INVESTIGATIONS OF SIGNALING PATHWAYS AND THEIR POTENTIAL BENEFITS IN COMBATING TRYPANOSOMATID DISEASES

by

SHARON KING KELLER

(Under the Direction of Silvia Moreno)

ABSTRACT

Trypanosomes are protist parasites, belonging to the order Kinetoplastida, characterized by the presence of a kinetoplast, a DNA-containing structure within the single mitochondrion of the parasite. This group is of great importance to the health of humans and domestic animals and has been the subject of much research. Signaling pathway such as the ones examined in this dissertation have been extensively studied in mammalian systems bringing to light knowledge that could be applied to elucidating the role of these pathways in these parasites. The extensive studies of the inositol 1, 4, 5-trisphosphate/diacylglycerol (IP_3/DAG) pathway in mammals and its implication in essential cellular process such as growth, differentiation, metabolism, among others, ignited interest in exploring the role of this pathway in the biology of the parasite. Targeting this pathway could render a way to disrupt the life cycle of the parasite. Our work on *Trypanosoma brucei* phosphatidylinositol phospholipase C demonstrates that this pathway is active in the parasites and could be involved in growth and infectivity. *T. brucei* has genetic tools that make it model system for exploring the effects of all parts of this pathway. Phosphodiesterase inhibitors have had success in targeting certain PDE families in humans. The parasite PDEC of *Trypanosoma cruzi* has structural similarity with human PDE4B, but we were

able to screen compounds that caused inhibitory effects, both *in vitro* and *in vivo*, selectively targeting the parasite PDE. This work demonstrated a role for PDEs in growth and in response to osmotic stress in parasites illustrating that even though the host and parasite PDEs are similar, the parasite enzyme can be selectively inhibited. The results from the compound testing allowed for the construction of a model that can be used to guide lead compound optimization and drug discovery. Our focus on both pathways have elucidated some fascinating similarities as well as differences compared to what is known from mammalian studies providing new insights in to the role of signaling in Trypanosomes.

INDEX WORDS: Trypanosomes, signaling, phosphatidylinositol phospholipase C, and phosphodiesterases

INVESTIGATION OF SIGNALING PATHWAYS AND THEIR POTENTIAL BENEFITS IN COMBATING TRYPANOSOMATID DISEASES

by

SHARON KING KELLER

AS, Athens Technical College, 2004

BS, University of Georgia, 2007

A Dissertation Submitted to the Graduate Faculty of The University of Georgia in Partial Fulfillment of the Requirements for the Degree

DOCTOR OF PHILOSOPHY

ATHENS, GEORGIA

2013

INVESTIGATIONS OF SIGNALING PATHWAYS AND THEIR POTENTIAL BENEFITS IN COMBATING TRYPANOSOMATID DISEASES

by

SHARON KING KELLER

Major Professor: Silvia Moreno

Committee: Roberto Docampo
Kojo Mensa-Wilmot
Rick Tarleton
Robert Sabatini

Electronic Version Approved:

Maureen Grasso
Dean of the Graduate School
The University of Georgia
August 2013

DEDICATION

I would like to dedicate this dissertation to my daughter, Brooklynn Adams, my husband, David Keller, and my parents, Jack and Brendel King. I would also like to dedicate this to my brother, Kenneth King, and sister-in-law, Joy King and nieces, Kendra and Kara. All of you have endlessly provided me with love, support, and prayers throughout my educational journey.

To Brooklynn, you are the source of inspiration for all that I have done. When I had you, I aspired to be more for you and for myself. You have been through all of this with me and have sacrificed things from yourself in order to go through this journey with me. I hope you have seen that you can do anything and get everything out of life that you may want. Now, it is your turn to go on this journey and I will be there for you.

To David, you have been a great source of strength and encouragement over these years. You have never ceased to believe in me even when I did not believe in myself. I love you and cannot wait to begin the next phase of our life together.

To my parents, I could not have done this without your love and support. You assisted me in taking care of Brooklynn when I needed the help so that I could prepare for school. Both of you have selflessly given so much to my educational pursuits that I will forever be in your debt.

To my brother, sister-in-law, and nieces, your love and support helped make this happen. We have shared many fun times and it seemed that those times came when I needed to laugh the most.

Thanks to you all. This has, undoubtedly, been the effort of our little family.

ACKNOWLEDGEMENTS

I would like to extend my deepest gratitude to my major professor, Dr. Silvia Moreno, for her guidance and encouragement throughout this project. She allowed me to try new things and push the boundaries on what I could accomplish. Dr. Moreno always taught me to never be satisfied and always strive for more. I would also like to thank my committee members, Dr. Roberto Docampo, Dr. Rick Tarleton, Dr. Kojo Mensa-Wilmot, and Dr. Robert Sabatini. The development of this project would not have been possible without their input and direction. I am forever thankful to all of my committee for expanding my view of and love for science.

I would like to thank all the members, past and present, of the Moreno lab and the Docampo lab for their support and encouragement. All of you have touched my life whether it was scientific advice or just a friendly word when I needed it the most. It was such fun to be a part of such a great group, not only of scientists, but of wonderfully, genuine people. Thanks to Christina Moore for exploring this project with me and for your beautiful cartoons.

My career here would not have been complete without the teaching mentoring I received from Dr. Kris Miller. Her deep love for and knowledge of teaching inspired me to develop my own teaching style. Words cannot express how much her teaching and mentoring have influenced the very teacher that I am and the one I hope to become. I owe a debt of gratitude to Dr. Denise Domizi for instilling in me the desire to seek out new and creative ways to teach. These are skills I will continue to develop. I would also like to thank Dr. Mark Farmer for his advice and support throughout my undergraduate and graduate career. He believed in me even when I did not and for that, I very thankful.

TABLE OF CONTENTS

Page

ACKNOWLEDGEMENTS v

LIST OF TABLES viii

LIST OF FIGURES ix

CHAPTER

1 GENERAL INTRODUCTION AND DISSERTATION STRUCTURE 1

1.1 General Introduction to Trypanosomes 1

1.2 Purpose and Significance of Dissertation 2

1.3 Structure of the Dissertation 2

2 LITERATURE REVIEW 4

2.1 The Disease, African Trypanosomiasis 4

2.2 Phosphoinositide Phospholipase C Role in Mammalian Systems 5

2.3 Role of Phosphoinositide Phospholipase C in *Trypanosoma cruzi* 6

2.4 IP_3 and IP_3 Receptor Role in Signaling 7

3 CA^{2+} REGULATION OF *TRYPANOSOMA BRUCEI* PI-PLC 9

Abstract 10

3.1 Introduction 11

3.2 Materials and Methods 12

3.3 Results 25

3.4 Discussion 32

References 39

4 LITERATURE REVIEW 61

4.1 The Disease, American Trypanosomiasis (Chagas) 61

4.2 Phosphodiesterases in Mammalian Cells 61

4.3 Phosphodiesterases in Trypanosomes 63

5 CHEMICAL VALIDATION OF PDEC AS A CHEMOTHERAPEUTIC TARGET 66

Abstract 67

5.1 Introduction 68

5.2 Materials and Methods 69

5.3 Results 76

5.4 Discussion 80

References 82

6 SUMMARY OF KEY FINDINGS AND FUTURE DIRECTION 99

6.1 Summary of Key Findings (PI-PLC) 99

6.2 Future Direction (PI-PLC) 101

6.3 Summary of Key Findings (PDEC) 102

6.4 Future Direction (PDEC) 103

LIST OF TABLES

Page

Table 3.1: Enzymatic kinetics comparison 45

Table 3.2: Primer sets used in cloning 57

Table 5.1: Structure of phosphodiesterase inhibitors 87

Table 5.2: Growth inhibitors 90

LIST OF FIGURES

Page

Figure 3.1: Role of myristoylation sequence 46

Figure 3.2: Role of identified amino acids for potential acylation 47

Figure 3.3: Endogenous localization 48

Figure 3.4: Enzymatic activity 49

Figure 3.5: Mutation of aspartate in calcium binding loop 51

Figure 3.6: Effect of TbPI-PLC down regulation by RNAi 52

Figure 3.7: Activity in parasites 53

Figure 3.8: Toxicity of overexpression by FACS analysis 54

Figure 3.9: Overexpression of PI-PLC results in susceptibility to PCD 55

Figure 3.10: Alignment of TbPI-PLC and mouse PLC ζ 56

Figure 3.11: Western blot of overexpression constructs 58

Figure 3.12: Composition of EF-Hand calcium binding loop 59

Figure 3.13: Mice infection 60

Figure 5.1: General approach to compound synthesis 92

Figure 5.2: Chemical structures 93

Figure 5.3: Inhibitor dose-response curves 94

Figure 5.4: Effect of PDEC inhibitors on cAMP levels 95

Figure 5.5: Regulatory volume decrease 96

Figure 5.6: Sequence alignment of *Trypanosoma cruzi* PDEC and human PDE4B 97

Figure 5.7: Homology modeling.....98

CHAPTER 1

GENERAL INTRODUCTION AND DISSERTATION STRUCTURE

1.1 General Introduction to Trypanosomes

Trypanosomes comprise a class of protozoan parasites within the superclass known as the kinetoplastids. Kinetoplastids are characterized by the possession of a kinetoplast which is a region of the mitochondrion that contains a high concentration of kDNA. Trypanosomes are exclusively parasitic organisms that possess one flagellum that is either free or attached to the cell surface at adhesion spots forming an undulating membrane. These parasites can infect multiple hosts and their impact, both human and economic toll, is staggering.

African trypanosomiasis is a systemic disease in which the pathogenic parasite, *Trypanosoma brucei*, is transmitted by the bite of a tsetse fly. These trypanosomes live in the blood, lymph node, and cerebrospinal fluid. *T. brucei* parasite can reproduce rapidly and invade organs of the body. African trypanosomiasis occurs in regions of sub-Saharan Africa in areas where poverty and weak health systems are rampant. Between 15,000 and 20,000 cases are reported annually. However, the World Health Organization estimates actual prevalence to be between 50,000 to 70,000 cases. Currently there are four drugs, suramin, pentamidine, melarsorprol, and eflornithine, available to treat African trypanosomiasis. Unfortunately, most are toxic and are effective only in certain stages of the disease (Kennedy, 2013).

American trypanosomiasis is a disease caused by the *Trypanosoma cruzi* parasite and occurs primarily in central and South America. Once inside the mammalian host, the parasites can invade any nucleated cell, invading organs, such as the heart, and potentially harming any

system of the host (Machado *et al*, 2013). Currently, it is estimated that approximately 8 million people are infected with about 30% projected to develop potentially the serious, life-threatening form of Chagas' disease (Bern *et al*, 2011). There are only 2 drug options available for treatment of Chagas, nifurtimox and benznidazole. Unfortunately, both have severe side effects such as skin reactions, vomiting, nausea, anorexia, neuropathy, and convulsions. Both agents require prolonged administration and have limited effectiveness especially in the chronic form (Pérez-Molina *et al*, 2013).

1.2 Purpose and Significance of Dissertation

The work presented in this dissertation highlights the complexity of signaling pathways in the Trypanosomatids and potential benefits these investigations may hold for treating and preventing disease. The role of phospholipases in the inositol 1, 4, 5-trisphosphate (IP_3)/diacylglycerol (DAG) signaling pathway has been extensively studied in mammalian systems as well as the role of phosphodiesterases in the regulatory signals involving cyclic adenosine monophosphate (cAMP). IP_3 and DAG are known to play role in mammalian cellular processes; however, much is unknown about this pathway in Trypanosomes. Phosphodiesterases (PDE) have garnered much attention in the past ten years with mammalian PDE-4 inhibitors being used to treat asthma, chronic obstructive pulmonary diseases, psoriasis, depression, as well as other diseases (Houslay, *et al*, 2005). In trypanosomes, a PDE has been demonstrated as playing a role in regulatory volume decrease (King-Keller *et al*, 2010), a process important to the parasites as they encounter osmolarity changes in their life-cycle.

1.3 Structure of the Dissertation

The dissertation is divided into six chapters. The second chapter is an introduction to phospholipases and their proposed functional roles. This is an overview of current literature

comprising a review of what is known about phospholipases from mammalian studies as well as studies in *Trypanosoma cruzi* and the potential significance of these enzymes in *Trypanosoma brucei.* Chapter 3 is a prepared manuscript that will be submitted for publication that describes the characterization of the phosphoinositide phospholipase C (PI-PLC) in *T. brucei.* We sought to demonstrate that this enzyme was indeed a phospholipase C as demonstrated in our enzymatic assays in which the activity was sensitive to calcium. This is a characteristic of PI-PLCs. Our analyses showed that the enzyme is active in parasites and may play a role in bioenergetics in the parasite (King-Keller *et al*, 2013). Chapter 4 is a literature review of phosphodiesterases and the use of phosphodiesterases inhibitors. We also discuss data from previous work highlighting interesting characteristics of *T. cruzi* phosphodiesterase C (TcPDEC). A previously published article validating TcPDEC as a potential drug target in *Trypanosoma cruzi* comprises chapter 5. A summary of key findings and future directions are discussed in chapter 6. The appendix is a book chapter discussing the role of acidocalcisomes in the stress response of *T. cruzi* in which phosphodiesterases play a role in the volume regulatory pathway (Docampo *et al*, 2011). Our work demonstrates the PI-PLC and TcPDEC are important and functional enzymes in signaling pathways. The investigations into the functions of these enzymes demonstrate their potential roles for investigation to the biology of the parasites and as potential chemotherapeutic targets.

CHAPTER 2

LITERATURE REVIEW

2.1 The Disease, African Trypanosomiasis

T. brucei has evolved a complex life cycle involving invertebrate and vertebrate hosts. In these hosts, the parasite undergoes morphological and metabolic changes that mediate the adaptation to a changing environment. When the tsetse fly ingests the parasite when feeding, the parasite migrates to the mid-gut of the insect, where it transforms into a procyclic trypomastigote and divides. Then the parasite migrates forward to the salivary gland where it transforms into the epimastigote form and further divides. In the salivary gland, the parasites can then transform into metacyclic trypomastigotes which is the only infective form to the vertebrate host (Figueiredo and Cross, 2010). Once inside the vertebrate host, the metacyclic trypomastigotes are changed into the bloodstream form and can multiply in the blood and lymph establishing the infection (Figueiredo and Cross, 2010). There are three subspecies of *T. brucei- T.b. brucei, T.b. gambiense, and T.b. rhodesiense.* These subspecies vary in infectivity of different hosts and in pathological manifestations (Figueiredo and Cross, 2010). *T.b. brucei* is a bloodstream parasite of African ruminants producing a disease called nagana (Steverding 2008). Symptoms include anemia, edema, watery eyes and nose, and fever. In a few days, the affected animal is emaciated and paralyzed and death is inevitable (Steverding, 2008). The human disease pathology depends on the causative parasite. *T.b. gambiense* is found in west and central Africa causing more than 90% of the reported cases. When present, the symptoms include severe headaches, sustained fever, alteration of mental state, and neurological disorders (Simarro *et al,* 2008). *T.b*

rhodesiense occurs in eastern and southern Africa. This form of the disease accounts for approximately 10% of reported cases (Brun and Balmer, 2006). The first symptoms are irregular fevers, occasional headaches, and pruritus (Simarro, 2008). After invading the blood and lymph systems, the disease proceeds to the central nervous system after crossing the blood-brain barrier (Simarro, 2008). If untreated, patients infected with *T. b. rhodesiense* will usually die within months or within years if infected with *T. b. gambiense* (Steverding, 2008). Human African trypanosomiasis decimated the people in many parts of the sub-Saharan Africa in the early 1900s. This impact led to efforts that nearly halted the transmission of the disease. However, lack of interest in disease surveillance caused the disease to slowly return (Simarro *et al*, 2008). Sleeping sickness and nagana have been huge obstacles in the development of rural Africa. The agricultural production needed to help sustain the people has also suffered due to these parasites and their resulting diseases. Human infections reduce labor resources and quality of life. Given the devastating effects of this disease, it is important to investigate new novel methods to control its spread and to treat those infected.

2.2 Phosphoinositide Phospholipase C role in Mammalian Systems

Phosphatidylinositiol phospholipase C (PI-PLC) is an intracellular enzyme that plays a vital role in signal transduction. The enzyme catalyzes the hydrolysis of phosphatidylinositol 4, 5-bisphosphate (PIP_2) to inositol 1, 4, 5-trisphospate (IP_3) and diacylglycerol (DAG) (Irvine, 1996). This catalysis occurs at the plasma membrane where the PIP_2 substrate is located. The enzyme catalyzes this hydrolysis of via a two-step mechanism involving Ca^{2+} as a cofactor (Rhee, 2001). IP_3 is soluble and diffuses through the cytoplasm, reacts with IP_3 receptors on the endoplasmic reticulum, and causes the release of intracellular calcium (Berridge, 1987). DAG remains attached to the plasma membrane and regulates phosphorylation by activating protein

kinases (Nishizuka, 1988). Mammalian PI-PLCs are involved in receptor-mediated signal transduction pathways (Williams, 1999). Thirteen mammalian PLC isozymes have been reported (Fukami *et al,* 2010). These isozymes have a modular arrangement of domains that achieve a regulated IP_3 and DAG production. Recent structural and functional studies have provided clues as to the roles of these domains in enzyme regulation and in interactions with the membrane (Paterson *et al*, 1995). It has been shown that the pleckstrin homology (PH) domain in PLC δ binds PIP_2 facilitating the access of the enzyme to the membrane surface (Paterson *et al,* 1995). The EF-hand domain may play an important part in stabilizing the fold of the enzyme as well as containing potential calcium binding sites (Williams, 1999). The X and Y domains form the two halves of the catalytic barrel (Fukami *et al,* 2010). The C2 domain crystal structure of the mammalian δ PLC shows evidence of Ca^{2+} binding sites (Suh *et al,* 2008). However, the exact role of these binding sites has not been elucidated and it thought that calcium may not bind there after all (Suh *et al,* 2008). The domain organization of the *Tb*PI-PLC includes homologous X and Y catalytic domains, an EF hand motif, a C2 domain similar to *T. cruzi*, but does not include a pleckstrin homology domain, which is characteristic of many PI-PLCs (Williams, 1999).

2.3 Role of Phosphoinositide Phospholipase C in *Trypanosoma cruzi*

The PI-PLC enzyme in *T. cruzi* has been previously described (Furuya *et al,* 2000; Okura *et* al, 2005; de Paulo Martins *et al,* 2010). Both *T. brucei* and *T. cruzi* PI-PLC have an *N*-terminal with a myristoylation consensus sequence (Furuya *et al*, 2000). *Tc*PI-PLC has been demonstrated to be lipid modified *in vivo* by analyzing metabolic labeling with [^{3}H] myristate and [^{3}H] palmitate (Furuya *et al,* 2000). In many eukaryotic cells, palmitoylation can play an important role in a protein's affinity for membranes and myristoylation is necessary for protein attachment to

membranes (Furuya *et al,* 2000). Using the anti-*Tc*PI-PLC antibody, the enzyme localized to the membrane in amastigotes, but demonstrated a diffuse localization throughout the cells in the epimastigote form. No detectable localization was observed in the trypomastigote form using this same antibody (Furuya *et al,* 2000). This data was supported by analysis of *Tc*PI-PLC mRNA using northern blot. It has been demonstrated that acylation of the *N*-terminal of *Tc*PI-PLC is responsible for directing the enzyme to the outer surface of amastigotes (de Paul Martins *et al,* 2010). In addition, studies have shown that the expression level of the enzyme changes during the different stages of differentiation. *Tc*PI-PLC expression increases in the differentiation of trypomastigotes into amastigotes (Furuya *et al,* 2000). This enzyme has been demonstrated to play a pivotal role in differentiation as antisense oligonucleotide-treated parasites of *T. cruzi* showed a slower rate of differentiation whereas overexpression of *Tc*PI-PLC mediated a faster differentiation rate (Okura, *et al,* 2005). Attempts to knock out the TcPI-PLC were lethal to the cells suggesting that the enzyme is essential (Furuya *et al,* 2000). However, genetic tools such as RNAi and conditional knockouts are not available in *T. cruzi*, but are viable options in *T. brucei,* making *T. brucei* an attractive model system for investigation of the enzyme's functional role.

2.4 IP_3 and IP_3 Receptor Role in Signaling

The second messenger IP_3 stimulates calcium release from intracellular stores through interaction with IP_3 receptors. Calcium in *T. brucei* appears to regulate cellular processes such as microtubule assembly (Dolan, 1986) and stimulate the release of VSG (Bowles *et al,* 1982). However, much is still unknown about the role of calcium signaling in Trypanosomes. The IP_3 ion channels are ~2700 amino acids and are similar to ryanodine receptors. These receptors are widely distributed among organisms as diverse as human, nematodes, and insects (Vazquez-

Martinez *et al,* 2003). IP_3 receptors contain six transmembrane domains and a large *N*-terminal region that is approximately ~2250 amino acids and extends into the cytoplasm (Vazques-Martinez *et al,* 2003). A single IP_3 binding site typically resides in the first 800 amino acids. IP_3 receptors possess a series of conserved domains including a putative IP_3-binding, ATP-binding, ryanodine homolog, and transmembrane domains (Ponting, 2000). While the transmembrane domain of these proteins does contain a motif for a Ca^{2+}-specific selectivity filter, amino acid residues important for IP_3 binding in mouse IP_3 receptors (Yoshikawa *et al,* 1996) are not well conserved in the predicted IP_3-binding domain of the *Tb*IP_3 receptor. IP_3 receptors are responsible for Ca^{2+} release by IP_3 after hydrolysis of PIP_2 by a phospholipase C. Recently the role of IP_3 receptors have been shown to play pivotal roles in different processes in Trypanosomes through the release of calcium. *Trypanosoma cruzi* IP_3 receptor genes expressed in DT40 cells lacking endogenous receptor genes caused calcium release from the endoplasmic reticulum (Hashimoto *et al,* 2013). Reduction or overexpression of the TcIP_3R in parasites resulted in defects in growth, transformation, and infectivity (Hashimoto *et al,* 2013). In *Trypanosoma brucei,* IP_3R was localized to acidocalcisomes and was able to release calcium in permeabilized cells (Huang e*t al,* 2013). RNAi caused a reduction in the calcium release from cells and caused defects in growth and infectivity (Huang *et al*, 2013). Collectively, this data suggests that the role of acidocalcisomes and calcium release is required for normal cellular functions in parasites.

CHAPTER 3

CA^{2+} REGULATION OF *TRYPANOSOMA BRUCEI* PHOSPHOINOSITIDE PHOSPHOLIPASE C

[1] King-Keller S., Moore C., Fang J., Docampo R., and Moreno, SN

To be submitted to *Eukaryotic Cell*

Abstract

A phosphoinositide phospholipase C (PI-PLC) has been characterized in *T. brucei*. The protein contains a domain organization characteristic of typical PI-PLCs, such as X and Y catalytic domains, an EF-hand calcium-binding motif, and a C2 domain, but lacks a pleckstrin homology (PH) domain. In addition, *Tb*PI-PLC contains an *N*-terminal myristoylation consensus sequence only found in trypanosomatid PI-PLCs. A peptide containing this *N*-terminal domain was shown to be *N*-myristoylated and palmitoylated and targeted to the plasma membrane. *Tb*PI-PLC enzymatic activity was stimulated by Ca^{2+} concentrations below cytosolic levels in the parasite, suggesting that the enzyme could be constitutively active. *Tb*PI-PLC hydrolyzes both phosphatidylinositol (PI) and phosphatidylinositol 4, 5-bisphosphate (PIP_2), with higher affinity for PIP_2, but does not hydrolyze glycosylphosphatidylinositol-anchored variant surface glycoprotein (GPI-VSG). We found that modification of a single amino acid in the EF-hand motif greatly affected its Ca^{2+} sensitivity and substrate preference. *Tb*PI-PLC localizes to intracellular vesicles and might use an intracellular source of PIP_2. Attempts to knockdown *Tb*PI-PLC expression by RNAi were unsuccessful but we show that the enzyme is active in parasites, can hydrolyze PIP_2, and thus contributes to the inositol 1,4,5-trisphosphate (IP_3)/diacylglycerol (DAG) pathway that was recently shown to be essential and required for growth and infectivity.

3.1 Introduction

Trypanosoma brucei is a protist parasite, which belongs to the order Kinetoplastida, characterized by the presence of a kinetoplast, a DNA-containing structure within the single mitochondrion of the parasite. *T. brucei* has a complex life cycle involving invertebrate and vertebrate hosts. The procyclic form is the proliferative form in the fly and the long slender bloodstream form is the proliferative form in the mammalian host. *T .b. brucei* is a parasite of African ruminants producing a disease called Nagana, while *T. b. gambiese* and *T. b. rhodesiense* are the subspecies that infect humans. Currently, approximately 50,000 people are infected annually with human African sleeping sickness, which is endemic in 36 sub-Saharan African countries (1). Efforts to understand the biology of the parasite are essential because they provide insights into novel ways by which we can disrupt the life cycle of the parasite and/or target the parasite while leaving the host unharmed.

The inositol 1,4,5-trisphosphate/diacylglycerol (IP_3/DAG) signaling pathway regulates many processes such as cell division, secretion, and differentiation in eukaryotic cells (2). The central enzyme in this pathway, the phosphoinositide phospholipase C (PI-PLC) catalyzes the hydrolysis of phosphatidylinositol 4,5-bisphosphate (PIP_2) to generate two second messengers, inositol 1,4,5-trisphospate (IP_3) and diacylglycerol (DAG) (3). IP_3 gates a channel in the endoplasmic reticulum, the IP_3 receptor (IP_3R), which releases calcium ion (Ca^{2+}) into the cytosol. DAG activates a protein kinase stimulating downstream signaling pathways (4). Previous work from our laboratory has characterized Ca^{2+} stores in *T. brucei* and found that these parasites store Ca^{2+} in an acidic compartment termed the acidocalcisome (5). Recently, a $TbIP_3R$ was shown to be a functional Ca^{2+} release channel located in *T. brucei* acidocalcisomes and to be essential for growth and the ability of the parasites to establish an infection (6). Considering the

central role that IP_3 plays in Ca^{2+} homeostasis we became interested in the characterization of the enzyme that can generate this second messenger, the *T. brucei* PI-PLC. Understanding the biochemical characteristics of this enzyme will help to understand the role of the IP_3 signaling in *T. brucei*, which could play an important role in the differentiation and adaptation of the parasite during its life cycle.

PI-PLCs in *T. brucei* and *T. cruzi* show some unique features not shared with any other PI-PLCs. For example, they have a myristoylation consensus sequence at their N-terminus instead of a pleckstrin homology (PH) domain that may play a role in the localization of the enzyme. N-myristoylation at the N-terminus was shown to be involved in the localization of the *Trypanosoma cruzi* PI-PLC to the plasma membrane (7). The trypanosomatid PI-PLCs have an overall domain organization that is most similar to the mammalian zeta type PI-PLC (PI-PLCζ) present in sperm (8). The PI-PLCζ is released into the oocyte upon fertilization where is activated by cytosolic Ca^{2+} levels and causes Ca^{2+} oscillations, which are responsible for the whole downstream cascade of signaling pathways leading to the development of the embryo (8, 9). In this work we have characterized the activity of the *Tb*PI-PLC and study its function and localization in the parasite as well as its potential regulation.

3.2 Materials and Methods

3.2.1 Chemicals and reagents

Plasmids

The pUB39 vector was a gift from George A.M. Cross (Rockefeller University, New York, NY). The $p2T7^{Ti}$ vector was a gift from John Donelson (University of Iowa, Iowa City, IA). The pET32 ligation and ligation independent cloning vectors were from Novagen. The pMOTag4H vector was from Thomas Seebeck (University of Bern, Bern Switzerland).

Chemicals and reagents

Qia gel extraction and MinElute PCR purification kit were from Qiagen. The Prime-a-Gene labeling system was from Promega. TRIzol reagent, Alexa 488 and 546 conjugated rat, rabbit, and mouse secondary antibodies from Invitrogen. Rabbit *Tb*VP1 antibody was a gift from Norbert Bakalara (Ecole Nationale Superieure de Chimie de Montpellier, Montpellier, France). Rabbit *Tb*BiP antibody was a gift from James Bangs (University of Wisconsin, Madison, Wisconsin). Purified anti-HA antibody was from Roche. *Tb*PPDK antibody was a gift from Frederiqe Bringaud (University of Bordeaux, Bordeaux, France). Commercial anti-PIP_2 was from VWR. AMAXA Human T-cell Nucleofector kit was purchased from Lonza. [^{3}H] myristate and palmitate for metabolic labeling were from NEN Life Science Products. Mouse anti-GFP monoclonal antibody was from Molecular Probes. Horseradish peroxidase (HRP)-conjugated goat anti-rabbit and goat anti-mouse IgG antibodies were from Santa Cruz Biotechnology. G fluoromount was from Southern Biotechnology. Pierce ECL western blotting substrate was from Thermo Fisher Scientific. Phire HS DNA polymerase was from Finnzymes. Clonetech His tag Superflow Cartridge. Gene Tailor Site-directed mutagenesis was from Invitrogen. Myo[^{3}H] inositol (7.27 Ci/mmol) and ^{3}H-PIP_2 (5.0 Ci/mmol) were from Perkin-Elmer (Waltham, MA). PIP_2 and PI were from Avanti-Polar Lipids, Inc. (Alabaster, AL).

3.2.2 Culture methods and in vitro growth analysis

Procyclic cells 29-13 co-expressing T7 RNA polymerase and Tet repressor were gifts from George A.M. Cross from Rockefeller University. Cells were grown in SDM-79 medium with hemin (7.5 μg/ml) and 10% FBS (heat inactivated, HI, and tetracycline free) at 27 ^{o}C with hygromycin (50 μg/ml) and G418 (15 μg/ml) (10). Single marker bloodstream (SM) parasites were a gift from George A.M. Cross and were grown in HMI-9 medium supplemented with 20%

FBS HI, tetracycline free and 2.5 μg/ml G418. Procyclic cells at a density of 1 x 10^6 cells were induced with 1 μg/ml of tetracycline and diluted every 2 days. Bloodstream form cells at a density of 1 x 10^4 were induced with 1 ug/ml of tetracycline and diluted daily.

3.2.3 Cloning of *Tb*PI-PLC

Cloning for N-terminal and N-terminal mutation overexpression in parasites

The *T. brucei* pUB39 expression vector was used for expression studies in parasites. The inserted fragment of VSG117 cDNA was removed by digestion with *Hind*III and *BamH*I. First, a primer pair to amplify the first eighteen amino acids, primer pair *Tb*PI-PLC $_{(1\text{-}18)}$ (Table 3.2) were generated to incorporate *Hind*III and *Xho*I sites. Secondly a pair of primers, GFP tag, were used to amplify the ORF of *Aequorea Victoria* GFP for incorporating of a XhoI site and a BamHI site (Table 3.2). The linearized fragments were co-ligated into *Hind*III and *BamH*I digested pUB39 to generate a pUB39/GFP to create a GFP fusion product. For the expression of the truncated version, a primer pair *Tb*PI-PLC $_{(19\text{-}714)}$, was used to for amplification of amino acids 19-714 and for incorporation of *Hind*III site and *Xho*I sites (Table 3.2). The fragment was cloned into the digested pUB39/GFP vector digested with *Hind*III and *Xho*I replacing the previously cloned myristoylation sequence with a truncated version. A forward primer (Table 3.2) and the reverse primer used previously was used to amplify GFP alone and clone into the pUB39 vector. All constructs were confirmed by sequencing (Yale University DNA Analysis Facility, New Haven, CT) and linearized by *Not*I digestion.

For studying the role of single amino acids of the *Tb*PI-PLC N-myristoylation consensus sequence, PCR-mediated point mutations were used to amplify the first eighteen amino acids and clone into the pUB39/GFP reporter system. Primers were designed for no mutation (WT);

ΔG2A mutant; ΔC4A mutant; ΔG2C4A mutant (Table 3.2). Mutations corresponding to amino acid changes are highlighted in bold.

Cloning, expression, and purification of recombinant PI-PLC

Primers were designed to amplify the *Tb*PI-PLC gene for cloning into pET32 ligation independent cloning system (Table 3.2). This system incorporates two histidine tags, both N-terminal and C-terminal plus creates a thioredoxin fusion tag that will facilitate obtaining soluble protein. The primers were used to amplify *Tb*PI-PLC gene from genomic DNA using Finnzymes Phire HS DNA polymerase. Qiagen PCR purification kit was used to purify PCR samples. To prepared insert to be compatible for ligation, the PCR product was treated with T4 DNA polymerase using manufacturer's protocol and incubating at 22℃ for 30 minutes and then subsequent inactivation of enzyme at 75℃ for 20 minutes. The manufacturer's protocol was used to anneal the insert into an EK/LIC vector. Ligation reaction was used to transform NovaBlue GigaSingles competent cells using manufacturer's protocol. Direct colony PCR was used to verify insert incorporation. Qiagen mini-prep plasmid kit was used to isolate plasmid and transformed expression bacteria, BL21DE2RIPL. The colonies were screened by digestion with *Nco*I and *Kpn*I. Colony 1 was tested for induction and five colonies were sent for sequencing. Colony 1 was confirmed by sequencing. One liter of LB was inoculated with *Tb*PI-PLCpET32 colony 1. Bacteria was grown at 37°C until OD_{600} ~ 0.6. IPTG was added to induction flasks at a final concentration of 1 mM and grown at 18˚for 3 hours. Bacteria were resuspended in 10 ml of lysis buffer: Wash buffer (0.5 M NaCl, 60 mM imidazole, 20 mM Tris-HCl (pH 7.9) plus lysozyme (100 μg/ml), bacterial His protease inhibitors, benzonase (2.5 units/ml), and 0.1% Triton-X-100. Bacteria were incubated on ice for 30 minutes then subjected to sonication for 1.5 minutes at 20 seconds on and 20 seconds off. The bacteria were then

centrifuged at 10,000g for 10 minutes at 4℃ for the removal of cell debris. The supernatant was passed through a 0.8 µM filter then through a 0.45 µM filter. Alternately, after sonication, the bacteria were centrifuged at 100,000g for 1 hour to render pellet and supernatant fractions (11). The Clonetech column was equilibrated (according to manufacturer's protocol), cleared sample passed through, and eluted with elution buffer containing: 0.5 M NaCl, 20 mM Tris-HCl and 1 M imidazole-HCl, pH 7.9. The elutions were pooled together and dialyzed overnight with 10 mM Tris-HCl, pH 7.0. Samples of the elutions were analyzed by SDS-PAGE for expression of protein at the corresponding size.

3.2.4 Cell transfections

Cells were transfected according to a published protocol (6). Approximately, 2.5 x 10^7 procyclic cells (in mid-log phase 5 x 10^6 cells/ml) were harvested and centrifuged at 1000g for 7 minutes. Cells were washed with Cytomix buffer containing 2 mM EGTA, 120 mM KCl, 0.15 mM $CaCl_2$, 25 mM HEPES, 5 mM $MgCl_2$, Glucose g mg/ml, BSA 0.1 mg/ml, and 1 mM hypoxanthine, pH 7.6 and resuspended in a volume of the same buffer at a density of 5 x 10^7 cells/ml. 500 µl of cells were added to 10 µg of linearized DNA in a 0.4 cm cuvette. The cuvette was electroporated with two pulses from a Bio-Rad Gene Pulser set at 1500 volts and 25 µF. The stable transfectants were selected using the appropriate antibiotic.
Approximately, 5 x 10^7 bloodstream cells were harvested and centrifuged at 1300g for 10 minutes and resuspended in 100 µl of AMAXA human T-cell nucleofector solution in a 2 mm gap cuvette. 10 µg of linearized DNA was added to the cuvette immediately. Electroporation was conducted with program X-001 using the AMAXA nucleofector. The stable transfectants were selected using the appropriate antibiotic.

3.2.5 Metabolic labeling

Metabolic labeling was performed as previously described (12). To analyze the roles of G2 and C4 residues in protein acylation and plasma membrane association, the N-terminal mutants and WT were metabolically labeled with either [9,10-^{3}H] myristate acid or [9,10-^{3}H] palmitate acid. Approximately 2 x 10^{8} bloodstream form cells from *Tb*PI-PLC$_{1-18}$ (wild type), G2A, C4A, G2C4A, and GFP alone were labeled for immunoprecipitation. The log phase cells in HMI-9 medium supplemented with 10% FBS, 10% serum plus, and supplemented with 5 µg ml^{-1} G418, 2.5 µg ml^{-1} phleomycin, and 1 µg ml^{-1} tetracycline were incubated with 25 µCi/ml of [9,10-^{3}H] myristate acid or 50 µCi/ml of [9,10-^{3}H] palmitate acid (NEN Life Science Products). After incubation for 4 hours at 37 °C, the cells were harvested and washed twice with cold PBS to remove any remaining serum proteins and excess label from medium. The cells were lysed in radioimmunoprecipitation analysis (RIPA) buffer (150 mM NaCl, 1.0% Nonidet P-40, 0.5% deoxycholic acid, 0.1% SDS, 50 mM Tris base, pH 7.5, NaN_3, and protease inhibitor mixture at a concentration of 10^{6}- 10^{7} cells per ml. The cell lysates were centrifuged at 21,000g for 20 minutes to remove debris. The supernatants were collected and incubated with the homogenous protein A/G agarose suspension (Roche Applied Science) for at least 3 hours on a rocking platform with gentle agitation. After centrifugation for 30 seconds at 12,000g the pre-absorbed supernatants were transferred to fresh tubes and incubated with 1 µg anti-GFP mouse monoclonal antibody (Molecular Probes) overnight with gentle agitation. The protein-antibody complex was selectively absorbed by further incubation with protein A/G agarose suspension for at least 3 hours or overnight at 4 °C on a rocking platform. The beads were collected by centrifugation for 30 seconds at 12,000g and washed twice with RIPA buffer, twice with high salt buffer (500 mM NaCl, 150 mM Tris base pH 7.5, 0.1% Nonidet P-40, and 0.05%

deoxycholic acid) and once with low salt buffer (50 mM Tris base, pH 7.5, 0.1% Nonidet P-40, 0.05% deoxycholic acid). For [9,10-^{3}H] myristate acid labeled proteins, the beads were mixed with and equal volume of 2X Laemmli sample (SDS) buffer without Tris base and boiled for 5 min. For [9,10-^{3}H] palmitate acid labeled proteins, the beads were suspended in an equal volume of non-denaturing 2X Laemmli sample buffer without Tris base, dithiotheritol or β-mercaptoethanol and boiled for 1-2 minutes to avoid breakage of the labile thioester bonds. After removing the protein A/G agarose by centrifugation for 20 seconds at 12,000g, the supernatants were subjected to SDS-PAGE electrophoresis. The [9,10-^{3}H] palmitate acid labeled proteins were treated with two 30 minutes washes with 1M hydroxylamine (pH 7.5) and 1 M Tris-HCl (pH 7.5). After treating with EN^{3}HANCE (NEN Life Science Products), the gels were dried and exposed to blue-sensitive x-ray films (Midwest Scientific) at -80℃

3.2.6 Epitope tagging

Forward and reverse primers were designed containing 100 nucleotides of the *Tb*PI-PLC ORF before the stop codon and the reverse complement of the 100 nucleotides of the 3' UTR followed by 21 nucleotides of the backbone of pMOTag4h, in frame (Table 3.2). The primers amplified the HA tagging cassette with hygromycin resistance gene from pMOTag4H. Amplification was verified by electrophoresis and DNA purified using Qiagen PCR purification kit, precipitated, and transfected into parasites following the one-step epitope tagging protocol previously published (13).

3.2.7 Western blot analysis

Cells were harvested and washed twice with PBS and lysed with RIPA buffer (150 mM NaCl, 20 mM Tris-HCl, pH 7.5, 1 mM EDTA, 1% SDS, and 0.1% Triton-X-100) with protease inhibitor cocktail (1 μg/ml aprotinin, 1 μg/ml leupeptin, 1 μg/ml pepstatin, 1 mM

phenylmethylsulfonyl fluoride (PMSF), and 2.5 u/ml of benzonase (6). Protein concentration was determined by Pierce BCA protein assay. Either total cell lysates or supernatant and pellet fractions (after centrifugation at 100,000g for 1 hour) were mixed with 4X Bio Rad laemmli loading buffer and directly loaded into SDS-PAGE gels. Electrophoresis was used to separate proteins and transferred onto a nitrocellulose membrane using a Bio Rad blotting apparatus. The membranes were blocked overnight in 5% nonfat milk in PBS-T (0.5% Tween-20) at 4℃. The membranes were washed and incubated either with the Roche rat anti-HA (1:100) or Molecular Probes rabbit anti-GFP (1:2000) for 1 hour. After thorough washing with PBS-T, the membranes were incubated with HRP-conjugated anti-Rat or anti-rabbit antibody (1:15000) for 1 hour. After washing five times with PBS-T, the immunoblots were visualized using Pierce ECL Western blotting substrate according to the manufacturer's protocol.

3.2.8 Fluorescence microscopy

Live cells were imaged using direct fluorescence. For immunofluorescence assays, parasites were washed with PBS and fixed with 4% paraformaldehyde in PBS, pH 7.4 for 1 hour. Cells were washed two times with PBS and adhered to 1 mg/ml poly-l-lysine coated coverslips. Cells were permeabilized with 0.3% Triton-X-100 in PBS, pH 7.4 for 3 minutes. Parasites were blocked for 1 hour at room temperature with a blocking solution containing: 50 mM NH_4Cl, 3% BSA, 1% fish gelatin, and 5% goat serum. Blocking solution was removed by washing with 1% BSA in PBS, pH 8.0. Cells were incubated with monoclonal Roche anti-HA antibody (1:20) and either the polyclonal rabbit antibody against TbVP1 (1:300), the rabbit anti-*Tb*BiP antibody (1:300), the mouse anti-*Tb*PPDK (1:30), or the mouse monoclonal anti-PIP_2 antibody (1:50) for 1 hour. Cells were washed with PBS, pH 8.0 and incubated with secondary antibodies Alexa 488-conjugated goat anti-rat (anti-HA) and/or Alexa 546-conjugated goat anti-rabbit/mouse at 1:1000

for 1 hour. The coverslips were mounted to glass slides using Southern Biotechnology fluoromount-G and counterstained with DAPI at 10 ug/ml. All images of parasites were captured using an Olympus 1X-71 inverted fluorescence microscope with a Photometrix Coolsnap CCD camera using the Delta Vision software from Applied Precision. Images were processed using the Softworx deconvolution software. Differential interference contrast and fluorescence images were captured under non-saturating conditions, using the same exposure times.

3.2.9 PI-PLC activity assay

Protein concentration was determined and recombinant enzyme was stored in 40% glycerol at -80 °C. Analysis of the enzymatic activity of PI-PLC was performed measuring the release of soluble IP_3 from the hydrolysis of [^{3}H] PIP_2. The standard reaction was performed as described (12). Briefly, the reactions contained 30,000 cpm of radioactive PIP_2 (or PI) and also contained cold PIP_2 (or PI) at varying concentrations and dried under nitrogen stream. Buffer included 20 mM Tris-HCl buffer pH 7.2, 2.5 mM EGTA, 100 mM NaCl and $CaCl_2$ in varying concentrations to obtain the calculated concentration of free calcium using the MaxChelator computer program. The phospholipid mixture was sonicated for 2 seconds. The reactions were initiated by the addition of 3.5 µg of enzyme followed by incubation at 30˚ for 20 min. The reaction was stopped by adding 500 µl of cholorform:methanol:HCl [100:100:0.6] and 150 µl of 5 mM EGTA in 1N HCl. Samples were centrifuged to separate organic and aqueous phases. The aqueous phase were removed and counted using a scintillation counter. Activity was analyzed for response to Ca^{2+} concentration, pH, time of reaction assay, and incubation temperature to establish activity parameters. K_m, V_{max}, and k_{cat} were calculated using nonlinear regression analysis using Prism software.

3.2.10 Labeling and purification of VSG

Parasites were labeled and VSG purified according to a published protocol (14). Parasites were labeled and VSG purified. *T. brucei* (2×10^9) were obtained from infected rats and washed in 2 ml of RPMI 1640. The cells were then incubated in a flask at 37 degrees for 15 minutes in a 5% CO_2 environment. BSA/ [^{3}H]-myristate complex was added to the cells and incubated for 2 hours at 37 degrees. Cells were washed in 10 ml of Bicine buffered saline (BBS; 50 mM bicine, 50 mM NaCl, 55 mM D-glucose, adjusted to pH 8.0 with sodium hydroxide) and resuspended in 4 ml of chilled hypotonic lysis buffer (10 mM sodium phosphate, pH 7, 1 ug/ml leupeptin, 0.1 mM TLCK (37 µl/ml), 5 mM p-CMPS) for harvesting of the radiolabeled VSG. Cell suspension was transferred to a 30 ml corex tube, incubated on ice for 15 min, and centrifuged at 7000g for 15 min at 4 ^{o}C to recover the membrane bound VSG from the pellet. The centrifugation was repeated and the pellet resuspended in 2 ml of 1% SDS to solubilize the VSG, then vortexed twice and heated at 100 degrees for 10 minutes. Subsequently, 20 ml of water saturated *n*-butanol at room temperature was added to the pooled aliquots. This mixture was centrifuged at 12,000g for 20 min at room temperature and the organic (top) phase was removed without disturbing the interphase. This removes extraneous lipids and leaves the VSG in the aqueous phase. The aqueous phase was re-extracted 5 times. The final extract is by the addition of 20 ml of *n*-butanol (not water saturated). The protein was recovered by centrifugation at 12,000g for 5 mins at room temperature. The precipitate was washed with anhydrous ether to remove the excess *n*-butanol and dry. The precipitate was dissolved by vortexing in 0.5 ml of 1% SDS and heat at 100 degrees for 10 mins. The sample was vortexed once more and the insoluble material was removed by centrifugation at 12,000g. The supernatant was transferred to a microcentrifuge tube. 500 µl of *n*-butanol was added for

extraction of the protein with repeated pipetting followed by centrifugation at 12,000g for 5 minutes at room temperature to resolve the phases. This step was repeated 4 or 5 times each time removing the butanol (top) phases. The pellet was resuspended in a small volume 1% NP-40 and heat at 100 degrees for 5 minutes. Enzymatic assay was performed as described (13) with the assay buffer described in PI-PLC activity assay.

3.2.11 Site-directed mutagenesis

The Invitrogen Gene Tailor site-directed mutagenesis system was used. Briefly, primers were designed to include overlapping regions and the creation of the nucleotide mutation, gac (aspartate) to gcc (alanine). With the aim to mutate aspartic 109 to alanine in the coding sequence of the TbPI-PLC, a primer pair (Table 3.2) was designed to incorporate this change. The *TbPI-PLC* gene was methylated, amplified using the mutated primers, and transformed in DH5α bacteria. The host cell circularizes the linear mutated DNA and digests the methylated template DNA. Colonies were screened by restriction digestion and plasmids were confirmed by sequencing. The mutated gene was digested with *BamH*I and *Sal*I and cloned into the ligation dependent pET32a. The expression of TbPI-PLC^{D109A} was done in BL21DE3 bacteria, purified as described above for the *Tb*PI-PLC, and assayed for activity using the same established parameters.

3.2.12 Generation of RNAi constructs

To knockdown the expression of the *Tb*PI-PLC gene by double stranded RNA expression, the p2T7^{Ti} vector was used. This utilizes dual inducible T7 promoters. A 500 base pair fragment corresponding to nucleotides 1304-1790 (shown in bold) was amplified using the following primers: *Tb*PI-PLC RNAi forward 5'-CCGCTCGAG**GAATTCAAGGGGTGCTGAAAAG**-3' (*Xho*I site) and *Tb*PI-PLC RNAi

reverse 5'- CGGGATCC**CCTGGGAAGACAGAAAGCT**- 3' (*BamH*I site) and cloned into the digested p2T7^{Ti} vector. The construct was verified by sequencing and purified for cell transfections.

3.2.13 Northern blot analysis

RNA was isolated with TRIzol reagent from Sigma-Aldrich and quantified. RNA samples of 10 µg were separated on 1% formaldehyde/agarose gels and then transferred to a Zeta Probe nylon membrane by overnight capillary transfer. The RNA was crosslinked to the membrane by baking at 80^{o}C. The same primer pair was used to generate probes and subsequently labeled with [α-^{32}P]-dCTP following the Prime-a-Gene labeling protocol. The β-tubulin was labeled and used as a loading control. The membranes were hybridized in 7% SDS, 0.5 M Na_2HPO_4, pH 7.2 buffer overnight at 65^{o}C in rotating hybridizer. Membranes were washed once with 1x SSC, 0.1% SDS at 65^{o}C and once with 0.1 x SSC, 0.1% SDS at 65°C for 30 min. The blots were visualized by autoradiography.

3.2.14 Parasite lysates for activity

Exponentially growing cells of procyclic 29-13, bloodstream form single marker, *Tb*PI-PLC OE, or *Tb*PI-PLC RNAi were harvested and washed twice with PBS (procyclic) or trypanosome dilution buffer (TDB), and subjected to freeze thaw by exposing cells to liquid nitrogen (5 minutes freeze and 1 minute of thaw at 37 ^{o}C) for 3-5 cycles or until cells were broken. The pellet was resuspended in approximately 200 µl of 20 mM Tris-HCl, pH 7.2. Protein concentration was measured using Thermo Scientific BCA protein assay kit and enzymatic activity assay was performed immediately. PI-PLC activity assay was carried out as previously described using 35 µg of total lysate in all reactions.

3.2.15 Flow cytometry

To quantify the amount of dead cells, the 29-13 parental line and transfectants overexpressing active PI-PLC were incubated ± tetracycline. Parasites were collected and washed twice with cold PBS and resuspended in 500 µl of manufacturer supplied 1X binding buffer. Propidium iodide was added at the final concentration recommended by manufacturer. Fluorescence was measured by FACS analysis and dead cells were as those stained positive for propidium iodide. Cells were also treated with 100 µM hydrogen peroxide (H_2O_2) for three hours and then labeled with propidium iodide to analyze susceptibility to apoptosis from overexpression of PI-PLC.

3.2.16 In vivo studies

Exponentially growing cells lines (WT and RNAi) were washed once in HMI-9 medium without selectable drugs and resuspended in the same medium. Eight-week-old BALB/C mice (5 mice per group) were infected with a single intraperitoneal injection of 2×10^4 bloodstream form parasites in 0.2 ml of HMI-9 medium. For the RNAi cells, single inoculums of non-induced cells were used in two sets of mice, one group being given 200 µg/ml doxycycline in 5% sucrose in drinking water and the other group supplied with drinking water containing 5% sucrose only. The drinking water with or without doxycycline was exchanged every 2-3 days, starting 3 days before infection and continuing through the process. Animals were fed ad libitum on standard chow. Presence of parasites were monitored and detected at day 3 post-infection. All animal experiments were carried out following protocols approved by the Institutional Animal Care and Use Committee (IUCAC) and the University of Georgia.

3.3 Results

3.3.1 Molecular characterization of *Tb*PI-PLC

Analysis of the *T. brucei* genome in the TriTryp database (http://tritrypdb.org) showed the presence of a putative phosphoinositide phospholipase C (*Tb*PI-PLC) gene (Tb.11.02.3780). The ORF consists of 2,145 bp predicting a protein of 714 amino acids with a molecular mass of 80.4 kDa. In addition to the highly conserved catalytic X (amino acids 246-392) and Y domains (amino acids 453-571), the *Tb*PI-PLC has an EF-hand domain (amino acids 95-130) at the N-terminal region and a C2 domain (amino acids 580-713) (Fig. 3.1A). The *Tb*PI-PLC EF-hand motif consist of approximately 36 amino acids in a helix-loop-helix arrangement (15). Within this motif, there is a 12-residue loop region (108-119) that has residues (aspartate and glutamate) in locations that may play a role in the binding of Ca^{2+} (16). The overall domain organization of the *Tb*PI-PLC is most similar to the mammalian sperm-specific PLCζ (AF435950) (Fig 3.1A). Sequence alignment shows an overall 27% identity and 40% similarity between *Tb*PI-PLC and mouse PLCζ proteins (Fig 3.11). However, one prominent difference between the *Tb*PI-PLC and the PLCζ is the presence of a N-myristoylation consensus sequence predicted by a NMT program (http://mendel.imp.univie.ac.at/myristate/) (Fig. 3.1A), which is highly similar to the N-myristoylation sequence of *Trypanosoma cruzi* (7).

3.3.2 Role of *N*-myristoylation sequence

In order to study the role of the N-myristoylation sequence, a series of green fluorescent protein (GFP) fusion constructs were generated and cloned into the pUB39 vector for overexpression in procyclic and bloodstream forms. The first 18 amino acids of the *Tb*PI-PLC sequence, *Tb*PI-PLC $_{(1-18)}$ fused to GFP, and the truncated PI-PLC, *Tb*PI-PLC $_{(19-714)}$, were transfected into procyclic (29-13) and bloodstream (single marker) forms. Cells were induced by

the addition of tetracycline (1 µg/ml) and lysates analyzed by Western blot for expression of the expected size protein with anti-GFP (Fig. 3.11). Direct fluorescence of live parasites demonstrated expression of *Tb*PI-PLC $_{(1-18)}$ localized to the plasma membrane (Fig. 3.1D) whereas localization of *Tb*PI-PLC $_{(19-714)}$ was cytosolic (Fig. 3.1C). This demonstrated that the N-myristoylation consensus sequence is sufficient for localization to the plasma membrane. To further study the role of single amino acids of the *Tb*PI-PLC N-myristoylation sequence, PCR-mediated point mutations, intact N-myristoylation sequence (WT), and the GFP reporter were used. Point mutations were introduced into the *Tb*PI-PLC $_{(1-18)}$ fused to GFP: ΔG2A, ΔC4A, and ΔG2C4A (Fig. 3.2A) and transgenic live parasites expressing these fusion proteins were analyzed by direct fluorescence. Mutating G2 or C4 disrupts the targeting to the plasma membrane and localizes the protein to the cytosol (Fig. 3.2B). To analyze the roles of G2 and C4 residues in protein acylation, the N-terminal mutants and WT were metabolically labeled with either [9, 10-^{3}H] myristate acid or [9, 10-^{3}H] palmitate acid. WT cells were both myristoylated and palmitoylated. However, the ΔG2A mutant, ΔG2C4A mutant, and GFP reporter were neither myristoylated nor palmitoylated. ΔC4A was myristoylated only (Fig 3.2C). This indicates that G2 is needed for both fatty acid modifications and C4 is necessary for palmitoylation only. We wanted to investigate metabolic labeling of the intact *Tb*PI-PLC enzyme; however, all attempts to overexpress the full length were unsuccessful. The overexpression was lethal in both procyclic and bloodstream form cells.

3.3.3 Endogenous localization

To determine the localization of endogenous *Tb*PI-PLC, in situ tagging was used to incorporate a tagging cassette at the C terminus end of one of the chromosomal copies of the *TbPI-PLC* gene (Fig. 3.3A). This strategy incorporates a 3XHA tag and a hygromycin resistance

gene. Western blot analysis using anti-HA confirmed the expression of the protein at the expected size (Fig. 3.3B). Localization was analyzed by immunofluorescence microscopy with anti-HA. *Tb*PI-PLC localizes to intracellular vesicles and further co-localization studies with intracellular markers of acidocalcisomes (vacuolar proton pyrophosphatase, *Tb*VP1) (17), ER *(Tb*BiP) (18), and glycosomes (pyruvate phosphate dikinase *Tb*PPDK) (19) showed that *Tb*PI-PLC did not co-localize with any of these markers (Fig. 3.3C). The localization of *Tb*PI-PLC to vesicles instead of to the plasma membrane was unexpected considering our data from the overexpression of the myristoylation sequence and the truncated version. However, it has been demonstrated that PLCs can utilize alternate sources of PIP_2. For example, the sperm specific PLCζ localized to distinct vesicles inside the egg (20). Likewise, PIP_2 was shown to localize distinct vesicular structures inside the egg cortex where PLCζ hydrolyzed this intracellular source of PIP_2 (20). We used anti-PIP_2 to study the distribution of PIP_2 with respect to the observed distribution of the HA tagged *Tb*PI-PLC (Fig. 3.3D). Our results demonstrated PIP_2 localization to vesicles throughout the cells with a similar distribution to *Tb*PI-PLC. In addition, we attempted to observe localization of the *Tb*PI-PLC gene in bloodstream forms, but our efforts were unsuccessful in tagging one of the alleles.

3.3.4 Expression, purification and activity of recombinant *Tb*PI-PLC

The *Tb*PI-PLC was expressed in bacteria and the purified protein was analyzed for its enzymatic properties. We investigated enzyme activity when subjected to the following concentrations of free calcium: 1 nM, 10 nM, 100 nM, 1 µM, 10 µM, 100 µM, 1 mM, and 10 mM. Other experimental data sets looked at enzyme activity using varied incubation time periods such as 0, 5, 10, 20, and 60 min (data not shown), various incubation temperatures (data not shown), and in various pH conditions (6.5, 7, 7.2, 7.5, 8, and 9). We observed a peak of

activity at a free Ca^{2+} concentration of 10 nM for PIP_2 and a peak of activity with PI when free Ca^{2+} was at 100 nM (Fig 3.4A). In addition, the enzyme was most active at a pH of 7.2 (Fig. 3.4B). Enzyme activity at different concentrations of PIP_2 (Fig. 3.4C) and PI (Fig 3.4D) was investigated and V_{max} and K_m were calculated for both substrates. The lower K_m for PIP_2 as the substrate indicates a preference of the enzyme for PIP_2 compared to PI. Enzymatic data was calculated and compared for both PIP_2 and PI as substrate. The enzyme prefers PIP_2 and has demonstrated more efficiency in hydrolyzing PIP_2 (Table 3.1).

In *Paramecium*, RNAi ablation of PLC resulted in the release of GPI-anchored proteins; suggesting a role for these enzymes in the hydrolysis of GPI-anchored proteins (20). To test if recombinant *Tb*PI-PLC enzyme can hydrolyze GPI-anchored proteins, we purified [^{3}H] myristate-labeled VSG to use as a possible substrate for the *Tb*PI-PLC (14). Hydrolysis of the labeled VSG was assayed according to a published (14) protocol, using calculated free calcium concentrations of 10 nM, 100 nM, 1 μM, and 1 mM. *Bacillus cereus* PI-PLC was used as a positive control (20). Recombinant *Tb*PI-PLC did not hydrolyze GPI-anchored VSG under the assay conditions whereas the bacterial PI-PLC was able to hydrolyze the labeled VSG (Fig. 3.4E).

3.3.5 Ca^{2+} binding motif mutation: effect on activity

The Ca^{2+} sensitivity of the recombinant *Tb*PI-PLC enzyme was surprisingly low when compared to the Ca^{2+} sensitivity of other PI-PLCs zeta type. For example the *Tc*PI-PLC has a peak of activity at approximately 10 μM (12) and PLCζ has a peak at approximately 1 μM (22). We also observed that the *Tb*PI-PLC enzyme showed lower activity (V_{max} 34.4 nmol min^{-1} mg^{-1}) when compared to other PLC enzymes such as *Tc*PI-PLC with a V_{max} of 0.93 μmol $min^{-1}mg^{-1}$ (12). EF hand motifs are the best-known Ca^{2+} binding motifs and are helix-turn-helix structural

domains that bind Ca^{2+} (23, 24, 25, 26). Twelve residues of the EF-hand structure typically form a pattern, Dx[DN]xDGx[ILV][DSTN]xxE, that is involved in the binding of the calcium ion (27). The binding of Ca^{2+} can have an effect on structural stability and can regulate activity (27). We compared the binding loop of *Tb*PI-PLC with binding loops of *Tc*PI-PLC (AF093565), and human PLCζ (NP_149114) (Fig 3.12). *Tb*PI-PLC has a negatively charged aspartic acid in the second residue position, creating a series of three negatively charged aspartates, which has not been observed in other loops. We hypothesized that changing this amino acid to alanine, as found in the *Tc*PI-PLC calcium-binding loop, would alter activity and Ca^{2+} sensitivity. Site-directed mutagenesis was used to change the aspartate in the 109th position (corresponding to the second residue in the binding loop) to alanine. The mutated protein was expressed and purified under the same conditions used for the *Tb*PI-PLC and assayed for the release of [^{3}H] IP_3 from [^{3}H] PIP_2. Interestingly, the enzyme exhibited an increase in activity with PIP_2 as substrate (Fig. 3.5A) and a substantial decrease of activity toward PI (Fig. 3.5B). However, no alteration of Ca^{2+} sensitivity was observed. This suggested that the binding of Ca^{2+} to the Ca^{2+} binding loop modulates the activity of the enzyme.

3.3.6 RNAi knockdown and effect on in vitro growth

Knockdown of *Tb*PI-PLC expression by inducible double-stranded RNA was performed in both procyclic and bloodstream form. Northern blot showed that the mRNA was down regulated after 2 days of induction by tetracycline for procyclics (Fig. 3.6A) compared to 29-23 (WT) and for bloodstream forms (Fig 3.6B) compared to single marker (WT). Procyclic form trypanosomes at a density of 1×10^6 cells were induced with 1 μg/ml of tetracycline and diluted every 2 days (Fig. 3.6C). Bloodstream form trypanosomes at a density of 1×10^4 were induced with 1 μg/ml of tetracycline and diluted daily (Fig. 3.6D). No in vitro growth defects were

observed for either procyclics or bloodstream form trypanosomes, suggesting that RNAi was not efficient in down-regulating *TbPI-PLC* protein levels. In addition, we used the RNAi cells to see if parasites were able to grow in a challenging environment by infecting mice. The parasites were able to grow normally and establish an infection (Fig. 3.13).

3.3.7 Functional role of TbPI-PLC in parasites

The classical diacylglycerol/IP_3 pathway includes the action of a phospholipase C that hydrolyzes PIP_2 to produce diacylglycerol (DAG) and IP_3. Recently, the presence of a functional $TbIP_3$ receptor and further evidence of a functional diacylglycerol/IP_3 pathway has been established (6). In this work, IP_3 released Ca^{2+} from acidocalcisomes of permeabilized *T. brucei* parasites and caused an increase of intracellular Ca^{2+} in live trypanosomes. In addition, knockdown of the *Tb*IP_3 gene caused defects in parasite growth and reduced the ability of the parasites to establish an infection (6). It was vital in our work to show that *Tb*PI-PLC can hydrolyze PIP_2 and can provide the second messenger that is used in this pathway. We prepared lysates of both procyclic and bloodstream form cells to be used as the enzyme source in the in vitro assay for hydrolysis of PIP_2. The lysates were tested at different Ca^{2+} concentrations and at different temperatures (30 and 37 °C). Activity was detected in both lysates, but more prominent in procyclic forms (Fig. 3.7A). A peak of activity was observed at 100 nM. This calcium concentration is in the range of the estimated intracellular Ca^{2+} concentration of procyclic forms (28). In bloodstream forms, activity appears to be very low. The low activity in bloodstream form and higher activity in procyclic forms is in agreement with previous data showing the presence of higher amounts of IP_3 in procyclics, and very low amounts in bloodstream form (28). To establish that our genetic manipulations were targeting the *Tb*PI-PLC enzyme, we prepared parasite lysates from cells overexpressing or down-regulating the expression of the enzyme for

activity analysis. The procyclic parental line (29-13), uninduced overexpressing parasites, and uninduced RNAi transgenic parasites demonstrated similar activities. However, induction of overexpression resulted in two-fold higher activity and induction of RNAi significantly reduced the amount of hydrolysis of PIP_2 (Fig. 3.7B). Collectively, this data shows that *Tb*PI-PLC enzyme activity was altered by our manipulations, is active in parasites, and can hydrolyze PIP_2 to produce the second messenger, IP_3.

3.3.8 Toxicity of *Tb*PI-PLC overexpression

To investigate whether overexpression of *Tb*PI-PLC-GFP affected cell viability we measured the propidium iodide permeability of procyclic forms after induction with tetracycline. We confirmed overexpression of the PI-PLC by testing for an increase in PIP_2 hydrolysis and observed a doubling of enzyme activity in the induced overexpression cells. Cells were incubated with and without tetracycline for 24 h and their permeability to propidium iodide was compared by FACS analysis. We observed a significant increase in propidium iodide cell labeling after tetracycline induction of *Tb*PI-PLC-GFP overexpression (Fig. 3.8D) as compared to that of 29-13 parental cell line (Fig. 3.8A) not labeled with PI, parental line labeled with PI (Fig. 3.8B), or labeled uninduced cells (Fig. 3.8C). The amount of dead cells increased from 0.35% in control 29-13 cells to 3.29% in the *Tb*PI-PLC-GFP overexpressing cells. Some increase was also observed in uninduced *Tb*PI-PLC-GFP cells (Fig. 3.8C) but was expected because of low level of expression of the construct in cells not incubated with tetracycline. The parental line had an average of 0.31 ± 0.07 of dead cells and the overexpressing had an average of 3.22 ± 0.08 from three independent experiments. To demonstrate that overexpression of *Tb*PI-PLC could make cells more susceptible to apoptosis, cells ± tetracycline were incubated with 100 µM of H_2O_2 and analyzed for an increase in dead cells. PI-PLC overexpression significantly increased the

amount of dead cells from 2.29% (Fig. 3.9C) to 3.31% (Fig. 3.9D) with H_2O_2 treatment. Figure 3.9 is a representative of two independent experiments. Treatment of parental line (Fig 3.9A & B) shows no effect from treatment of H_2O_2.

3.4 Discussion

Our laboratory has described the presence of a functional inositol phosphate/diacylglycerol pathway in *T. brucei* (6, 28). However, the enzyme that generates the second messengers in this pathway in *T. brucei* has not been explored until now. In this work, we demonstrated that the gene product is similar to the mammalian sperm-specific PLCζ, but contains a myristoylation consensus sequence not found in the mammalian PLC. The myristoylation consensus sequence was shown to play a role in targeting to the plasma membrane and was shown to be metabolically labeled by myristate and palmitate. The endogenous enzyme localizes to intracellular vesicles and may represent an alternate localization pathway under certain conditions, such as the lack of fatty acid modification. The enzyme is active at low concentrations of Ca^{2+} and site-directed mutagenesis suggests that Ca^{2+} binding in the EF-hand domain may modulate its activity. The enzyme prefers PIP_2 and is more efficient in hydrolyzing PIP_2 as substrate. Knockdown of the *Tb*PI-PLC mRNA by inducible double-stranded RNA did not cause any effects on growth. However, we demonstrated that the enzyme is functional, more detectable in the procyclic than bloodstream forms. In addition, overexpression of an active form of the enzyme appears to be lethal by overstimulation of the IP_3/DAG pathway.

The *Tb*PI-PLC gene product of 714 amino acids has a domain organization that is most similar the sperm-specific mammalian PLCζ, with the exception of an N-myristoylation sequence (1-18 amino acids) similar to the sequence previously described in *Trypanosoma cruzi* (7). Mammalian PLCζ and *Tb*PI-PLC lack the pleckstrin homology (PH) domain that is essential

for localization of mammalian PLC δ (20) to the plasma membrane. The importance of the absence of PH domains and the presence of a NLS and myristoylation sequence in PLC ζ and trypanosome PI-PLCs, respectively, is unknown. It is possible that the lack of the PH domain allows for other localizations rather than exclusively to the plasma membrane. In the case of the myristoylation sequence, the presence of fatty acid modifications would determine if the enzyme localizes to the plasma membrane. However, this work demonstrates the requirement for these acylation events for localization to the plasma membrane. Our observations of endogenous localization may provide insight as to why an alternative localization is needed. Immunofluorescence assays highlighted endogenous localization to intracellular vesicles rather than to the plasma membrane as expected from the N-terminal overexpression data. Intracellular localization of a phospholipase C has recently been described for the sperm-specific PLC ζ (20). PLC ζ was shown to localize to internal vesicles when injected in mouse eggs. PIP_2 also localized to vesicles with the same pattern as the PLC ζ demonstrating that the enzyme is utilizing an intracellular source of PIP_2 rather than at the plasma membrane (20). Assays measuring the changes in plasma membrane PIP_2, and the effects of PIP_2 depletion in the plasma membrane and in the intracellular vesicles showed that neither PLC ζ nor sperm hydrolyzed any measurable amount of plasma membrane PIP_2. Instead, the enzyme hydrolyzed an intracellular membrane source of substrate (20). We used immunofluorescence with anti-PIP_2 to study PIP_2 distribution in the parasite and observed localization to intracellular vesicles with a similar pattern as the *Tb*PI-PLC. This suggests the *T. brucei* enzyme may use an intracellular source of substrate. The amount of PIP_2 in the plasma membrane is approximately 1% of the total phospholipid content of cells (29). It could be that the needed *Tb*PI-PLC activity of the cells requires targeting the cells to areas of higher concentrations of substrate. The possibility also

exists of specific *T. brucei* palmitoyl acyltransferases (PAT) in the localization of enzymes. Twelve PATs have been identified, but TbPAT7 only was identified as necessary for proper localization of calflagins to the flagellar membrane (30). It is possible that a currently unidentified PAT may be responsible for localization to the intracellular vesicles rather than to the plasma membrane. Also, we cannot rule out the possibility that the enzyme may localize to the plasma membrane in bloodstream form parasites. Differences in localization in different forms of the parasite have also been demonstrated for the *T. cruzi* PI-PLC (12). Our attempts to tag one of the chromosomal copies in bloodstream form were unsuccessful. The expression profile from the TriTrypDB shows a 2-fold down regulation of expression in bloodstream form. Our hypothesis is that *Tb*PI-PLC expression is under the control of the 3' UTR (31). Our attempts to integrate the HA tag-hygromycin resistance cassette into the *Tb*PI-PLC gene may have resulted in the down regulation of the *Tb*PI-PLC expression as well as the expression of the hygromycin gene causing the parasites to be susceptible to hygromycin. Similar results were demonstrated with the 3' UTR of GPI-PLC. GPI-PLC is expressed only in bloodstream form cells. In this study, a G418 resistance gene under the control of the 3' UTR of GPI-PLC was expressed in bloodstream form cells. When the bloodstream form cells were differentiated into procyclics, there parasites became sensitive to G418 demonstrating that the 3' UTR plays a role in regulation (32). Collectively, the data from N-terminal overexpression and endogenous localization highlighted interesting differences in localization in which the precise mechanism for translocation is unclear. Until the localization of PLC ζ to intracellular vesicles was demonstrated (20), the only known localization of PLCζ was in the pronuclei of activated mouse eggs (33, 34, 35). This localization appeared to correlate with a loss of PLCζ function (20). PLC ζ has a putative nuclear localization sequence (NLS) (9), but the timing and the mechanism of

the how this sequence functions in localization is unknown. Recently, the N-myristoylated *Tb*ARL6 demonstrated localization to vesicles throughout the parasite body and was identified as a potential binding partner of tubulin (36). A G2A mutant of *Tb*ARL6 showed a localization to subpellicular microtubules at the plasma membrane (36). The hypothesis is that the myristoylation sequence could act like a 'switch' with accumulation at regions of high binding partner (tubulin) concentration unless myristoylated which would then allow for vesicular localization (36). *Tb*PI-PLC may be targeted to vesicles with a higher concentration of PIP_2, but when certain interactions occur, such as fatty acid attachment, the enzyme could be localized to the plasma membrane. The mechanism surrounding the switch of one localization to another is unknown. Localization of the previously described PLC ζ may also require a specific combination of interactions for binding to intracellular membranes and in the absence of these interactions, pronuclei localization occurs (20).

Enzymatic activity was assayed at differing calcium concentrations and activity was sensitive to these differences demonstrating that the gene product was indeed a phospholipase C. We observed peaks of activity at 10 nM of calcium with PIP_2 as the substrate and 100 nM with PI as the substrate. Both values are in range of the estimated calcium concentration for both procyclic (90-100 nM) and bloodstream forms (20-30 nM) (28). These findings suggest that the enzyme is constitutively active. In DT40 B lymphocytes, IP_3R mediated calcium release was required to maintain a basal low-level of calcium. The mitochondrial uptake of this released calcium is required for enough NADH production to support oxidative phosphorylation (37). Bloodstream form energy metabolism is based on glycolysis whereas procyclics have a functional mitochondrion and electron transport chain (38). RNAi knockdown of key enzymes demonstrated that substrate level phosphorylation is required for growth of procyclic form cells

(38). Our data suggests that the *Tb*PI-PLC could be constitutively active and could play a role in the bioenergetics of procyclics through the generation of IP_3.

Previous work has shown that *T. cruzi* glycosylinositol phospholipid anchored glycoproteins anchors can possess either a glycerolipid or ceramide (39). *Tc*PI-PLC was shown to hydrolyze inositolphosphoceramides during differentiation from trypomastigotes to amastigotes (39). We tested *Tb*PI-PLC to see if it had the ability to hydrolyze GPI anchored proteins, but observed that the enzyme does not hydrolyze GPI-anchored proteins as is the case with some PLCs (20), but prefers PIP_2 as substrate highlighted by a lower K_m and higher efficiency with PIP_2.

We observed a high sensitivity to low amounts of calcium by the recombinant, but much lower activity when compared to previously described PLCs, such as *Tc*PI-LC (12). The twelve residues of the calcium binding loop, with a pattern of Dx[DN]xDGx[ILV][DSTN]xxE, have been shown to regulate calcium sensitivity or activity, or both (40). The *Tb*PI-PLC loop has an aspartate in the second position of the loop that is not been observed in other loops. Site-directed mutagenesis of this aspartate to alanine increased activity with respect to PIP_2 and decreased activity with respect to PI as substrate suggesting the enzyme is regulated by calcium. In addition, this demonstrates that the EF-hand domain is responsible for the enzyme sensitivity to calcium instead of the C2 domain.

Using an inducible double-stranded RNA system, *Tb*PI-PLC expression was knocked down after two days of induction with tetracycline for procyclics and bloodstream forms and confirmed by northern blot. Transcript level was also assayed for parental lines, 29-13 for procyclics and single marker for bloodstream forms. Growth curve analysis was performed for each transfectant and parental cells, but no growth defect was observed. This supports findings

that no fitness loss was associated with *Tb*PI-PLC knockdown (41). Knockdown in both forms we tested was not complete and it is possible that sufficient protein was expressed to carry out its function. It is also possible that another enzyme could compensate for the reduction in function of the *Tb*PI-PLC. In addition, knockdown in bloodstream form showed no defects in the establishment of acute infection (data not shown). Our attempts to generate a knockout of both alleles were lethal to cells. In addition, our attempts to create a conditional knock out by expressing an ectopic copy before knocking out the second copy caused the cells to stop growing and slowly die. Collectively, these results suggest that the enzyme may be essential.

We prepared lysates of procyclics, bloodstream form, overexpressing (non-induced and induced), and RNAi cells (non-induced and induced to investigate the activity of the enzyme in the parasites. Activity was detected in both procyclics and bloodstream, but was more detectable in procyclics supporting previous data that detected higher amounts of IP_3 in procyclics (28). We also established that our manipulations of expression resulted in the expected effects in PLC activity. When overexpression was induced, we detected more than twice the activity and when we induced RNAi, we observed a reduction in activity. This demonstrates that the enzyme is active in parasites and can hydrolyze PIP_2 generating the second messenger, IP_3, of the IP_3/DAG signaling pathway.

Understanding the contribution of the *Tb*PI-PLC enzyme to the IP_3/DAG pathway is important as this pathway is known to be involved in various cellular processes (2) and could explain why attempts to overexpress the full length enzyme in procyclics and bloodstream form were unsuccessful. Overexpression was particularly lethal in bloodstream where there is also a two-fold down regulation of PI-PLC expression. We could only overexpress the truncated form, *Tb*PI-PLC $_{(19\text{-}714)}$, in procyclics. It is unclear as to why the inclusion of the myristoylation

sequence could not be overexpressed in procyclics. We hypothesize that the cumulative effect of the lethality of overexpression and an increase of myristate consumption was detrimental to the cells (42). To examine the effects of overexpression of the *T. brucei* PI-PLC, we used flow cytometry to analyze dead cells labeled by propidium iodide. We observed an increase of dead cells from overexpression of the truncated form (shown to be enzymatically active) compared to the parental cells and controls. Overstimulation of the IP_3/DAG pathway could cause an increase of intracellular calcium leading to an increase of mitochondrial calcium. This overload of calcium has been shown to increase superoxide radicals and trigger programmed cell death in *T. cruzi* (43). This could also explain why the aspartate in the calcium binding loop in the EF-hand may regulate activity of the enzyme. The enzyme is sensitive to low amounts of calcium and may be constitutively active. However, this could be harmful to the cells unless the activity is reduced and this may have been accomplished by this one amino acid difference.

Calcium signaling in *T. brucei* has been implicated in bloodstream form surface coat release (44) and in differentiation from bloodstream form to procyclic (45). Recently, it has been described that *Tb*IP_3R-mediated calcium signaling plays a role in cell growth and infectivity (6). However, much is still unknown about the role of calcium in this parasite. Our recombinant work illustrates that this enzyme can hydrolyze PIP_2 and provide the IP_3 involved in intracellular calcium release mediated through the IP_3 receptor. In addition, this work shows the enzyme is functional in the parasites, describes the regulatory role of calcium for *T.brucei* PI-PLC activity through the EF-hand domain, and illustrates how this enzyme could play a role in vital parasite processes through the IP_3/DAG pathway.

References

1. **Brun R, Blum J, Chappius F, Burri C.** 2010. Human African Trypanosomiasis. Lancet **375**: 148-159.
2. **Berridge M.J.** 2009. Inositol trisphosphate and calcium signaling mechanisms. Biochim Biophys Acta. **1793**: 933-940.
3. **Rhee S.** 2001. Regulation of Phosphoinositide-specific phospholipase C. Annu. Rev. Biochem. **70**: 281-312.
4. **Miyakawa T, Mizushima A, Hirose K, Yamazawa T, Bezprozvanny I, Kuroaski T, Iino, M.** 2001. Ca^{2+}-sensor region of IP_3 receptor controls intracellular Ca^{2+} signaling. EMBO J. **20**: 1674-1680**.**
5. **Docampo R, Scott DA, Vercesi AE, Moreno SN.** 1995. Intracellular Ca^{2+} storage in acidocalcisomes of *Trypanosoma cruzi.* Biochem. J. **310**: 1005-1012.
6. **Huang G, Bartlett J, Thomas A, Moreno SNJ, Docampo, R.** 2013 **Acidocalcisomes** of *Trypanosoma brucei* have an inositol 1, 4, 5-trisphosphate receptor that is required for growth and infectivity. Proc. Natl. Acad. Sci. **110**: 1887-92.
7. **de paulo Martin V, Okura M, Maric D, Engman D, Vieira M, Docampo R, Moreno SNJ.** 2010 Aclyation-dependent export of *Trypanosoma cruzi* Phosphoinositide-specific phospholipase C to the outer surface of amastigotes. J. Biol. Chem **285**: 30906-30917.
8. **Saunders CM, Larman MG, Parrington J, Cox LJ, Royse J, Blayney LM, Swann K, Lai FA.** 2002. PLCζ: a sperm-specific trigger of Ca^{2+} oscillations in eggs and embryo development. Development. **129**: 3533-3544.

9. **Swann K, Saunders CM, Rogers NT, Lai, FA.** 2006. PLCζ: A sperm protein that triggers Ca^{2+} oscillations and egg activation in mammals. Semin. Cell Dev. Biol. **17**: 264-273.

10. **Ochatt CM, Bütikofer P, Navarro M, Wirtz E, Boschung M, Armah D, Cross GA.** 1999. Conditional expression of glycosylphophatidylinositol phospholipase C in *Trypanosoma brucei.* Mol Biochem Parasitol. **103**: 35-48.

11. **Bangs JD, Uyetake L, Brickman MJ, Balber AE, Boothroyd, JC.** 1993. Molecular cloning and cellular localization of a BiP homologue in *Trypanosoma brucei.* J. Cell Sci. 105: 1101-1113.

12. **Furuya T, Kashuba C, Docampo, R, Moreno SNJ.** 2000. A novel phosphatidylinositol-phospholipase C of *Trypanosoma cruzi* that is lipid modified and activated during trypomastigote to amastigote differentiation. J. Biol. Chem. **275**: 6428-6438.

13. **Oberholzer M, Morand S, Kunz S, Seebeck T.** 2006. A vector series for rapid PCR-mediated C-terminal in situ tagging of *Trypanosoma brucei* genes. Mol. Biochem. Parasitol. **145**: 117-120

14. **Mensa-Wilmot K, Morris JC, al-Qahtani A, Englund PT.** 1995. Purification and use of glycosylphophatidylinositol phospholipase C. Method Enzymol. **250**: 641-55.

15. **Kretsinger RH, Nockold CE.** 1973. Carp muscle calcium-binding protein II. Structure determination and general description. J. Biol. Chem. **248**: 3313-26.

16. **Moncrief ND, Kretsinger RH, Goodman M.** 1990 Evolution of EF-hand calcium modulated proteins. I. Relationship based on amino acid sequence. J. Mol. Evol. **30**: 522-562.

17. Lermercier G, Espiau B, Ruiz FA, Vieira M, Luo S, Baltz T, Docampo R, Bakalara N. 2004. A pyrophosphatase regulates polyphosphate metabolism in acidocalcisomes is essential for *Trypanosoma brucei* virulence in mice. J. Biol. Chem. **279**: 3420-3425.

18. Bangs JD, Uyetake L, Brickman MJ, Balber AE, Boothroyd JC. 1993. Molecular cloningand cellular localization of a BiP homologue in *Trypanosoma brucei.* Divergent ER retention signals in a lower eukaryote. J. Cell Sci. **105**: 1101-1113.

19. Bringaud F, Baltz D, Baltz T. 1998. Function and molecular characterization of a glycosomal PPi-dependent enzyme in trypanosomatids, pyruvate, phosphate dikinase. Proc. Natl. Acad. Sci. **95**: 7963-68

20. Yu Y, Nomikos M, Theodoridou M, Nounesis G, Lai FA. 2011. PLCζ causes Ca^{2+} oscillations in mouse eggs by targeting intracellular and not plasma membrane $PI(4,5)P_2$. Mol. Biol. Cell. **23**: 371-380.

21. Klöppel C, Müller A, Marker S, Simon M. 2009. Two isoforms of eukaryotic phospholipase C in *Paramecium* affecting transport and release of GPI-anchored proteins in vivo. Eur. J .Cell Biol. **88**: 577-592.

22. Kouchi Z, Fukami K, Shikano T, Oda S, Nakamura Y, Takenawa T, Miyazaki S. 2004. Recombinant phospholipase C ζ has high Ca^{2+} sensitivity and induces Ca^{2+} oscillations in mouse eggs. J. Biol. Chem. **279**: 10408-10412.

23. Gifford JL, Walsh MP, Vogel HJ. 2007. Structure and metal-ion-binding properties of the Ca^{2+}-binding helix-loop-helix EF-hand motifs. Biochem J. **405**: 199-221.

24. Grabarek, Z. 2006. Structural basis for diversity of the EF-hand calcium binding proteins. J. Mol. Biol. **359**: 509-25.

25. Kretsinger, RH. 1976. Evolution and function of calcium-binding proteins. Int. Rev. Cytol. **46**: 323-93.

26. Stynadka NC, James MN. 1989. Crystal structure of the helix-loop-helix calcium binding proteins. Annu. Rev. Biochem. **58**: 951-98.

27. Rigden DJ, Woodhead DD, Wong PWH, Galperin MY. 2011. New structural and functional contexts of the Dx[DN]xDG motif: insights into evolution of calcium-binding proteins. PLoS One. **6:** e21507.

28. Moreno SN, Vercesi AE, Pignataro OP, Docampo R. 1992. Calcium homeostasis in *Trypanosoma cruzi* amastigotes: presence of inositol phosphates and lack of an inositol 1, 4, 5-trisphosphate-sensitive calcium pool. Mol. Biochem. Parasitol. **52:** 251-61.

29. Nomikos M, Mulgrew-Nesbitt A, Pallavi P, Mihalyne G, Zaitseva I, Swann K, Lai FA, Murray D, McLaughlin S. 20017. Binding of phosphoinositide-specific phospholipase C-ζ (PLC-ζ) to phospholipid membranes. J. Biol. Chem. **282**: 16644-16653.

30. Emmer BT, Souther C, Toreillo KM, Olson CL, Epting CL, Engman DM. 2006. Identification of a palmitoyl acyltransferase required for protein sorting to the flagellar membrane. J Cell Sci. **122**: 867-74.

31. Clayton C, Shapira M. 2007. Post-transcriptional regulation of gene expression in trypanosomes and leishmanias. Mol. Biochem. Parasitol. **156**: 93-101.

32. Webb H, Burns R, Ellis L, Kimblin N, Carrington, M. 2005. Developmentally regulated instability of the GPI-PLC mRNA is dependent on a short-lived protein factor. Nucl Acids Res. **33:** 1503-1512.

33. Yoda A, Oda S, Shikano T, Kouchi Z, Awaji T, Shirakawa H. 2004. Ca^{2+} oscillation-inducing phospholipase C zeta expressed in mouse eggs is accumulated to the pronucleus during egg activation. Dev. Biol. **268**: 245-57.

34. Larman MG, Saunders CM, Carroll J, Lai FA, Swann K. 2004. Cell cycle-dependent Ca^{2+} oscillations in mouse embryos are regulated by nuclear targeting of PLCζ. J. Cell Sci. **117**: 2513-2521.

35. Sone Y, Ito M, Shirakawa H, Shikano T, Takeuchi H, Kinoshita, K. 2005. Nuclear translocation of phospholipase C-zeta, an egg activating factor, during early embryonic development. Biochem. Biophys. Res. Commun. **330**: 690-4.

36. Price HP, Hodgkinson MR, Wright MH, Tate EW, Smith BA, Carrington M, Stark M, Smith, DF. 2012. A role for the vesicle-associated tubulin binding protein ARL6 (BBS3) in flagellum extension in *Trypansoma brucei*. Biochim. Biophys. Acta. **1823**: 1178-1191.

37. Cárdenas C, Miller RA, Smith I, Bui T, Molgó J, Müller M, Vais H, Cheung K, Yang J, Parker I, Thompson C, Birnbaum M, Hallows KR, Foskett JK. 2010. Essential regulation of cell bioenergetics by constitutive IP_3 receptor Ca^{2+} transfer to mitochondria.

38. Bochud-Alleman N, Schneider A. 2002. Mitochondrial substrate level phosphorylation is essential for growth of procyclic *Trypanosoma brucei.* J. Biol. Chem. **277:** 32849-32854.

39. Salto ML, Bertello LE, Vieira M, Docampo R, Moreno SN, de Lederkremer RM. 2003. Formation and remodeling of inositolphosphoceramide during differentiation of *Trypanosoma cruzi* from trypomastigote to amastigote. Eukaryot Cell. **2:** 756-768.

40. Drayer L, Meima ME, Derks MWM, Tuik R, van Haastert PJM. 1995. Mutation of an EF-hand Ca^{2+} binding motif in phospholipase C of *Dictyostelium discoideum:* inhibition of activity but no effect on Ca^{2+}-dependence. Biochem. J. **311**: 505-510.

41. Alsford S, Turner DJ, Obado SO, Sanchez-Flores, A, Glover L, Berriman M, Hertz-Fowler C, Horn D. 2011. High-throughput phenotyping using parallel sequencing of RNA interference targets in the African trypanosome. Genome Res. **21:** 915-924.

42. Price HP, Güther M, Ferguson M, Smith DF. 2010. Mristoyl-CoA: protein *N*-myristoyltransferase depletion in trypanosomes causes avirulence and endocytic effects. Mol. Biochem. Parasitol. **169:** 55-58.

43. Irigoín F, Inada NM, Fernandes MP, Piacenza L, Gadelha FR, Vercesi, AE, Radi, R. 2009. Mitochondrial calcium overload trigger complement-dependent superoxide-mediated programmed cell death in *Trypanosoma cruzi.* Biochem. J. **418:** 595-604.

44. Bowles DJ, Voorheis HP. 1982. Release of the surface coat from the plasma membrane of intact bloodstream forms of *Trypanosoma brucei* requires Ca^{2+}. FEBS Lett. **139:** 17-21.

45. Stojdl DF, Clarke MW. 1996. *Trypanosoma brucei*: Analysis of cytoplasmic Ca^{2+} during differentiation of bloodstream stages in vitro. Exp. Parasitol. **83:** 134-146.

Table 3.1 Enzymatic kinetics comparison

Comparison of *Tb*PI-PLC substrate hydrolysis activities with both substrates demonstrating the enzyme prefers PIP_2 as a substrate and has a higher efficiency in the hydrolysis of PIP_2.

substrate	K_m (μM)	V_{max} (nmol min^{-1} mg^{-1})	K_{cat} (min^{-1})	k_{cat}/K_m (M^{-1} min^{-1})
PIP_2	4.1 ± 0.7	34.4 ± 1.0	0.27 ± 0.008	6.6×10^4
PI	22.6 ± 4.6	13.5 ± 0.8	0.11 ± 0.007	1.2×10^4

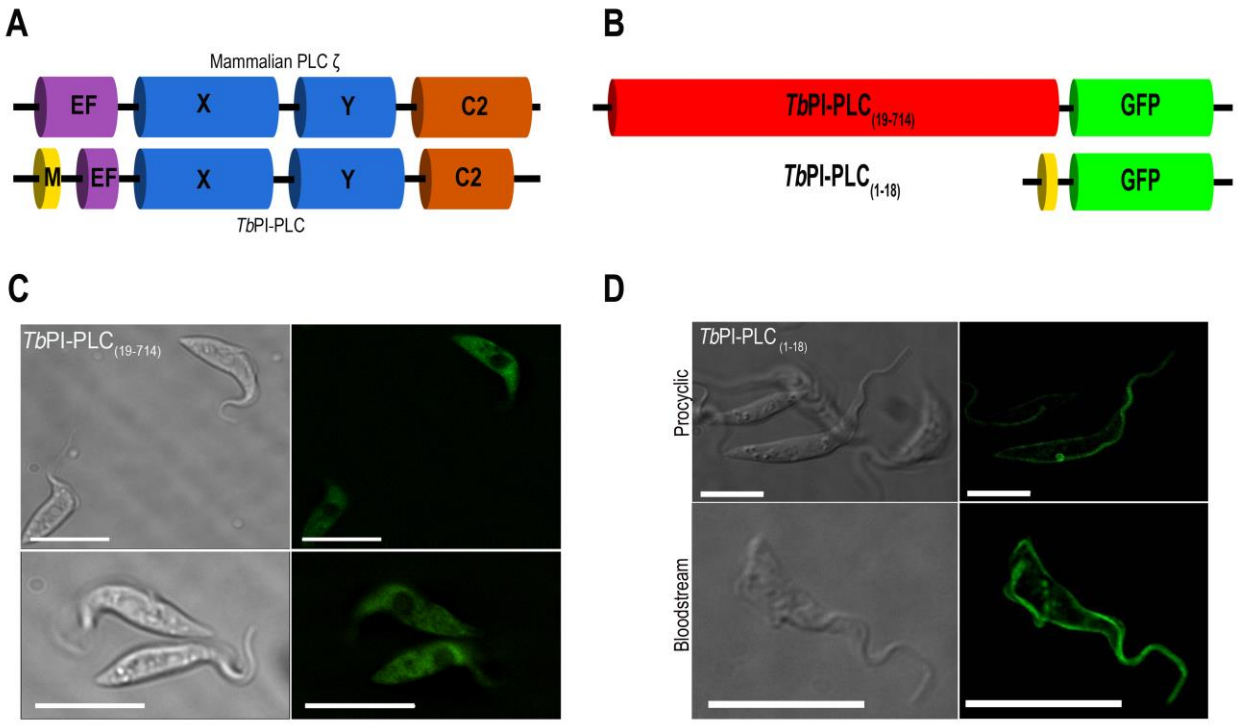

Figure 3.1: Role of myristoylation sequence

(A) Overall domain organization of *Tb*PI-PLC and mammalian PLC ζ. (B) Constructs overexpressing the first eighteen amino acids, *Tb*PI-PLC $_{(1-18)}$ or a truncated form, *Tb*PI-PLC $_{(19-714)}$. (C) Cells expressing the truncated for *Tb*PI-PLC $_{(19-714)}$ localizes to the cytosol. (D) In contrast, *Tb*PI-PLC $_{(1-18)}$ localizes to the plasma membrane and flagellum.

Figure 3.2: Role of identified amino acids for potential acylation

(A) Site-directed mutagenesis was used to mutate glycine-2 (G2A), cysteine (C4A), and a double mutant (G2C4A). (B) Direct fluorescence demonstrated all mutations ablated plasma membrane and flagellum localization in the bloodstream form. (C) To study effect on lipid modification, mutants were labeled with [^{3}H]-myristate and [^{3}H]-palmitate and immunoprecipitated with anti-GFP. G2A disrupted both labeling events while C4A ablated palmitate labeling only. No labeling was observed with G2C4A or GFP alone (control).

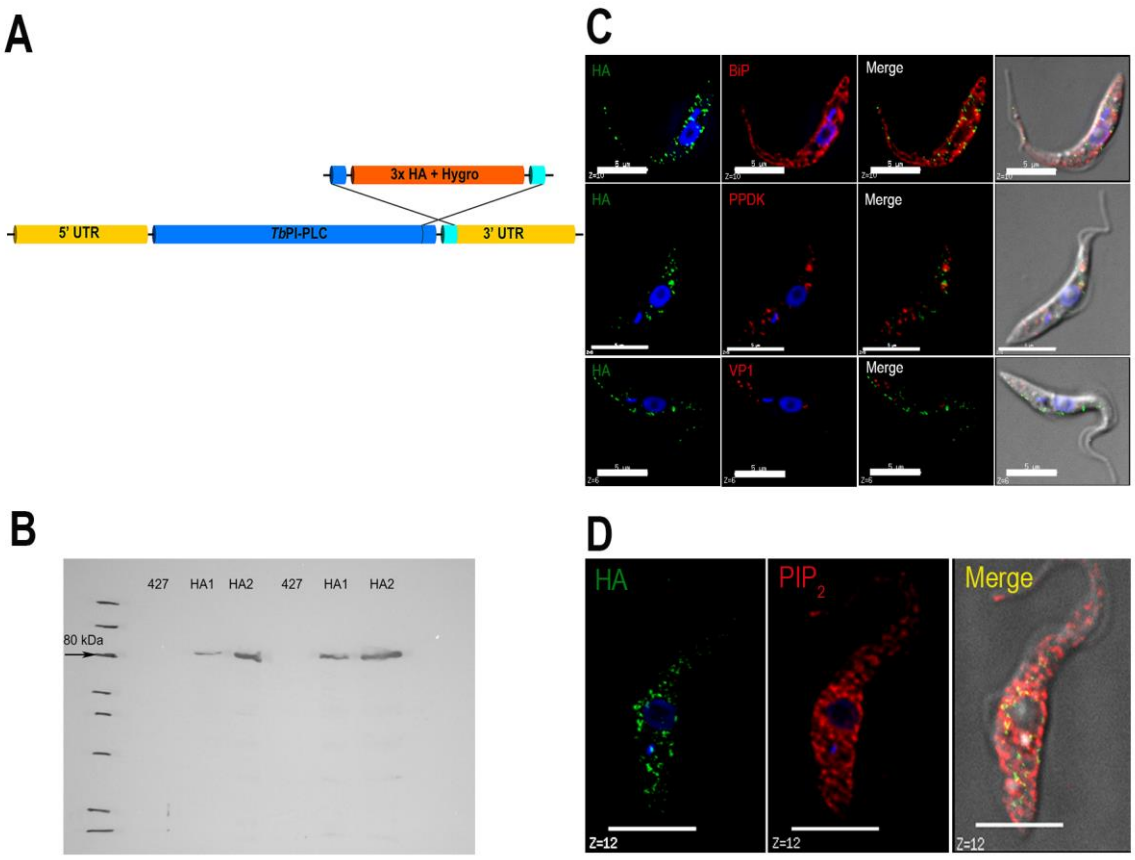

Figure 3.3: Endogenous localization

(A) In situ tagging was used to incorporate a tagging cassette into one of the chromosomal copies of the *Tb*PI-PLC gene. (B) Western blot confirmed the tagging of the enzyme in two different transfectants (HA1 and HA2) at the expected size of 80 kDa. (C) Immunofluorescence with anti-HA demonstrated vesicle localization. No co-localization with the ER, glycosomes, or acidocalcisomes was observed. (D) Intracellular localization of PIP_2 with similar distribution pattern as the *Tb*PI-PLC.

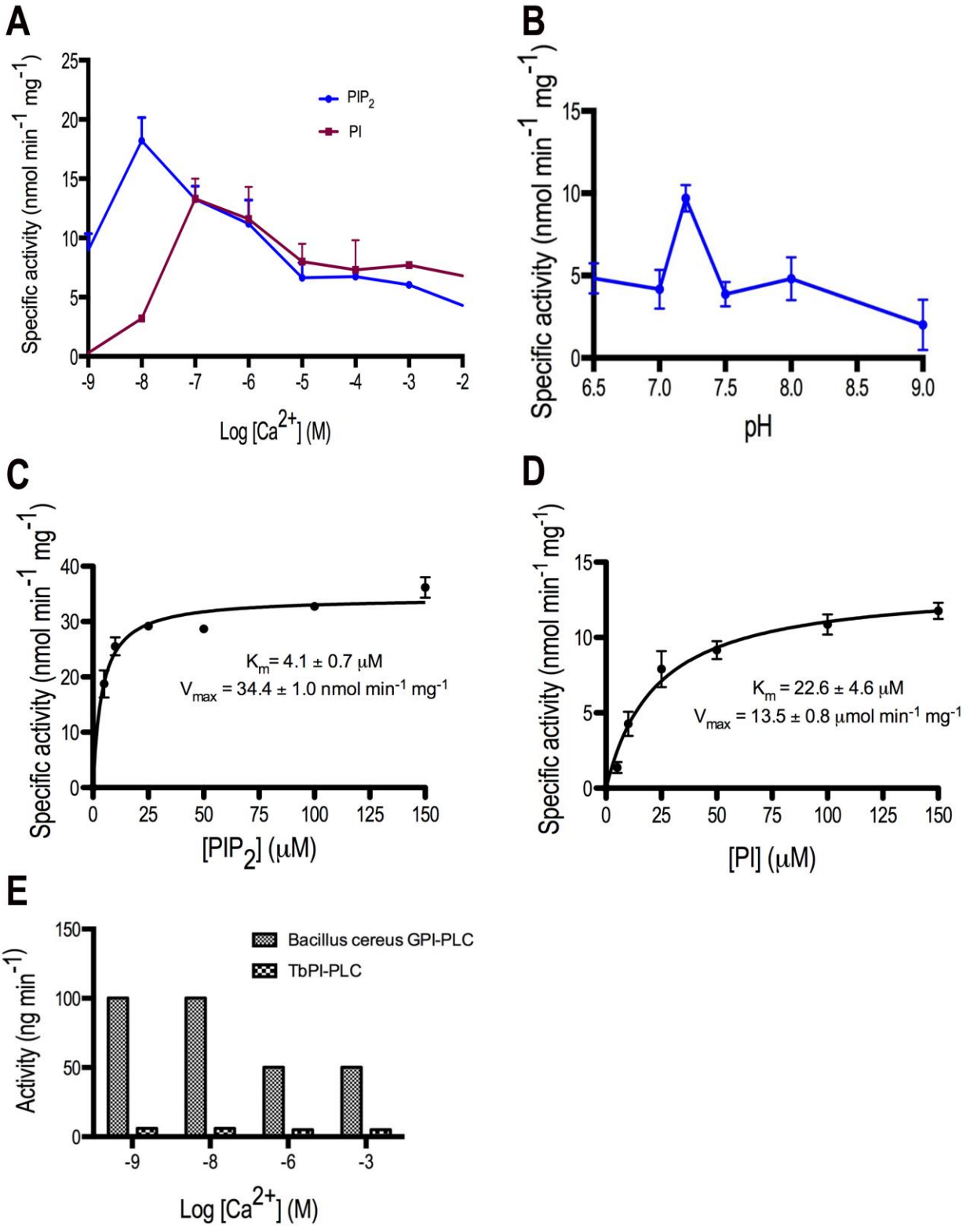
A
Specific activity (nmol min-1 mg-1)
PIP2
PI
Log [Ca2+] (M)
B
Specific activity (nmol min-1 mg-1)
pH
C
Specific activity (nmol min-1 mg-1)
Km= 4.1 ± 0.7 μM
Vmax = 34.4 ± 1.0 nmol min-1 mg-1
[PIP2] (μM)
D
Specific activity (nmol min-1 mg-1)
Km = 22.6 ± 4.6 μM
Vmax = 13.5 ± 0.8 μmol min-1 mg-1
[PI] (μM)
E
Activity (ng min-1)
Bacillus cereus GPI-PLC
TbPI-PLC
Log [Ca2+] (M)

Figure 3.4: Enzymatic activity

(A) Enzymatic activity was assayed by the release of [^{3}H]-IP_3 from the hydrolysis of [^{3}H]-PIP_2 or PI. The activity was stimulated by calcium with peaks of activity between 10-100 nM for PIP_2 and PI, respectively. (B) A peak of activity was observed at a pH of 7.2. Activity was assayed with respect to substrate concentration demonstrating a preference for PIP_2 (C) as substrate compared to PI (D). Since some PLCs can hydrolyze GPI-anchored proteins, parasites were incubated with radiolabeled myristate to allow for incorporation into VSG. (E) Assay for hydrolysis of GPI-anchored proteins was conducted as described. The *Tb*PI-PLC did not hydrolyze the VSG whereas the *Bacillus cereus* (control) hydrolyzed the purified labeled VSG (n=2). All other values are mean ± SE (n=3).

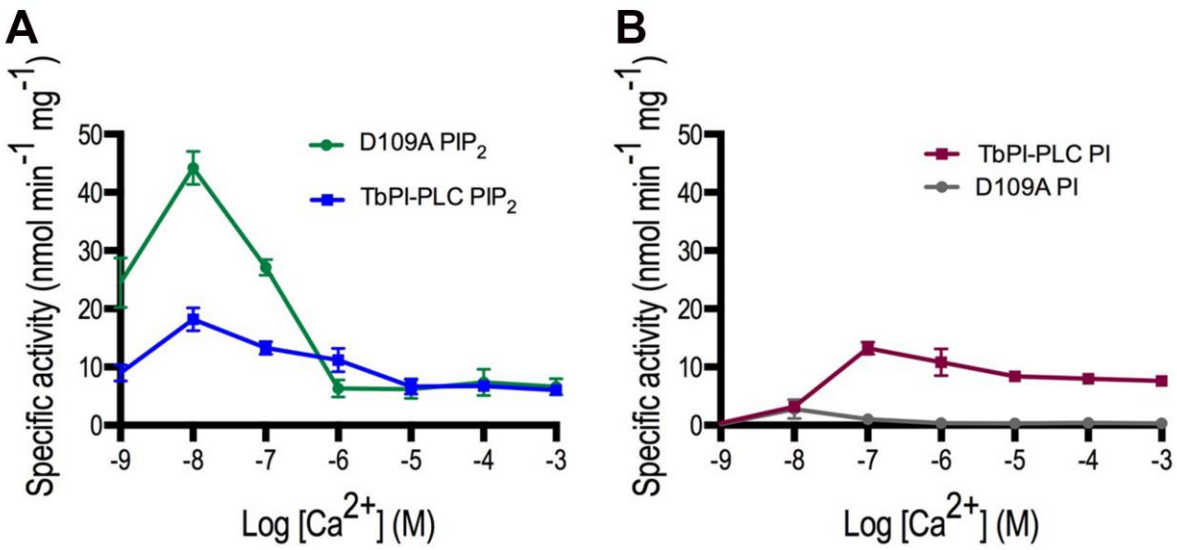

Figure 3.5: Mutation of aspartate in calcium binding loop

Site-directed mutagenesis was used to create a mutation of aspartate to an alanine in the calcium binding loop corresponding to the amino acid in the 109th position. (A) The mutation increased activity with PIP_2 as substrate with the incorporated amino acid change. (B) When PI was used as a substrate, little to no activity was observed from the mutated enzyme. All values are mean ± SE (n=3).

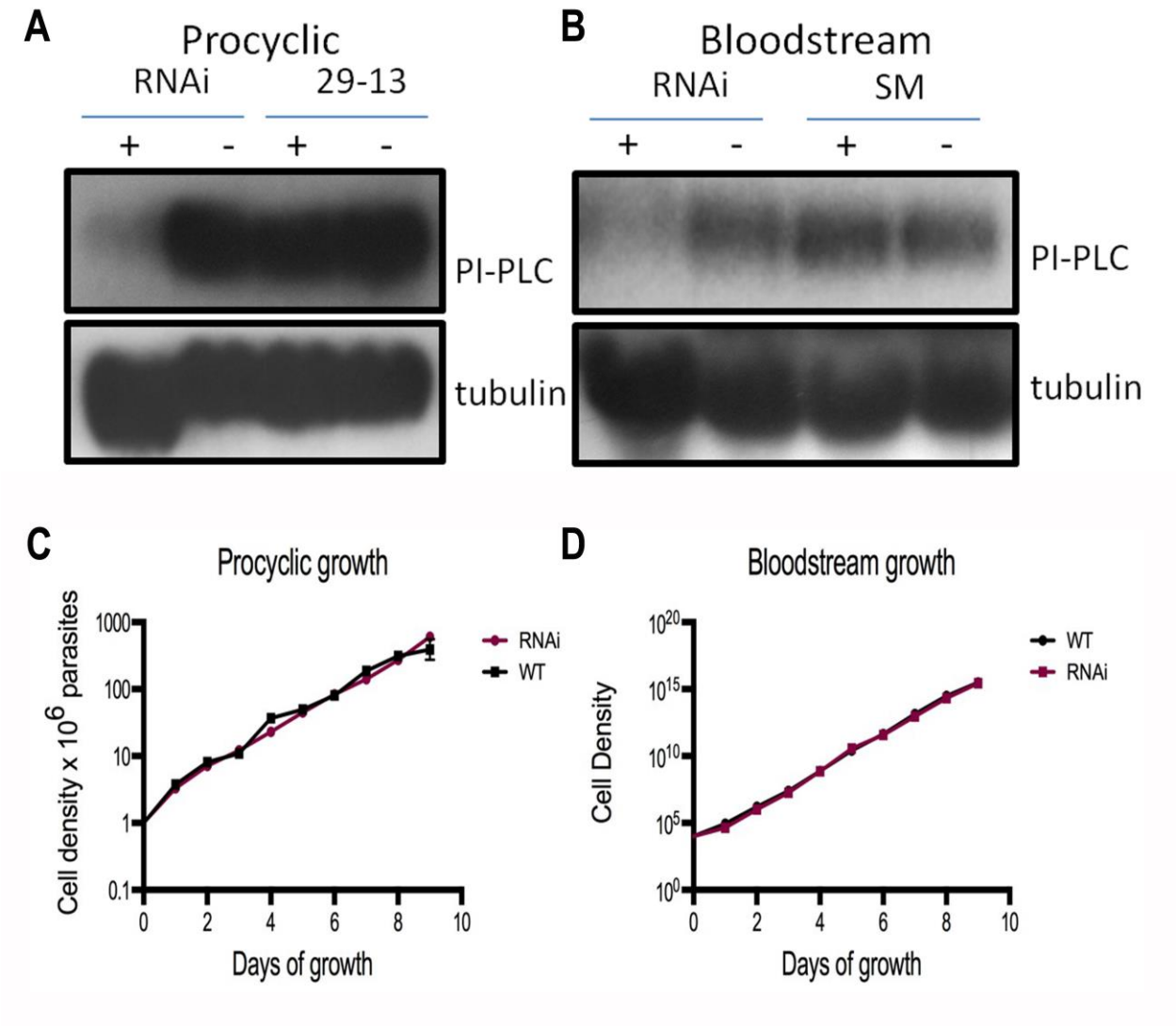

Figure 3.6: Effect of *Tb*PI-PLC down regulation by RNAi

Northern blot analysis of PI-PLC knock grown in the presence (+) or absence (-) of tetracycline. (A) Expression was knocked down in procyclics, RNAi cells, compared to parental cell line (29-13) and in bloodstream forms (B) compared to parental cell line (SM or single marker). Inhibition of *Tb*PI-PLC expression did not have a growth effect on procyclics (C) or bloodstream forms (D) when compared to parental cells (WT).

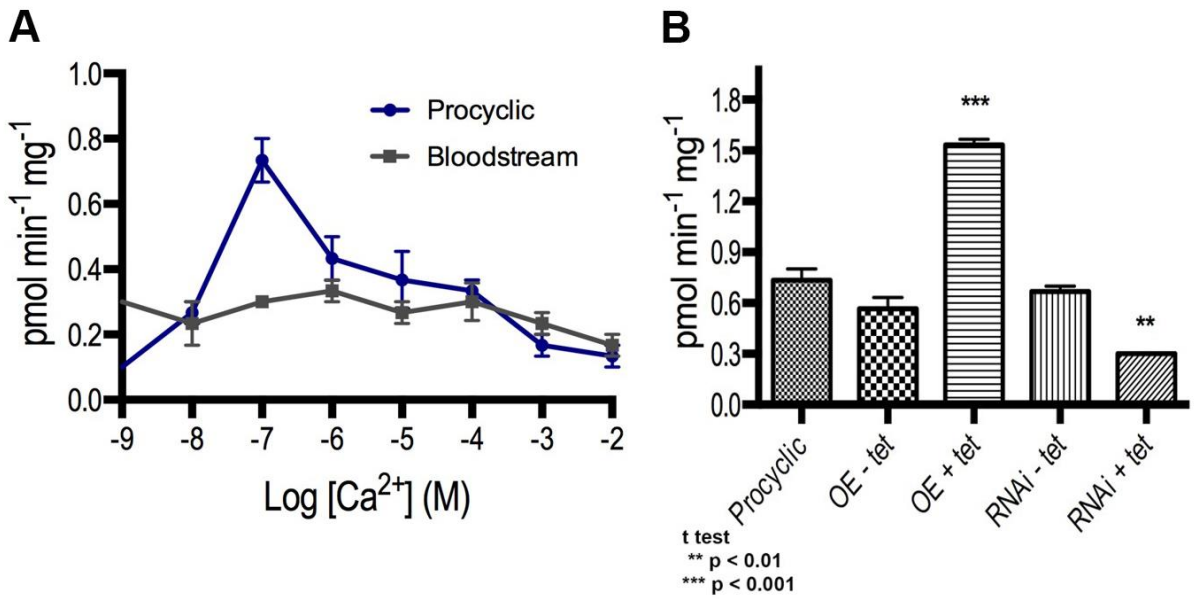

Figure 3.7: Activity in parasites

Hydrolysis activity PIP_2 was measured using an established protocol with prepared parasite lysates. (A) Activity was detected in procyclic and bloodstream form parasites. A peak of activity in procyclics was measured at 100 nM. (B) In procyclics, a significant increase of activity was measured in parasites overexpressing the *Tb*PI-PLC enzyme as well as a significant reduction of activity in parasites after induction of RNAi. All values are mean ± SE (n=3).

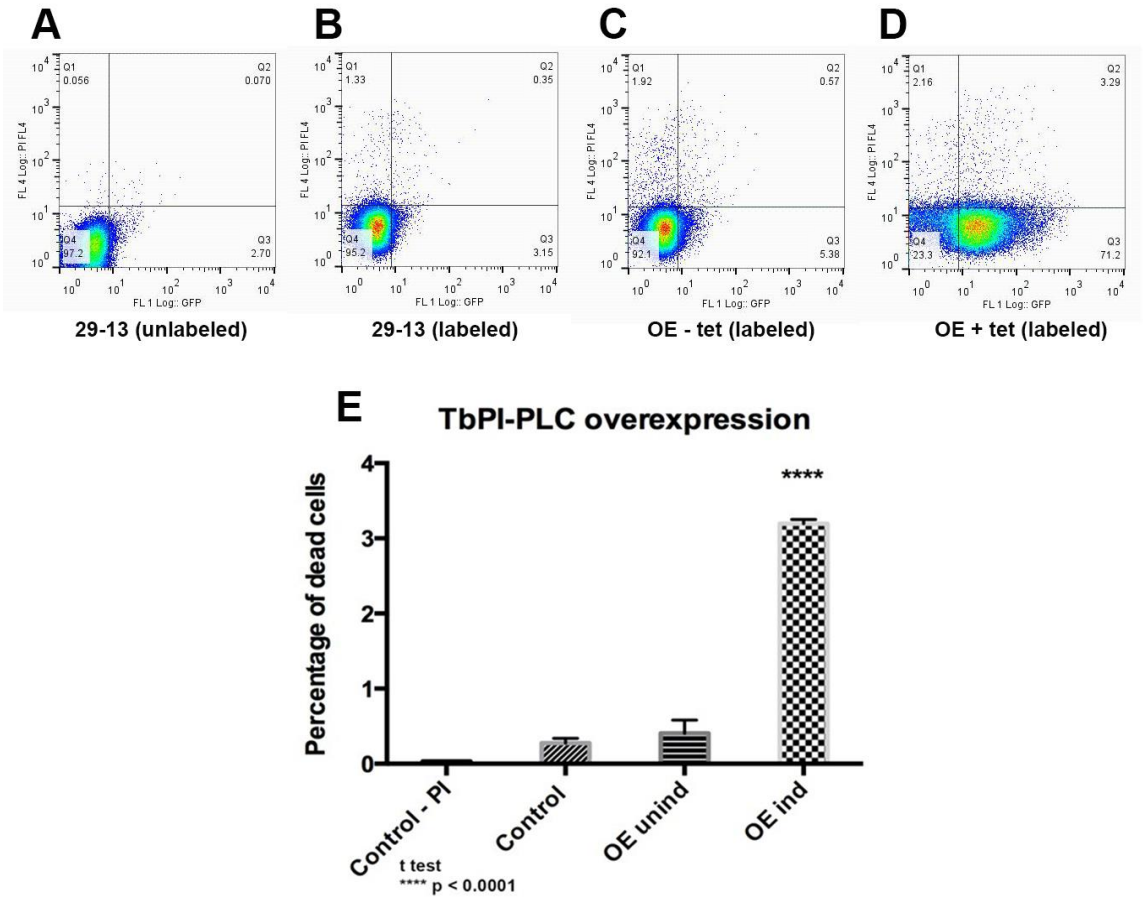

Figure 3.8: Toxicity of overexpression by FACS analysis

Cells induced for 24 hours with tetracycline were labeled with propidium iodide and analyzed by FACS analysis immediately for fluorescence. (A) 29-13 (parental line) unlabeled by propidium iodide. (B) Parental line labeled with propidium iodide demonstrating very few dead cells. (C) Non-induced overexpressing cells stained with propidium iodide. (D) Induced overexpressing cells demonstrating an increase in labeling by propidium iodide. (E) Means from three independent experiments demonstrate a significant increase of dead cells after 24 hour induction of TbPI-PLC. PanelA-D are from one representative experiment. All means are ± SD.

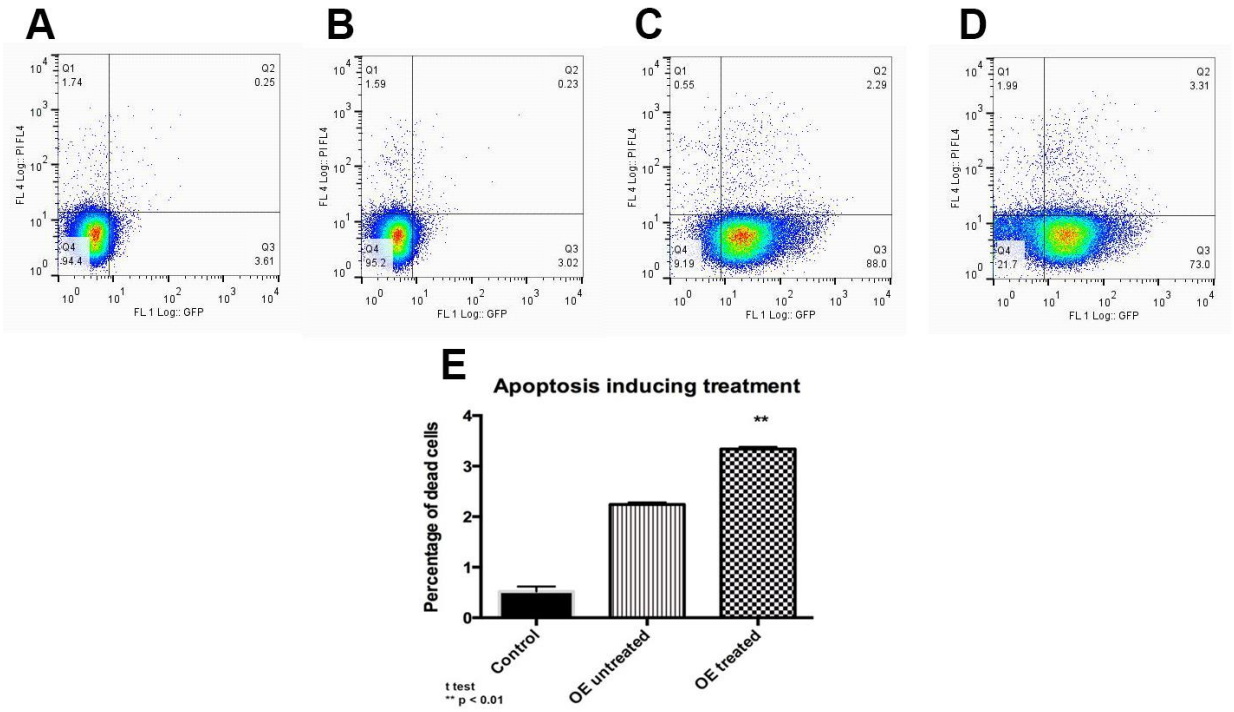

Figure 3.9: Overexpression of PI-PLC results in susceptibility to PCD

Parental cells and overexpressing cells were incubated ± tetracycline for 24 hours with and subjected to ± treatment with 100 µM of H_2O_2 for three hours. Cells were subsequently labeled with propidium iodide and analyzed by FACS analysis immediately for fluorescence. (A) Parental line without tetracycline and without treatment with H_2O_2. (B) Parental line incubated with tetracycline and treated with H_2O_2. (C) *Tb*PI-PLC overexpressing cells not induced with tetracycline but treated with H_2O_2. (D) *Tb*PI-PLC overexpressing cells induced and treated with H_2O_2. (E) Induced overexpressing cells demonstrated a significant increase in dead cells after treatment with H_2O_2 compared to the uninduced, highlighting PI-PLC overexpression may make cells more susceptible to apoptosis. Representative of two independent experiments.

Supplementary Tables and Figures

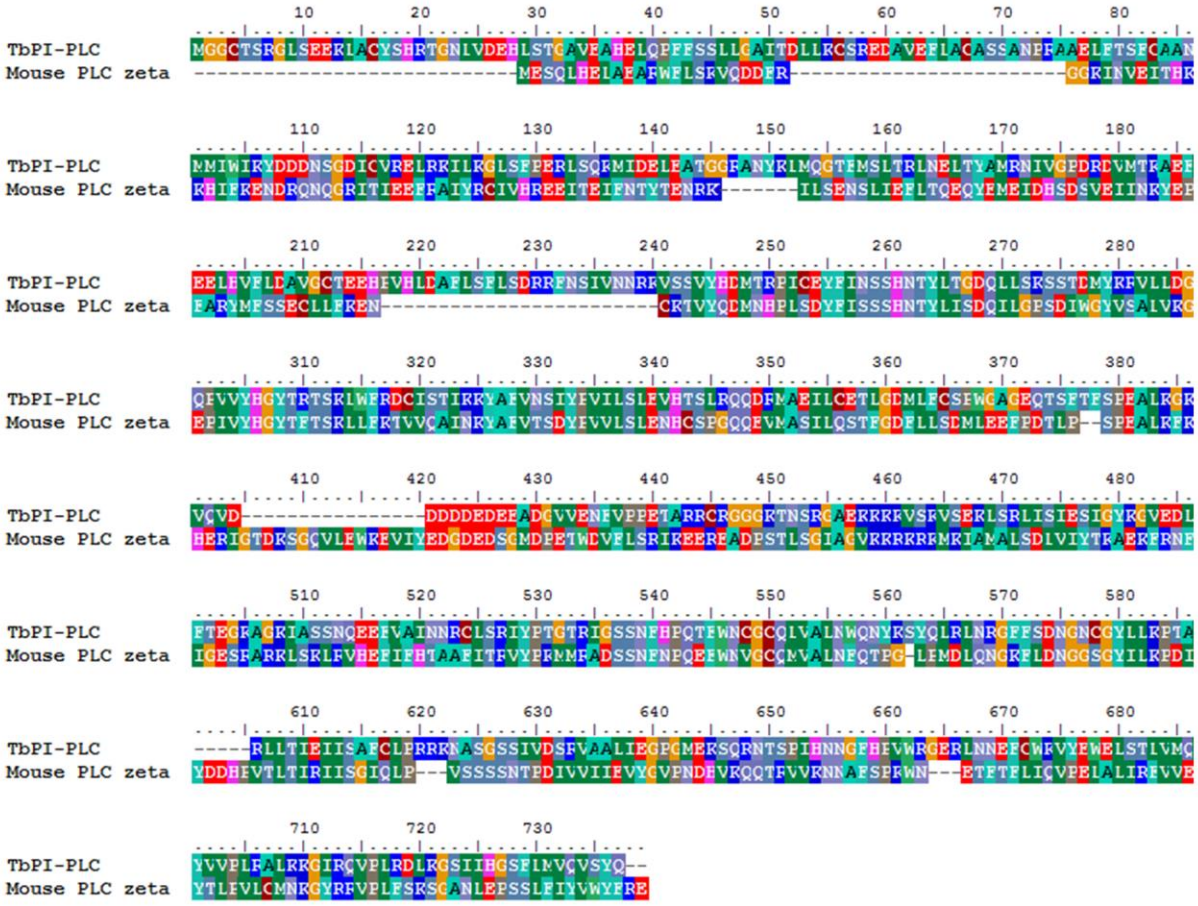

Figure 3.10: Alignment

CLUSTAL W alignment of *Tb*PI-PLC and mouse PLC ζ highlighting 27% identity and 40% similarity.

Table 3.2: Primer sets used in cloning

Primers used for cloning. Nucleotides underlined are for incorporation of restriction sites or backbone of target vector for amplification. Nucleotides in bold are for incorporation of amino acid changes.

Construct	Primer pair
*Tb*PI-PLC$_{(1-18)}$	For 5'-CAAGCTTATGGGAGGGTGTACCTCACGTGGGCTCTCA-3' Rev 5'-CTCGAGGGAGTAACATGCGAGTTTCT-3'
*Tb*PI-PLC$_{(19-714)}$	For 5'-AAGCTTATGCACCGTACCGGCAACCTCGTT-3' Rev 5' CTCGAGCTGATAAGATACTTGAACCATT-3'
GFP tag	For 5'-CTCGAGGGAGTAACATGCGAGTTTCT-3' Rev5'-GGGATCCTTACTTGTACAGCTCGTCCAG-3'
GFP alone	For 5'- CCAAGCTTATGGTGAGCAAGGGCGAGGAG- 3' Rev 5'-GGGATCCTTACTTGTACAGCTCGTCCAG-3'
WT ΔG2A ΔC4A ΔG2C4A	For 5'- CAAGCTTATGGGAGGGTGTACCTCACGTGGGCTCTCA- 3' For 5'- CAAGCTTATG**GCA**GGGTGTACCTCACGTGGGCTCTCA- 3' For 5'- CAAGCTTATGGGAGGG**GCA**ACCTCACGTGGGCTCTCA- 3' For 5'- CAAGCTTATG**GCA**GGG**GCA**ACCTCACGTGGGCTCTCA- 3'
*Tb*PI-PLCpET32	For 5'- GACGACGACAAGATGGGAGGGTGTACGTCACGTGGGCTC-3' Rev 5- GAGGAGAAGCCCGGTTACTACTGATAAGATACTTGAACCAT- 3'
*Tb*PI-PLCHA tag	For 5'- TTACGTGCCCTAAAAAAAGGAATTCGCCAGGTCCCCCTTCGAGAC CTCAAAGGATCTATTATACATGGCTCTTTTTTAATGGTTCAAGTATC TTATCAGGGTACCGGGCCCCCCCTCGAG- 3' Rev 5'- AGCTACGCTGTGAAGACCATGGCACAACATGGTGCCATAAAGTCG GGTACATGCAACGCACACTTGTAACCCAATTGAAGAACACGATAT TCTCAAACTCTGGCGGCCGCTCTAGAACTAGTGGAT- 3'
*Tb*PI-PLCpET32D109A	For 5'-TGATATGGATAAAGTACGACGCCGACAACAGCGG-3' Rev 5'-GTCGTACTTTATCCATATCATCATGAACTT-3'

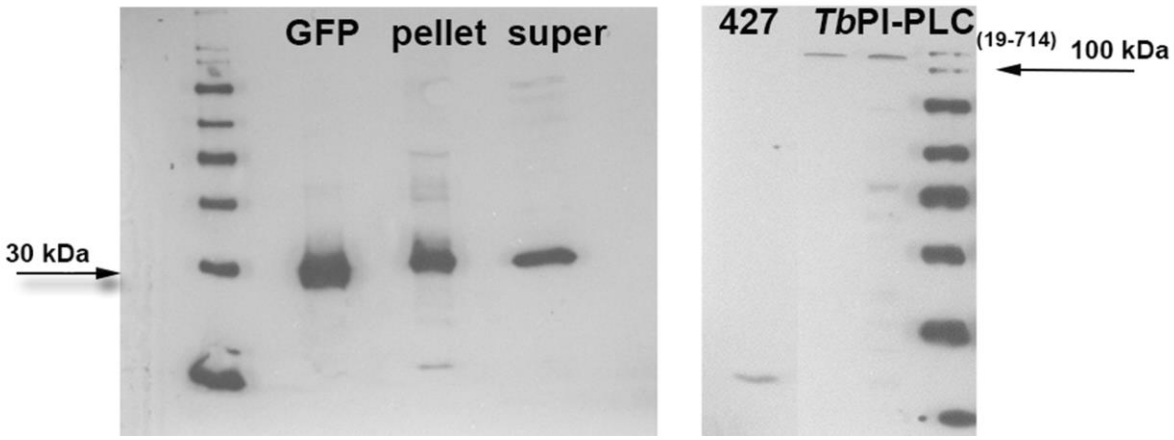

Figure 3.11: Western blot of overexpression constructs

Western blot with anti-GFP demonstrating the overexpression of *Tb*PI-PLC $_{(1-18)}$ at the expected size of 35 kDa (left). Western blot confirming the overexpression of *Tb*PI-PLC $_{(19-714)}$ at the expected size of 110 kDa.

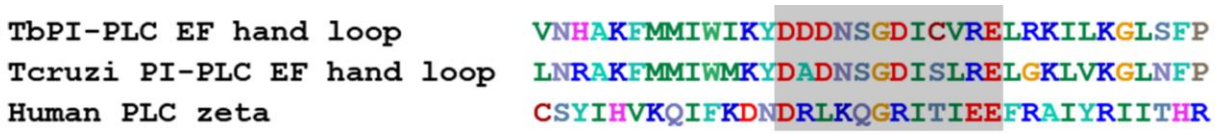

Figure 3.12: Composition of EF-hand calcium binding loop

A series of three aspartates were observed in the calcium binding loop of the *Tb*PI-PLC EF-hand (gray box) and compared to the loops of other calcium sensitive enzymes. This extra aspartate was not observed in the other loops.

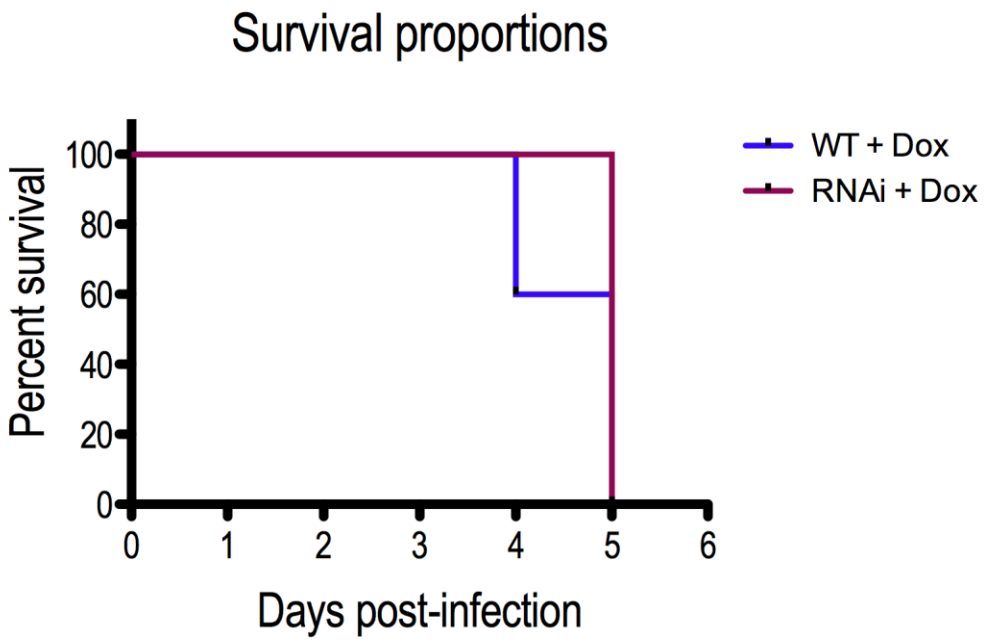

Figure 3.13: Mice infection

Groups of five mice were inoculated with single marker (WT) or RNAi transgenic bloodstream form parasites. Mice were give doxycycline to induce RNAi. All mice were dead by day 5 post-infection.

CHAPTER 4

LITERATURE REVIEW

4.1 The Disease, American trypanosomiasis (Chagas)

American trypanosomiasis is a disease caused by the *Trypanosoma cruzi* parasite and occurs primarily in central and South America. The main source of transmission is by biting reduviid bugs in which the parasites are released in the feces. The parasites can enter the mammalian host via mucosal tissues causing the Romaña sign or through broken skin such as the bite site causing a chagoma. The disease can also be transmitted by blood transfusion, organ transplants, and from mother to fetus. Some patients may initially present with mild flu-like symptoms such as fever and swollen lymph nodes. However, most are asymptomatic and remain asymptomatic for years. The chronic form is the leading cause of death associated with Chagas by causing severe damage to the heart (apical aneurysm) and intestinal system (megacolon and megaesophagus). There are only 2 drug options available for treatment of Chagas, nifurtimox and benznidazole. Unfortunately, both have severe side effects such as skin reactions, vomiting, nausea, anorexia, neuropathy, and convulsions. Both agents require prolonged administration and have limited effectiveness especially in the chronic form (Pérez-Molina *et al*, 2013).

4.2 Phosphodiesterases in Mammalian Cells

Phosphodiesterases are enzymes that degrade cyclic adenosine monophosphate (cAMP) and cyclic guanosine monophosphate (cGMP), two ubiquitous second messengers (Beavo, 1995). These second messengers are synthesized from adenosine triphosphate (ATP) and guanosine triphosphate (GTP) by adenylyl cyclase and guanylyl cyclase, respectively (Joen *et al*, 2005).

These cyclic nucleotides can activate other enzymes such as protein kinase A and protein kinase G thus affecting the phosphorylation of other substrates such as ion channels, transcription factors, and other substrates in cellular processes (Jeon *et al,* 2005). Phosphodiesterases provide the only mechanism for degrading these messengers (Houslay *et al*, 2005), providing excellent targets for chemotherapeutic discovery.

There are a total of 21 PDE isoforms group into 11 different families with most functioning in the hydrolysis of both cAMP and cGMP (DeNinno, 2012). The majority of the PDE families can hydrolyze both cyclic nucleotide compounds while some are specific for either cAMP or cGMP (DeNinno, 2012). However, they differ in substrate specificity, distribution, and regulatory mechanisms (Lakics *et al,* 2010). Understanding these differences and exploring recent achievements in the determination of 3D structures provide opportunities to generate new drugs that are selective and effective for its intended target (Jeon *et al,* 2005). After the introduction of moderately selective PDE5 inhibitors used for the treatment of erectile dysfunction, the interest in PDEs greatly increased. Through the regulation of cyclic nucleotide signaling, PDEs have become implicated as having very diverse physiological functions. PDE4 inhibitors have been used to treat asthma (Schudt *et al,* 1995; Schudt *et al,* 1999) and chronic obstructive pulmonary disease (COPD) (MacIntyre, 2004) and show promise in the treatment of rheumatoid arthritis (Dyke and Montana, 1999), and depression (Houslay, 2001). PDE1 has been suggested as playing roles in Parkinson's disease (Kakkar *et al,* 1996; Kakkar *et al,* 1997) and Alzheimer's disease (Sorimachi *et al,* 1997; Li *et al,* 1998; Saido *et al,* 1994; Croall and Demartino, 1991; Saito *et al,* 1993. In addition, PDE3 is a potential target for the development of drugs to treat type 2 diabetes (Jeon *et al,* 2005). The further development of PDE inhibitors have failed to match the success of PDE5 inhibitors. However, current efforts focus on targeting

PDE catalytic sites and regulatory domains show promise (DeNinno 2012). These efforts involve a more targeted approach to drug design and include investigating structure, function, localization, and expression of the PDEs and their different isoforms. A targeted approach may be more successful and provide the key to unlocking the next generation of PDE inhibitors.

4.3 Phosphodiesterases in Trypanosomes

In trypanosomes, cAMP has been shown to play roles in growth, differentiation, and osmoregulation (Rangel-Aldao *et al,* 1988; Naula and Seebeck, 2000; Seebeck *et al,* 2001; Rohloff *et al,* 2004). Recent studies have identified families of adenylyl cyclases and PDEs that can regulate cAMP levels; however, complete understanding of this pathway is lacking (Laxman and Beavo, 2007). The first demonstration of PDE activity was from bloodstream form lysates of *T. brucei gambiense* more than 30 years ago (Walter, 1974). The completion of sequenced genomes has revealed four different phosphodiesterase families in the kinetoplastids, the trypanosomes and *Leishmania major* (Laxman and Beavo, 2007). All four families belong to Class I group of PDEs as in mammals and are designated as A, B, C, or D (Laxman and Beavo, 2007). The first family to be cloned and identified was in *T. brucei* and is designated as family B (Rascon *et al,* 2002; Zoraghi and Seebeck, 2002; Zoraghi *et al,* 2001) with recent orthologs characterized in *T. cruzi* (D'Angelo *et al,* 2004; Diaz-Benjumea *et al,* 2006). The PDEB families specifically degrade cAMP and are insensitive to most mammalian PDE inhibitors (Laxman and Beavo, 2007). The second family identified, PDEC, was characterized in *T. cruzi* and is currently the only trypanosome PDE that can hydrolyze both cAMP and cGMP (Kunz *et al,* 2005). TcrPDEC is unusual in that the catalytic domain is in the middle of the polypeptide chain (Kunz *et al,* 2005) instead of in the C-terminal part as is characteristic for class I PDEs (Laxman and Beavo, 2007). Also, TcrPDEC contains a FYVE-type domain at the N-terminus (Kunz *et al,*

2005). Classical FYVE domains are known to interact with phosphatidylinositol-3-phosphate and locate to endosomal membranes, but the FYVE domain of TcrPDEC is required for localization to the contractile vacuole, where the enzyme plays a role in regulatory volume decrease (RVD) (Rohloff and Docampo, 2008) and for PDE activity (Schoijet e*t al,* 2011). An increase in cAMP levels during hyposmotic stress in epimastigotes causes fusion of the aquaporin from acidocalcisomes to the contractile vacuole complex (CVC) transferring metabolites to the CVC. This creates an osmotic gradient causing water to enter the organelle leading to a release of excess water out the flagellar pocket (Rohloff and Docampo, 2008; Rohloff *et al,* 2004). Inhibition of the TcrPDEC stimulated volume recovery of epimastigotes subjected to hyposmotic stress demonstrating the TcrPDEC could be regulating the level of cAMP in osmotic stress response (Schoijet *et al,* 2011). The ability to regulate volume and response to osmotic stress is important to these parasites in their life cycle as they must adapt to different environments in the vector and mammalian host.

The catalytic domains of parasite PDEs were shown to be closely related to the human PDEs as they are to each other using comparative sequence analysis (Seebeck *et al,* 2011). This garners emphasis on the efforts to design drugs specifically for the intended target. In the past, the development of anti-parasitic drugs have occurred either by chance and/or repurposing drugs for other uses or by strategies that target the parasite target without harming the host (Seebeck *et al,* 2011). However, it has been suggested that an alternative approach would be to use the established technology targeting the human PDE to target the closely related parasite PDE (Seebeck *et al,* 2011). Medicinal chemistry has demonstrated that it is possible to target specific PDEs families (PDE4 inhibitor for COPD and PDE5 inhibitors for erectile dysfunction) in

humans even though they are closely related and could address the host versus parasite specificity issues (Seebeck *et al*, 2011).

Through sequence analysis and activity testing, mutations have inactivated PDECs in *T. brucei, T. evansi*, and *T. congolense* (Wang *et al, 2012).* In *T. brucei*, this gene is regulated and expressed similarly to the active PDEC gene in *T. cruzi* (Wang *et al*, 2012). These findings are interesting as they suggest the inactive PDEC may have another function. In addition, the TcrPDEC1 crystal structure demonstrated the presence of a pocket, called a "P-pocket" that is near the active site and unique to kinetoplastids (Wang *et al*, 2012). In kinetoplastids, this pocket is accessible whereas in human PDEs this pocket is blocked by two resides or is lacking altogether (Wang *et al*, 2012). This could provide a target area for the development of parasite specific PDE inhibitors. Collectively, an active PDEC in *T. cruzi*, but not in other kinetoplastids and the presence of the P-pocket may be valuable aspects affecting future drug design.

CHAPTER 5

CHEMICAL VALIDATION OF PHOSPHODIESTERASE C AS A CHEMOTHERAPEUTIC TARGET IN *TRYPANOSOMA CRUZI*, THE ETIOLOGICAL AGENT OF CHAGAS DISEASE

[1]King-Keller S., Li M., Smith A., Zheng S., Kaur G., Yang X., Wang B., and R. Docampo. 2010 *Antimicrobial Agents and Chemotherapy*. 54:3738-3745.

Reprinted here with permission from the publisher.

Abstract

Trypanosoma cruzi phosphodiesterase C (TcrPDEC) is a novel and rather unusual PDE that, unlike all other class I PDEs, has its catalytic domain localized in the middle of the polypeptide chain, is able to hydrolyze cGMP, although it prefers cAMP, and has a FYVE-type domain in its *N*-terminal region (16). TcrPDEC shows homology to the mammalian PDE4 family members. PDE4 inhibitors are currently under development for the treatment of inflammatory diseases, such as asthma, chronic pulmonary diseases, and psoriasis, as well as for treating depression and serving as cognitive enhancers. We therefore tested a number of compounds originally synthesized as potential PDE4 inhibitors on *T. cruzi* amastigote growth, and we obtained several useful hits. We then conducted homology modeling of *T. cruzi* PDEC and identified other compounds through virtual screening as potential inhibitors. Testing of these compounds on amastigote growth and on the recombinant TcrPDEC activity resulted in several potent inhibitors. The most potent inhibitors were found to increase the cellular concentration of cAMP. Preincubation of cells in the presence of one of these compounds stimulated volume recovery after hyposmotic stress, in agreement with their TcrPDEC inhibitory activity *in vitro*, providing chemical validation of this target. The compounds found could be useful tools in the study of osmoregulation in *T. cruzi*. In addition, their further optimization could result in the development of new drugs against Chagas disease and other trypanosomiases.

5.1 Introduction

The morbidity and mortality associated with Chagas disease exceeds those of better-known infectious diseases such as malaria, tuberculosis and AIDS, in North, Central and South America. Millions of people are affected by this trypanosomiasis. No vaccine is available to prevent this disease and drug treatments have serious side effects or are not completely effective (34).

Trypanosoma cruzi, the etiologic agent of Chagas disease, experiences dramatic changes in osmolarity as it passes through its diverse life-cycle stages. Cyclic adenosine monophosphate (cAMP)-mediated fusion of acidocalcisomes, which are lysosome-related organelles, to the contractile vacuole complex (CVC) results in translocation of a water channel or aquaporin, and water movement leading to the decrease in volume (regulatory volume decrease) that occurs after hyposmotic stress (28). This pathway is terminated by the action of a *T. cruzi* cAMP phosphodiesterase C (TcrPDEC) (28) that is located in the CVC (Schoijet *et al* 2010). This is a novel and rather unusual PDE that, unlike all other class I PDEs, has its catalytic domain localized in the middle of the polypeptide chain (2, 16). In general, PDEs have unique *N*-terminal regulatory domains and the catalytic domain is located near their *C*-terminus (17). TcrPDEC is the only trypanosome PDE identified to date capable of hydrolyzing cGMP, although it prefers cAMP as a substrate (16). Additionally, TcrPDEC is unusual in that its *N*-terminal region contains a FYVE-type domain, a functional domain that has not been found in any PDE so far (2, 16). It should be possible to design inhibitors that are selective for the trypanosome PDEs and do not cause toxic effects owing to actions on mammalian PDEs. In this regard, there is good evidence that it is possible to obtain selective inhibitors against particular PDEs in humans, as for example the case of sildenafil (for erectile dysfunction) (11).

We tested several compounds initially designed as potential PDE4 inhibitors (37) or obtained by virtual screening, against *T. cruzi* amastigote growth and TcrPDEC activities. In addition, we report that several of these compounds inhibit TcPDEC *in vivo* as shown by their effects on cyclic AMP levels and on regulatory volume decrease after hyposmotic stress of these parasites, providing chemical validation for this potential drug target.

5.2 Materials and Methods

5.2.1 Culture methods

T. cruzi (Y strain) trypomastigotes were obtained as described previously (36). L_6E_9 myoblasts were exposed to 2,000 rad of gamma radiation and plated on 75 cm^2 flasks at a density of 1 x 10^7 cells/flask and incubated in Dulbecco's Minimum Essential Medium (DMEM) containing 20% fresh fetal calf serum. After 24 hours of incubation at 35°C in a 7% CO_2 atmosphere, the cells were exposed to a suspension of 5 x 10^7 trypomastigotes in the same medium. Eight hours later, the flasks were washed with Hanks solution, pH 7.2. A second wash with Hanks was performed 72 hours post-infection. After 4-5 days, the trypomastigotes were harvested from the supernatants and final concentration of parasites was determined using a hemacytometer.

L_6E_9 myoblasts were cultured as described before (5). Myoblasts were cultured in 100 mm x 20 mm Corning dishes with DMEM medium and incubated at 35°C. The myoblasts were passed every 3-4 days checking for confluency and density. The myoblasts were washed three times with Hanks solution, pH 7.2, and detached from the dishes by incubating with 0.25% pancreatin in Hanks solution. Cell suspension was centrifuged at 800 rpm for 10 min. Supernatant was aspirated from the tube and pellet was reconstituted with 2 ml of DMEM per dish collected. Approximately 0.4 ml of suspension was added to newly prepared dishes with DMEM. PDE-deficient *S. cerevisiae* strain PP5 transformed with the construct containing the

entire full-length open reading frame of TcrPDEC was obtained from Dr. Thomas Seebeck, University of Bern, Switzerland. The cells were grown and maintained in SC-leu medium (16).

5.2.2 Chemicals and reagents

Fetal calf serum, DMEM, and Hanks were purchased from Sigma. [2, 8-^{3}H] Adenosine 3', 5'-cyclic phosphate (28.1 Ci/mmol), ammonium salt and [5, 6-^{3}H] uracil (37.1 Ci/mmol) were purchased from Perkin Elmer. The HitHunter cAMP II assay was from GE Healthcare. All other reagents were analytical grade.

5.2.3 Growth Inhibition assay

Gamma-irradiated L_6E_9 myoblasts (0.8×10^7 cell/plate) in DMEM medium containing 20% fetal calf serum were plated in either 12 or 24-well tissue culture plates (Corning Glass Works) and incubated at 35°C in a 7% CO_2 atmosphere for 24 hours as described before (36). After 24 hours, cells are washed once and fresh DMEM plus 20% fetal calf serum was added containing 4.17×10^6 trypomastigotes per well if 12-well plates were used. If 24-well plates were used, the concentrations were adjusted accordingly. After 2 hours of incubation at 35°C in a 7% CO_2 atmosphere, the wells were washed two times with Hanks solution, pH 7.2. At this time, 0.5-1 µCi of [5, 6-^{3}H] uracil/well were added. To investigate intracellular amastigote replication, drugs were added in concentrations of 0.5, 1, 5, 20, and 50 µM in duplicate. The plates were incubated for an additional 70 hours. The incorporation of the [^{3}H]-uracil into trichloroacetic acid (TCA)-precipitable material was measured at this time period. The supernatants from the monolayers were aspirated and the cells were dissolved in 1.3 ml of 1% sodium dodecyl sulfate containing 100 µg of cold uracil per ml. This was transferred to glass tubes and 3 ml of 5% TCA was added. The tubes were incubated on ice for 15 min. The precipitates were collected on glass fiber filters (Whatman GF/B) by using a sampling manifold (Millipore, Bedford, MA). The filters were

washed twice with 5% TCA and once with 95% ethanol. The filters were placed in 4 ml of scintillation fluid (MP Biomedicals). Radioactivity was measured using a Beckman Coulter LS 6500 multipurpose scintillation counter. The percent inhibition of uracil incorporation was calculated using the following formula: [(A-B)/ A] x 100. A is the mean counts per minute of infected control treated myoblasts and B is the mean counts per minute of infected drug-treated myoblasts. Then the labeling of the uninfected controls was subtracted yielding the [^{3}H]-uracil incorporation that could be attributed to intracellular amastigotes. The calculation of IC_{50} was performed as described previously (22). Briefly, the percent of growth inhibition was plotted as a function of drug concentration by fitting the values to the rectangular hyperbolic function: $I= (I_{max} C)/ (IC_{50}+C)$. I equals the percent of inhibition, I_{max} equals 100% inhibition, C is the concentration of the inhibitor, and IC_{50} is the concentration for 50% growth inhibition. The regression analyses were performed using Sigma Plot 5.0.

5.2.4 Yeast cell lysis.

Yeast cell lysis was performed as described (2) with minor modifications. Yeast cells were grown to OD_{600} = 0.8-1.5 and harvested. The harvested cells were washed two times with H_2O and the pellet was stored at -80°C. The pellet was thawed on ice and suspended in ice-cold extraction buffer (50 mM HEPES pH 7.5, 100 mM NaCl, plus mammalian cell protease inhibitor cocktail (Sigma-Aldrich). Cells were lysed by grinding with glass beads (450-600 µm) by 3 cycles of 30 seconds of grinding and 30 sec of incubation on ice. They were kept in ice until sedimented and the supernatant was decanted. The supernatant was centrifuged at 2,500 *g* for 10 min at 4°C. The resulting supernatant was centrifuged at 100,000 *g* for 1 hour. The supernatant was saved to make sure the activity was in the pellet fraction only. The pellet was resuspended in 200 µl of extraction buffer with 5% glycerol plus anti-protease cocktail.

5.2.5 Phosphodiesterase activity

Phosphodiesterase activity was assayed according to the method of Thompson and Appleman (32) with minor modifications (16). Activity was determined in 40 mM Tris-HCl pH 8, 5 mM $MgCl_2$, 50 µM of unlabeled cAMP. Each assay contained 50,000 cpm ^{3}H-labeled cAMP (adenosine 3', 5'-cyclic phosphate, ammonium salt from Perkin Elmer). Ten µg of enzyme were added to each reaction plus potential inhibitor compounds in concentrations of 0.1, 0.5, 1, 5, and 10 µM. The reaction was done in a total volume of 100 µl for 10 min at 30°C. The reaction was stopped by heating at 100°C for 1 min. The reaction was incubated again for 30 min at 30°C adding 40 µl of snake venom (King Cobra: 2 mg/ml in 10 mM Tris-HCl pH 8). A solution (20 µl) containing 50 mM EDTA and 5 mM adenosine was added to stop the second reaction. Then, 1 ml of a suspension containing 33% of anion exchange resin AG1-X4 (200-400 mesh) and 30% ethanol in water was added. The mixture was well mixed, sedimented, and 0.4 ml of the supernatant was added to 2 ml of scintillation fluid and counted in the same counter as above. The percent of inhibition and IC_{50} were calculated with the same formulas as above.

5.2.6 Cyclic AMP determinations

T. cruzi epimastigotes were suspended at a concentration of 1 x 10^8 cells per ml and incubated with or without PDE inhibitor for 10 min in Dulbecco's PBS supplemented with 5 mM glucose. Aliquots of 0.5 ml were taken at 1 min and 5 min post-incubation, centrifuged, and resuspended in 100 µl of PBS and 400 µl of 50 mM sodium acetate, pH 5.5, preheated to 95 °C. The samples were heated at 95 °C for 5 min. Then the samples were centrifuged, supernatants collected, and stored at -20°C. The cAMP measurements were done using the GE Healthcare HitHunter cAMP II assay using protocol 1 as described by its manufacturer. The determinations were performed

by calculating for each sample the amount of increase or decrease of cAMP comparing each to the control (without inhibitor) as indicated by the increase or decrease of luminescence.

5.2.7 Homology modeling

We developed a theoretical model for *T. cruzi* PDEC by using homology modeling based on human PDE4B crystal structure (PDB entry: 1XMY) with 28% sequence identity (3). The rough model was solvated by using the TIP3P water model, subjected to 500-steps of molecular mechanics minimization and molecular dynamics simulations at 300 K for 1.0 ns using the SANDER module in AMBER 8 program (4). This optimized homology model can be used as input for the structure-based virtual screening.

5.2.8 Virtual screening

Docking-based virtual screening with our PDEC homology model was conducted against the Maybridge database, containing about 60,000 compounds. The 3D structures of the compounds were built with hydrogen atoms added. Then AM1-BCC partial charges were assigned (14, 15, 33). This docking-based virtual screening was conducted by following similar procedures we reported elsewhere (19, 20). The position and conformation of each compound were optimized first by the anchor fragment orientation and then by the torsion minimization method implemented in the DOCK 6 program (7, 24). Fifty conformations and a maximum of 100 anchor orientations for each compound were generated, and all of the docked conformations were energy minimized by 100 iterations following procedures as described in literature (24). The docked molecules were ranked based on the sum of the van der Waals and electrostatic energies implemented in the DOCK 6 program to obtain the top 1000 compounds. After collecting the top hits, re-analysis of virtual screening results was conducted using drug-like property criteria (25) by the FILTER 2.0.1 software (9). We then performed consensus scoring

evaluation (8) by ChemScore (6, 26) PLP (35) ScreenScore (31) ChemGauss and ShapeGauss (23) implemented in the FRED 2.2.3 software (9) as well as hydrogen bond and hydrophobic profiles checked by the IDEA 8.8 software (13) As the final step, a manual binding orientation and conformational analysis was performed to obtain the final 30 hits for biological evaluation.

5.2.9 Regulatory volume decrease

Epimastigotes were collected and washed twice with isotonic chloride buffer (Iso-Cl buffer, 137 mM NaCl, 4 mM KCl, 1.5 mM KH_2PO_4, 8.5 mM Na_2PO_4, 20 mM HEPES, 11 mM glucose, 1 mM $CaCl_2$, 0.8 mM $MgSO_4$, pH 7.4). The osmolarity of the buffer was adjusted to 300 ± 5 mOsm as verified by an Advanced Instruments 3D3 Osmometer (Norwood, MA). The washed cells were resuspended in Iso-Cl buffer to a cell density of 1 x 10^8.ml^{-1} cells. The cells were distributed in 96-well plates with 150 µl per well in triplicate and hyposmotic stress was induced by 1:1 dilution of cell suspension with sterile deionized water, resulting in a final osmolarity of 150 mOsm. The absorbance changes at 550 nm were recorded every 6 s for 10 min using a SpectraMax M2e plate reader (Molecular Devices) (29).

5.2.10 General chemistry

All reagents were purchased from Acros and Aldrich. 3-{1-[3-Methoxy-4-(pyridin-2-yloxy)-phenyl]-but-1-enyl}-quinoline (**7**) was synthesized according to literature procedure (37). Microwave heating was performed in the single-mode microwave cavity of a Discover Synthesis System (CEM Co.), and all microwave reactions were conducted in a heavy-walled glass vials sealed with Teflon septa. ^{1}H-NMR, ^{13}C-NMR and DEPT spectra were recorded at 400 and 100 MHz, respectively, on a Bruker 400 NMR spectrometer. Combustion analyses and mass spectra were performed by the analytical and the mass spectrometry facilities at Georgia State

University. Compounds **2a**, **3b**, **4a-b** and **5a-u** were synthesized according to literature procedures reported earlier (37).

5.2.11 Synthesis of 1-[4-Difluoromethoxy-3-(pyridin-2-yloxy)-phenyl]-1-quinolin-3-yl-butan-1-ol (6a) by nucleophilic addition to the ketones 5l

To ketones **5l** (1 mmol) in THF (5 mL), was added dropwise 3-quinolyllithium at -78 °C. The resulting mixture was stirred overnight, during which time the reaction was allowed to gradually warm from -78 °C to rt, and quenched with water. The aqueous layer was extracted three times with ethyl acetate. The combined organic solution was dried over $MgSO_4$, filtered and evaporated. The residue was purified by flash chromatography to afford **6a**. Yield: 24 %. ^{1}H-NMR ($CDCl_3$): 8.80 (1H, d, J = 7.2 Hz), 8.26 (1H, s), 8.03 ~ 7.95 (2H, m), 7.79 (1H, d, J = 8.0 Hz), 7.66 ~ 7.64 (2H, m), 7.52 (1H, m), 7.37 (1H, s), 7.27 (1H, d, J = 10.0 Hz), 7.20 (1H, d, J = 8.4 Hz)), 6.98 ~ 6.59 (2H, m), 6.40 (1H, t, J = 74.4 Hz), 3.20 (1H, s, br), 2.32 (2H, m), 1.43 (1H, m), 1.25 (1H, m), 0.93 (3H, t, J = 7.2 Hz). ^{13}C-NMR ($CDCl_3$): 162.9 (s), 149.5 (d), 147.2 (d), 146.6 (s), 145.2 (s), 144.8 (s), 142.6 (s), 139.6 (d), 139.1 (s), 132.4 (d), 129.9 (d), 129.5 (d), 128.7 (d), 128.0 (d), 127.4 (s), 126.9 (d), 123.7 (d), 122.0 (d), 121.7 (d), 118.7 (triplet, J =253 Hz, d), 111.1 (d), 77.3 (s), 43.9 (t), 16.9 (t), 14.3 (q). HRMS-ESI (+): Calc. for $C_{25}H_{23}FN_2O_3$: 437.1598. Found: 437.1668 $[M+H]^+$.

5.2.12 Synthesis of 3-{1-[3-Methoxy-4-(pyridin-2-yloxy)-phenyl]-butyl}-quinoline (8)

To a solution of 3-{1-[3-Methoxy-4-(pyridin-2-yloxy)-phenyl]-but-1-enyl}-quinoline (**7**) (0.30 g, 0.80 mmol) in ethanol (5 mL) was added 10% Pd/C (0.03 g) as catalyst and the mixture was hydrogenated at room temperature overnight. The reaction mixture was quenched with saturated brine. The aqueous solution was extracted with ethyl acetate three times. The combined organic solution was washed with brine and dried over $MgSO_4$, filtered, concentrated. The residue was

purified by flash chromatography to afford 0.11g (38 %) of **8**. ^{1}H-NMR ($CDCl_3$): 8.85 (1H, d, J = 2.0 Hz), 8.13 (1H, m), 8.08 (1H, d, J = 8.0 Hz), 7.98 (1H, d, J = 2.0 Hz), 7.79 (1H, d, J = 7.6 Hz), 7.67 ~7.63 (2H, m), 7.54 (1H, d, J = 7.2 Hz)), 7.07 (1H, d, J = 8.4 Hz), 6.95 ~ 6.86 (4H, m), 4.13 (1H, t, J = 8.0 Hz), 3.72 (3H, s), 2.15 (2H, m), 1.38 (2H, m), 0.98 (3H, t, J = 7.2 Hz). ^{13}C-NMR ($CDCl_3$): 163.7 (s), 151.8(d), 151.7 (s), 147.5 (d), 146.9 (s), 141.7 (s), 141.2 (s), 139.1 (d), 137.7 (s), 133.5 (d), 129.1 (d), 128.8 (d), 128.1 (s), 127.6 (d), 126.7 (d), 122.9 (d), 120.3 (d), 118.0 (d), 112.4 (d), 110.6 (d), 56.0 (q), 48.6 (d), 29.7 (t), 21.1 (t), 14.0 (q). HRMS-ESI (+): Calc. for $C_{25}H_{25}N_2O_2$: 385.1838. Found: 385.1908 $[M+H]^+$.

5.3 Results

5.3.1 Homology modeling

In the absence of a well-defined experimentally determined structure, homology modeling provides a rational alternative for developing a reasonable 3D working model to guide drug discovery efforts. It needs to be noted that homology modeling of proteins is currently the most accurate method for predicting 3D structure, yielding models suitable for a wide spectrum of applications, such as mechanism investigation, structure-based drug development or virtual screening (10). We previously successfully conducted a number of homology modeling studies for various disease-related protein targets, including the Nonstructural Protein NS1 protein of the H5N1 strain of human influenza viruses (21) and human α_{1A}-adrenergic receptor (18).

We previously worked on developing inhibitors for mammalian PDE4 (37). *T. cruzi* PDEC has 28% sequence identity with human PDE4B (PDB entry: 1XMY), for which the crystal structure is available (Fig. 5.6) (3). By using homology modeling following previously published procedures (4, 14) we built a working model for *T. cruzi* PDEC. Specifically, the rough model was solvated by using the TIP3P water model, subjected to 500-steps of molecular

mechanics minimization and molecular dynamics simulations at 300 K for 1.0 ns using the SANDER module in AMBER 8 program (15). After structural optimization and validation, the PDEC homology model showed great similarity to the PDE4B template with a low RMSD value of 2.5 Å (Fig. 5.7).

5.3.2 PDE and parasite growth inhibition

Because of the structural similarity between the homology model of PDEC and PDE4B crystal structure, in our initial effort of searching for *T. cruzi* PDEC inhibitors, we tested a number of compounds generated for our PDE4 inhibition project (37). The synthesis of most of these compounds has been reported (37). Figure 5.1 describes the general approach. Among all the compounds, **6a** and **8** have not been reported yet. Table 5.1 shows the structures of all the compounds tested. It was found that some of them (ZL-N series) were excellent inhibitors of the parasite without toxicity to the host cells (Table 5.2). Many such compounds exhibited IC_{50} values in the low micromolar range. These values compare favorably with the inhibition obtained with nifurtimox and benznidazole, the drugs currently used against Chagas disease, whose IC_{50}s values under similar experimental conditions are 2.8 and 3.7 μM, respectively (36).

Among all these compounds, some showed paralell activities for both PDE4 and PDEC or preferential inhibition of PDE4. This is not surprising since these two enzymes show a high degree of homology and structural similarity based on computational results and the compounds were designed for PDE4. Among those compounds are Zl-N-98 (IC_{50} of 2.2 and 0.082 μM for PDEC and PDE4 respectively), ZL-N-99 (IC_{50} of 5.4 and 5.2 μM for PDEC and PDE4 respectively), ZL-N-100 (IC_{50} of 5.3 and 1.1 μM for PDEC and PDE4 respectively), ZL-N-101 (IC_{50} of 2.5 and 0.18 μM for PDEC and PDE4 respectively), ZL-N-106 (IC_{50} of 4.4 and 0.667 μM for PDEC and PDE4 respectively), ZL-N-107 (IC_{50} of 3.2 and 0.626 μM for PDEC and

PDE4 respectively), and ZL-N-120 (IC_{50} of 3.2 and 0.022 μM for PDEC and PDE4 respectively). However, for the purpose of minimizing side effects in humans, we are more interested in those that preferentially inhibited PDEC and their structural features. Several compounds showed 4- to 30-fold selectivities for PDEC over PDE4. These are ZL-N-66 (IC_{50} of 3.5 and 71 μM for PDEC and PDE4 respectively), ZL-N-67 (IC_{50} of 4.0 and 60 μM for PDEC and PDE4 respectively), ZL-N-68 (IC_{50} of 5.1 and 100 μM for PDEC and PDE4 respectively), ZL-N-69 (IC_{50} of 5.6 and 24 μM for PDEC and PDE4 respectively), ZL-N-81 (IC_{50} of 3.1 and 93 μM for PDEC and PDE4 respectively), and ZL-N-115 (IC_{50} of 2.5 and 44 μM for PDEC and PDE4 respectively).

By examining the structures of the selective PDEC inhibitors, one can see that these compounds have the bulky cyclic substituent at the 4-position (ZL-N-66-69, 81) or does not have a bulky substituent (ZL-N-115). Such findings are very reasonable since a bulky substituent at the 3-position of the aryl ring is known to enhance binding for PDE4, and substitution at the 4-position disfavors binding to PDE4. Therefore, lack of a bulky substitution or moving it to the 4-position all results in poor affinity for PDE4. Such results indicate that future optimization work should focus on substitution patterns similar to that of ZL-N-66-69, ZL-N-81, or ZL-N-115 in order to further improve selectivity.

5.3.3 Virtual screening

In order to search for additional PDEC inhibitors, we used the homology model (Fig. 5.7) and conducted virtual screening against the Maybridge database containing about 60,000 compounds using DOCK 6 following procedures described in earlier publications (19, 20, 33). Twenty five compounds were identified for biological evaluation. Fig. 5.7 shows the docking conformations

of these 25 compounds in the binding site of the PDEC homology model and Fig. 5.2 depicts their chemical structures.

We then tested the compounds identified from virtual screening (PDEC series, Table 5.2 and Fig. 5.2) against *T. cruzi* infective stages *in vitro* and found that some of them were specific inhibitors of the parasite. Many such compounds exhibited IC_{50} values in the low micromolar range against the enzyme, but were not as effective against the parasites.

5.3.4 PDE inhibition *in vivo*

To confirm that the most effective compounds were able to inhibit *T. cruzi* PDEC *in vivo*, and therefore chemically validate the enzyme as a drug target, we assayed their ability to increase cyclic AMP concentration in intact epimastigotes. Fig. 5.4 shows that compounds ZLN55, ZLM66, ZLN68, and ZLN82 significantly increased the levels of cAMP after their incubation for 1 to 5 min with epimastigotes, with ZLN82 being the most active compound. Fig. 5.3 shows a dose-response curve using different concentrations of ZLN82. To confirm that ZLN82 was inhibiting TcrPDEC, the isozyme that is involved in terminating cAMP signaling during osmotic stress (28), we preincubated epimastigotes for 10 min with ZLN82 and followed the rate of volume recovery during hyposmotic stress by light scattering. Fig. 5.5 shows that when the cells were subjected to a 50% reduction in osmolarity (from 300 to 150 mOsm) swelling led to a decrease in absorbance at 550 nm. Volume recovery led to an increase in absorbance, which reached values equivalent to the initial values after 5 min. ZLN82 preincubated cells did not swell as much as control cells and initiated volume recovery sooner than wild type cells (Fig. 5.5).

5.4 Discussion

We report here the inhibition of TcrPDEC and growth of *T. cruzi* amastigotes by two series of PDE inhibitors, one obtained by screening of compounds previously synthesized as inhibitors of human PDE4 (37), and a second based on virtual screening of a chemical library after homology modeling of the enzyme and pharmacophore identification. Both approaches resulted in the identification of novel inhibitors of the parasite enzyme and growth.

It is very important to note that the active compounds identified from our human PDE4 project (37) were not considered very active against human PDE4, i.e., those were unsuccessful inhibitors of human PDE4. Such results suggest that TcrPDEC structure is sufficiently different from human PDE4, which should allow the identification of very selective inhibitors of TcrPDEC without cross reactivity against human PDEs. It is understood that low micromolar concentrations of inhibitors are not necessarily very impressive by the "normal" drug discovery standards. However, these numbers compare favorably with the IC_{50} values obtained with nifurtimox and benznidazole (36), the drugs currently used against Chagas disease, under similar experimental conditions (Table 5.2). Starting from a potency level of clinically used drugs for further structural optimization is a very reasonable position in this particular case. The concentrations inhibiting amastigote growth and the recombinant enzyme activity were of the same order and there was good correlation between both activities. Although we cannot rule out the possible inhibition of other enzymes by some of these compounds, the ability of these inhibitors to increase the levels of cyclic AMP and improve the regulatory volume decrease after hyposmotic stress of live parasites is in agreement with their inhibitory activity against TcrPDEC, and thus chemically validate this enzyme as a potential drug target.

The consequences of cyclic AMP intoxication in trypanosomes are not known and may include stimulation of different pathways that could lead to cell death. In yeast, accumulation of cyclic AMP leads to a marked heat-shock sensitivity (27) while in macrophages it leads to activation of pathways mediated by protein kinase A and cyclic AMP response-element-binding protein (CREB) pathway (1). *T. cruzi* possesses a cyclic AMP-regulated protein kinase A regulatory subunit that associates with the PKA catalytic subunit (12). The *T. cruzi* genome also has several predicted cyclic AMP binding proteins but their functions are not clear (17). Trypanosomatid PDEs are highly resistant to mammalian PDE inhibitors (17). Unfortunately, this different sensitivity of trypanosomatid PDEs to mammalian PDEs inhibitors was overlooked in many experiments where inhibitors of mammalian PDEs were used uncritically for studying cyclic AMP effects in different trypanosomatids (30). Although many of these inhibitors did have an effect on trypanosomes, the effects observed may not be due entirely to cyclic AMP (30). Our identification of a number of TcrPDEC inhibitors that were shown to increase cyclic AMP in intact parasites and stimulate their regulatory volume decrease will greatly facilitate the understanding of the role of this nucleotide in osmoregulation as well as in proliferation and differentiation. Considering the fact that there are no really effective therapies available, the present work has also potential to make a major impact in the chemotherapy of Chagas disease.

References

1. **Agarwal, N., G. Lamichhane, R. Gupta, S. Nolan, and W. R. Bishai.** 2009. Cyclic AMP intoxication of macrophages by a *Mycobacterium tuberculosis* adenylate cyclase. Nature **460:**98-102.

2. **Alonso, G. D., A. C. Schoijet, H. N. Torres, and M. M. Flawia.** 2006. TcPDE4, a novel membrane-associated cAMP-specific phosphodiesterase from *Trypanosoma cruzi*. Mol Biochem Parasitol **145:**40-9.

3. **Card, G. L., B. P. England, Y. Suzuki, D. Fong, B. Powell, B. Lee, C. Luu, M. Tabrizizad, S. Gillette, P. N. Ibrahim, D. R. Artis, G. Bollag, M. V. Milburn, S. H. Kim, J. Schlessinger, and K. Y. Zhang.** 2004. Structural basis for the activity of drugs that inhibit phosphodiesterases. Structure **12:**2233-47.

4. **Case, D. A., T. E. Cheatham, 3rd, T. Darden, H. Gohlke, R. Luo, K. M. Merz, Jr., A. Onufriev, C. Simmerling, B. Wang, and R. J. Woods.** 2005. The Amber biomolecular simulation programs. J Comput Chem **26:**1668-88.

5. **Docampo, R., S. N. Moreno, and A. E. Vercesi.** 1993. Effect of thapsigargin on calcium homeostasis in *Trypanosoma cruzi* trypomastigotes and epimastigotes. Mol Biochem Parasitol **59:**305-13.

6. **Eldridge, M. D., Murray, C.W., Auton, T.R., Paolini, G.V., Mee, R.P.** 1997. Empirical scoring functions: I. The development of a fast empirical function to estimate the binding affinity of ligands in receptor complexes. J. Comput. Aided Mol. Des. **11:**425-445.

7. **Ewing, T. J., Makino, S., Skillman, A.G., and Kuntz, I.D.** 2001. DOCK 4.0: search strategies for automated molecular docking of flexible molecule databases. J. Comput. Aided Mol. Des. **15:**411-428.

8. **Feher, M.** 2006. Consensus scoring for protein-ligand interactions. Drug Discov Today **11:**421-8.

9. **FRED.** 2007. Fast rigid exhaustive docking. *In* I. OpenEye Scientific software (ed.), Santa Fe, NM.

10. **Ginalski, K.** 2006. Comparative modeling for protein structure prediction. Curr. Opin. Struct. Biol. **16:**172-177.

11. **Goldstein, I., T. F. Lue, H. Padma-Nathan, R. C. Rosen, W. D. Steers, and P. A. Wicker.** 1998. Oral sildenafil in the treatment of erectile dysfunction. Sildenafil Study Group. N Engl J Med **338:**1397-404.

12. **Huang, H., L. M. Weiss, F. Nagajyothi, H. B. Tanowitz, M. Wittner, G. A. Orr, and Y. Bao.** 2006. Molecular cloning and characterization of the protein kinase: A regulatory subunit of *Trypanosoma cruzi*. Mol Biochem Parasitol **149:**242-5.

13. **IDEA.** 2007. Breadth Technology, Taipei, Taiwan.

14. **Jakalian, A., Bush, B.L., Jack, D.B., and Bayly, C.I.** 2000. Fast, efficient generation of high quality atomic charges. AM1-BCC model: I. Method. J. Comput. Chem. **21:**132-146.

15. **Jakalian, A., Jack, D.B., and Bayly, C.I.** 2002. Fast, efficient generation of high-quality atomic charges. AM1-BCC model: II. Parameterization and validation. J. Comput. Chem. **23:**1623-1641.

16. **Kunz, S., M. Oberholzer, and T. Seebeck.** 2005. A FYVE-containing unusual cyclic nucleotide phosphodiesterase from *Trypanosoma cruzi*. FEBS J **272:**6412-22.

17. **Laxman, S., and J. A. Beavo.** 2007. Cyclic nucleotide signaling mechanisms in trypanosomes: possible targets for therapeutic agents. Mol Interv **7:**203-15.

18. **Li, M., H. Fang, L. Du, L. Xia, and B. Wang.** 2008. Computational studies of the binding site of alpha1A-adrenoceptor antagonists. J Mol Model **14:**957-66.

19. **Li, M., Y. J. Huang, P. C. Tai, and B. Wang.** 2008. Discovery of the first SecA inhibitors using structure-based virtual screening. Biochem Biophys Res Commun **368:**839-45.

20. **Li, M., N. Ni, H. T. Chou, C. D. Lu, P. C. Tai, and B. Wang.** 2008. Structure-based discovery and experimental verification of novel AI-2 quorum sensing inhibitors against Vibrio harveyi. ChemMedChem **3:**1242-9.

21. **Li, M., and B. Wang.** 2007. Homology modeling and examination of the effect of the D92E mutation on the H5N1 nonstructural protein NS1 effector domain. J Mol Model **13:**1237-44.

22. **Ling, Y., G. Sahota, S. Odeh, J. M. Chan, F. G. Araujo, S. N. Moreno, and E. Oldfield.** 2005. Bisphosphonate inhibitors of *Toxoplasma gondii* growth: in vitro, QSAR, and in vivo investigations. J Med Chem **48:**3130-40.

23. **McGann, M. R., H. R. Almond, A. Nicholls, J. A. Grant, and F. K. Brown.** 2003. Gaussian docking functions. Biopolymers **68:**76-90.

24. **Moustakas, D. T., Lang, P.T., Pegg, S., Pettersen, E., Kuntz, I.D., Brooijmans, N., Rizzo, R.C.** 2006. Development and validation of a modular, extensible docking program: DOCK 5. J. Comput. Aided Mol. Des. **20:**601-619.

25. **Muegge, I.** 2003. Selection criteria for drug-like compounds. Med Res Rev **23:**302-21.

26. **Murray, C. W., Auton, T.R., Eldridge, M.D.** 1998. Empirical scoring functions. II. The testing of an empirical scoring function for the prediction of ligand-receptor binding affinities and the use of Bayesian regression to improve the quality of the model. J. Comput. Aided Mol. Des. **12:**503-519.

27. **Nikawa, J., P. Sass, and M. Wigler.** 1987. Cloning and characterization of the low-affinity cyclic AMP phosphodiesterase gene of *Saccharomyces cerevisiae*. Mol Cell Biol **7:**3629-36.

28. **Rohloff, P., A. Montalvetti, and R. Docampo.** 2004. Acidocalcisomes and the contractile vacuole complex are involved in osmoregulation in *Trypanosoma cruzi*. J Biol Chem **279:**52270-81.

29. **Rohloff, P., C. O. Rodrigues, and R. Docampo.** 2003. Regulatory volume decrease in *Trypanosoma cruzi* involves amino acid efflux and changes in intracellular calcium. Mol Biochem Parasitol **126:**219-30.

30. **Seebeck, T., R. Schaub, and A. Johner.** 2004. cAMP signaling in the kinetoplastid protozoa. Curr Mol Med **4:**585-99.

31. **Stahl, M., and M. Rarey.** 2001. Detailed analysis of scoring functions for virtual screening. J Med Chem **44:**1035-42.

32. **Thompson, W. J., and M. M. Appleman.** 1971. Cyclic nucleotide phosphodiesterase and cyclic AMP. Ann N Y Acad Sci **185:**36-41.

33. **Tsai, K. C., S. H. Wang, N. W. Hsiao, M. Li, and B. Wang.** 2008. The effect of different electrostatic potentials on docking accuracy: a case study using DOCK5.4. Bioorg Med Chem Lett **18:**3509-12.

34. **Urbina, J. A., and R. Docampo.** 2003. Specific chemotherapy of Chagas disease: controversies and advances. Trends Parasitol **19:**495-501.

35. **Verkhiver, G. M., Bouzida, D., Gehlaar, D.K., Rejto, P.A., Arthurs, S., Colson, A.B., Freer, S.T., Larson, V., Luty, B.A., Marrone, T., Rose, P.W.** 2000. Deciphering common failures in molecular docking of ligand-protein complexes. J. Comput. Aided Mol. Des. **14:**731-751.

36. **Yan, W., and S. N. Moreno.** 1998. A method to assess invasion and intracellular replication of *Trypanosoma cruzi* based on differential uracil incorporation. J Immunol Methods **220:**123-8.

37. **Zheng, S., G. Kaur, H. Wang, M. Li, M. Macnaughtan, X. Yang, S. Reid, J. Prestegard, B. Wang, and H. Ke.** 2008. Design, synthesis, and structure-activity relationship, molecular modeling, and NMR studies of a series of phenyl alkyl ketones as highly potent and selective phosphodiesterase-4 inhibitors. J Med Chem **51:**7673-88.

Table 5.1: Structures of PDE inhibitors tested

No.	R_1	R_2	R_3	Structure	Drug
2a	$-CHF_2$	H	H	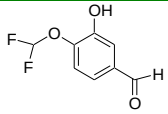	2GK30
3b	$-CH_3$		H	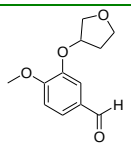	2GK23
4a	$-CH_3$		*n*-Pr	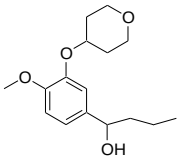	2GK13
4b	$-CH_3$		*n*-Pr	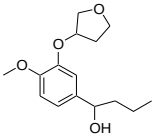	2GK25
5a	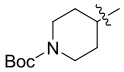	$-CH_3$	*n*-Bu	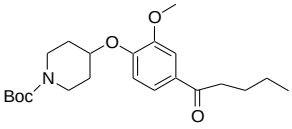	ZL-N-81
5b	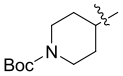	$-CH_3$	*n*-Pr	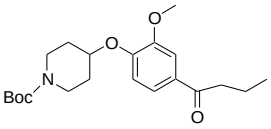	ZL-N-82
5c		$-CH_3$	*n*-Pr	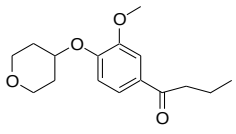	ZL-N-67
5d		$-CH_3$	*n*-Bu	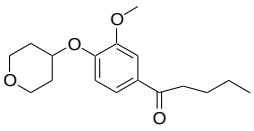	ZL-N-66

5e		-CH_3	*n*-Pr	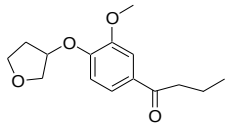	ZL-N-69
5f		-CH_3	*n*-Bu	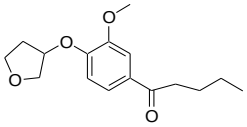	ZL-N-68
5g	-CH_3		*n*-Pr	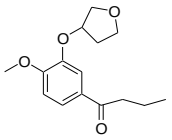	2GK16
5h	-CH_3		*n*-Bu	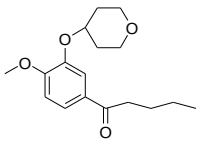	2GK37
5i	-CH_3		-$(CH_2)_2$cyclohexyl	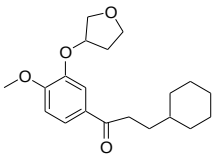	2GK50
5j	-CH_3		-$(CH_2)_2$Ph	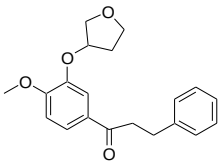	2GK53
5k	-CH_3		-CH_2cyclohexyl	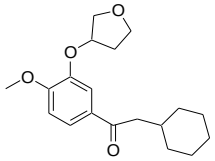	2GK57
5l	-CHF_2	2-py	*n*-Pr	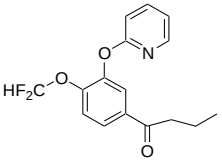	ZL-N-35
5m	-CHF_2		*n*-Pr	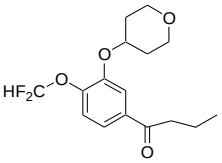	ZL-N-55

5n	-CHF_2		- $(CH_2)_2$cyclohexyl	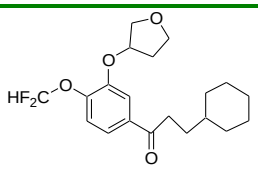	ZL-N-100
5o	-CHF_2		-$(CH_2)_2$Ph	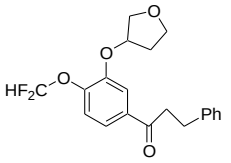	ZL-N-101
5p	-CHF_2	-CHF_2	-$(CH_2)_2$Ph	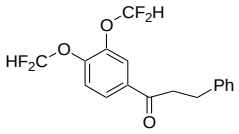	ZL-N-98
5q	-CHF_2	-CHF_2	-CH_2-cyclohexyl	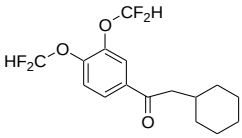	ZL-N-99
5r	-CHF_2	-CHF_2	-$(CH_2)_3$Ph	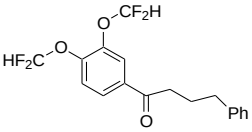	ZL-N-115
5s	-CHF_2		*i*-Bu	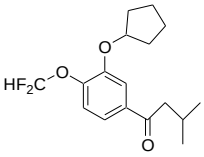	ZL-N-120
5t	-CHF_2		-CH_2-cyclohexyl	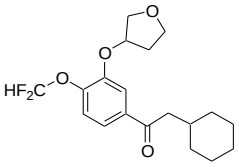	ZL-N-106
5u	-CHF_2		-$(CH_2)_3$Ph	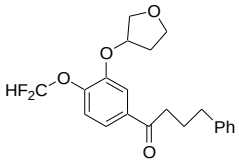	ZL-N-107
6a	-CHF_2	2-pyridinyl	3-quinolinyl	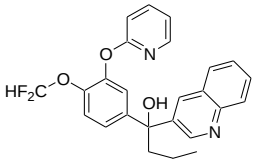	ZL-N-39
8	2-pyridinyl	-CH_3	3-quinolinyl	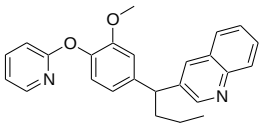	ZL-N-43

Table 5.2 Growth Inhibition

Amastigote growth inhibition experiments were conducted using L_6E_9 myoblasts infected with Y strain *T. cruzi* by measuring [5,6-^{3}H]uracil incorporation 3 days post-infection. Asterisks (*) indicate that the compounds were cytotoxic for host cells at the concentration indicated. Compounds showing no cytotoxicity on host cells when tested at 1 and 25 μM were retested at 5 different concentrations to obtain their IC_{50}s, except for compound PDEC11(**), which percent inhibition at 1 and 25 μM were 51% and 98%, respectively, and was not cytotoxic to host cells. Results are expressed as means ± S.E.M, except for the less potent compounds.

Phosphodiesterase activity of recombinant enzyme was assayed as described under Materials and Methods. Results are means ± S.E.M. of three different experiments.

[#]For comparison, the IC_{50}s for the GK and ZL-N series obtained against the human PDE4 activity (ref. 7) are shown between parentheses.

	Growth Inhibition	Recombinant Assay			Growth Inhibition	Recombinant Assay
		IC_{50} (in µM)				
Drug	**IC_{50} (in µM)**	**PDEC (PDE4)[#]**		**Drug**	**IC_{50} (in µM)**	**IC_{50} (in µM) PDEC**
2GK13	10	> 10	(>100)	PDEC1	> 25	> 10
2GK16	68	> 10	(0.43)	PDEC2	> 25	10
2GK23	122	> 10		PDEC3	> 25*	> 10
2GK25	471	> 10	(>100)	PDEC4	> 25*	> 10
2GK30	11	> 10		PDEC5	> 25	3.8 ± 2.4
2GK37	2.1 ± 0.8	> 10	(0.72)	PDEC6	> 10	> 10
2GK50	6.1 ± 5.1	> 10	(1.9)	PDEC7	> 10	> 10
2GK53	5.6 ± 2.0	> 10	(2.3)	PDEC9	> 10	> 10
2GK57	1.7 ± 0.4	4.9 ± 2.5	(2.6)	PDEC10	> 10	> 10
ZL-N-35	10.3	3.5 ± 2.6	(40)	PDEC11	> 1**	4.1 ± 2.9
ZL-N-39	3.8 ± 1.1	3.9 ± 3.0	(6)	PDEC12	5.4 ± 3.0	7.0 ± 2.7
ZL-N-43	1.9 ± 0.9	3.3 ± 2.2	(6)	PDEC13	> 10	> 10
ZL-N-55	1.6 ± 0.7	4.8 ± 1.9	(0.35)	PDEC14	> 10	10
ZL-N-66	5.2 ± 2.1	3.5 ± 1.7	(71)	PDEC15	> 10	> 10
ZL-N-67	4.0 ± 1.7	4.0 ± 1.6	(60)	PDEC16	4.8 ± 2.6	6.3 ± 2.8
ZL-N-68	1.8 ± 0.3	5.1 ± 3.1	(100)	PDEC17	6.4 ± 2.7	4.6 ± 0.5
ZL-N-69	3.7 ± 0.7	5.6 ± 1.4	(24)	PDEC18	> 25*	4.3 ± 2.2
ZL-N-81	3.8 ± 1.0	3.1 ± 1.5	(93)	PDEC19	3.3 ± 3.1	5.5 ± 1.9
ZL-N-82	3.3 ± 1.0	6.5 ± 2.0	(29)	PDEC20	< 1*	> 10
ZL-N-98	2.3 ± 0.4	2.2 ± 1.2	(0.082)	PDEC21	<1*	2.4 ± 1.4
ZL-N-99	5.7 ± 2.6	5.4 ± 1.5	(5.2)	PDEC22	<1*	4.5 ± 3.3
ZL-N-100	5.8 ± 2.3	5.3 ± 1.4	(1.1)	PDEC23	> 10*	> 10
ZL-N-101	3.1 ± 0.8	2.5 ± 1.3	(0.18)	PDEC24	< 1*	3.6 ± 1.3
ZL-N-106	4.4 ± 1.4	2.5 ± 1.4	(0.667)	PDEC25	> 10*	> 10
ZL-N-107	3.1 ± 0.8	3.2 ± 0.5	(0.626)			
ZL-N-115	7.7 ± 4.0	2.5 ± 2.5	(44)			
ZL-N-120	3.6 ± 1.8	3.2 ± 2.5	(0.022)			

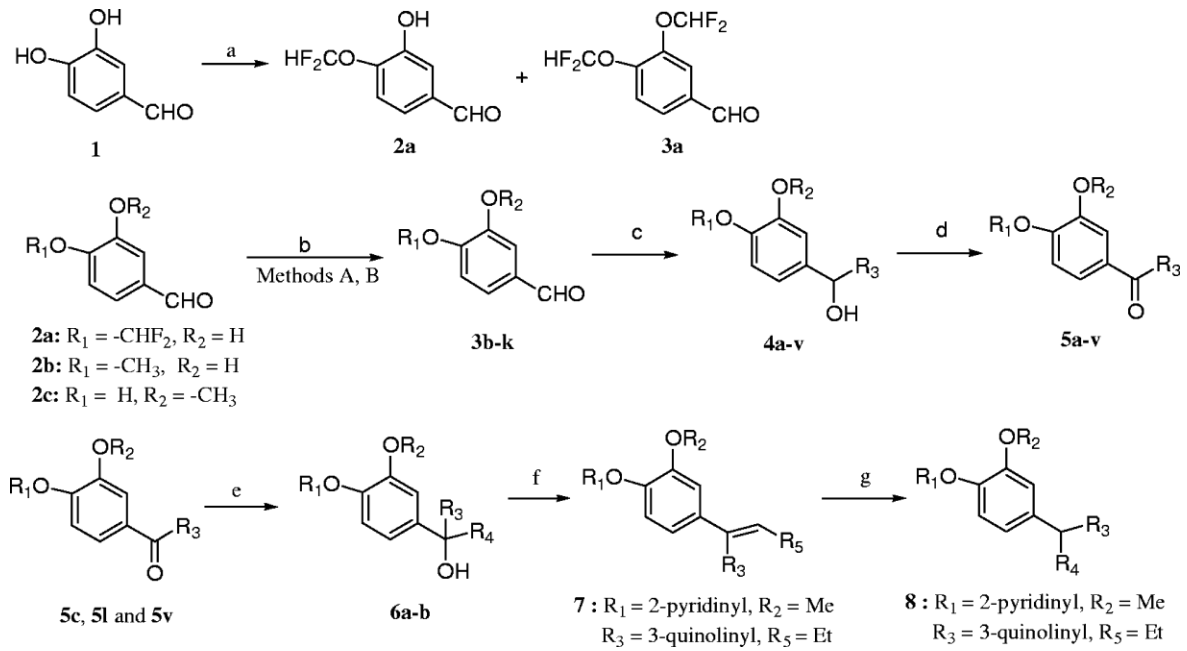

Figure 5.1

(a) CClF2COOMe, Cs2CO3, *N*,*N*-dimethylformamide; (b) (i) method A, R1OH or R2OH, PPh3, *t*-BuO2CNANCO2Bu-*t*, THF; method B, R1Br or R2Br, CsCO3, DMF; (c) R3Li or R3MgBr, THF, _78°C; (d) pyridinium chlorochromate, dichloromethane; (e) R4Br, *n*-BuLi, THF, _78°C or *n*-BuLi, THF, _78°C; (f) AcOH, H2SO4, 80°C; (g) H2, Pd/C, RT.

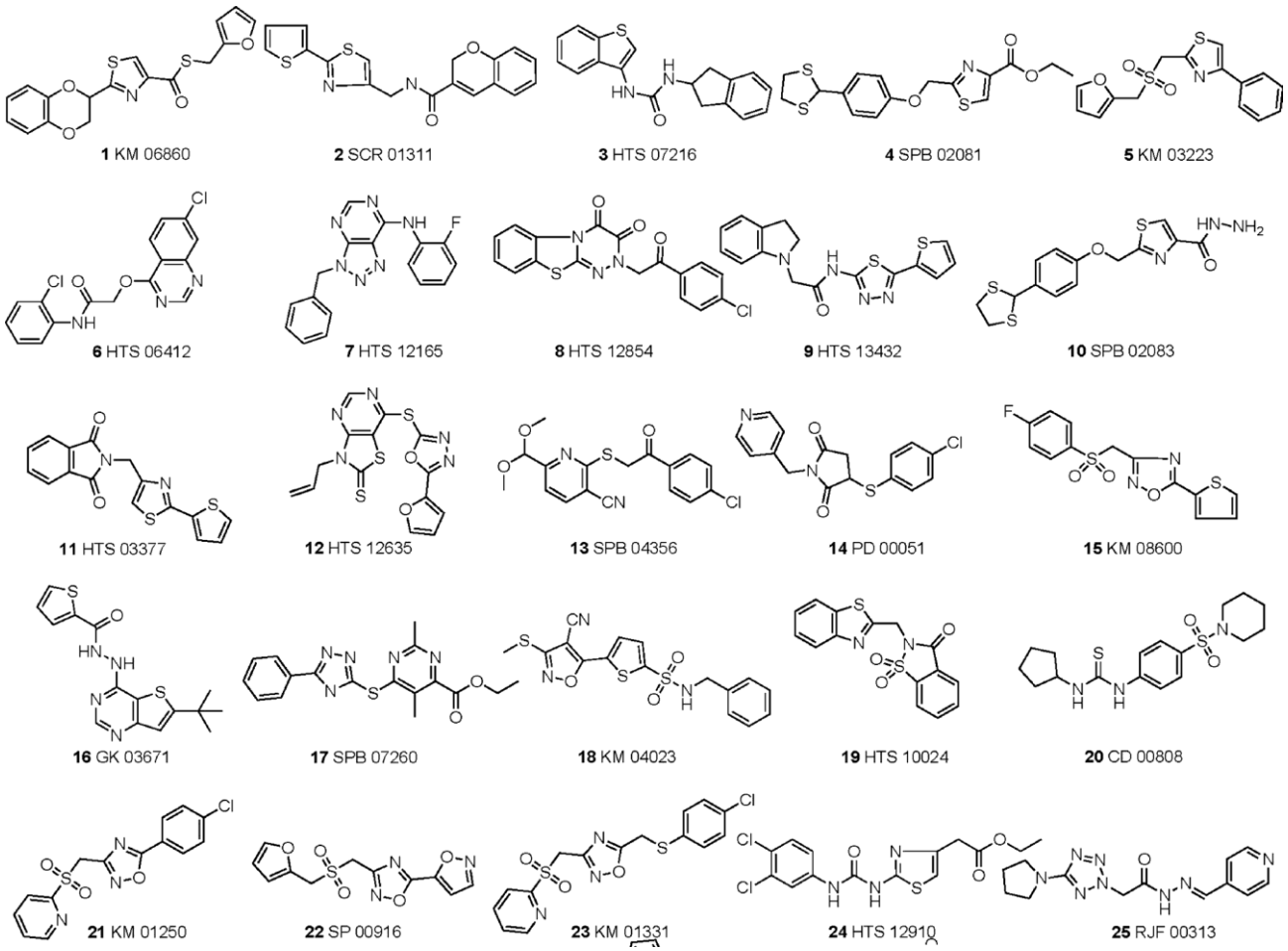

Figure 5.2

The chemical structures of all compounds obtained from virtual screening tested for PDEC inhibitory activity.

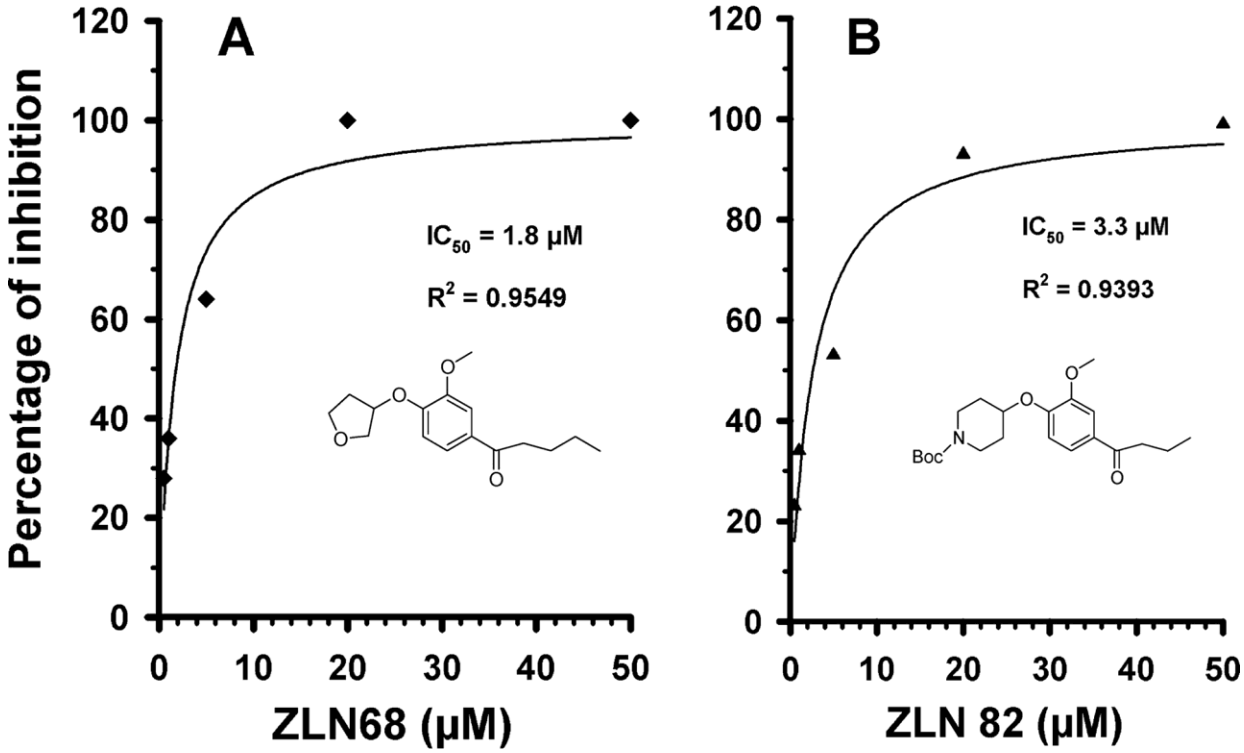

Figure 5.3

Typical dose-response curves for *in vitro* amastigote growth inhibition by two inhibitors, ZLN68 and ZLN82.

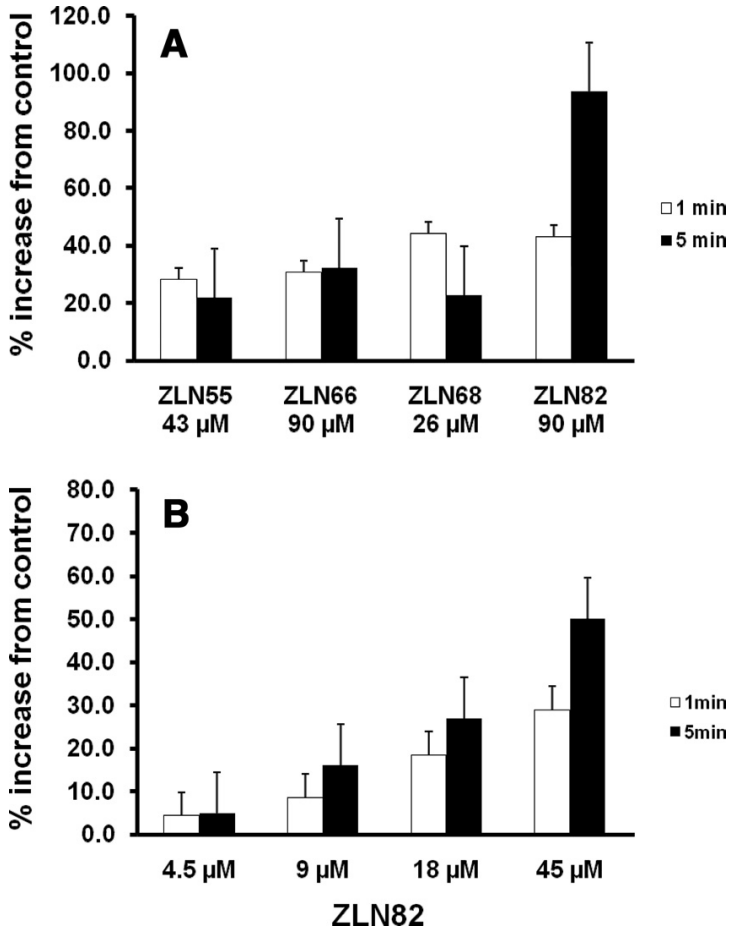

Figure 5.4

Effect of PDEC inhibitors on epimastigote cyclic AMP levels. The cAMP increase was calculated by comparing the luminescent signal from each sample with that of the control using the HitHunter cAMP kit as described in Materials and Methods. Control values were 8.5 ± 0.9 pmol/10^9 cells. (A) Each sample was incubated with about 5 to 10 times the TcrPDEC IC50 for each compound (ZLN55, 43 µM; ZLN66, 90 µM; ZL82, 90 µM) except for ZLN68 (26 µM). The results are means ± SD of data from 3 experiments, each one in duplicate. (B) Each sample was incubated with the concentrations of ZLN82 indicated. The cAMP increase was calculated as described above. The results are means ± SD of data from two experiments, each one carried out in duplicate.

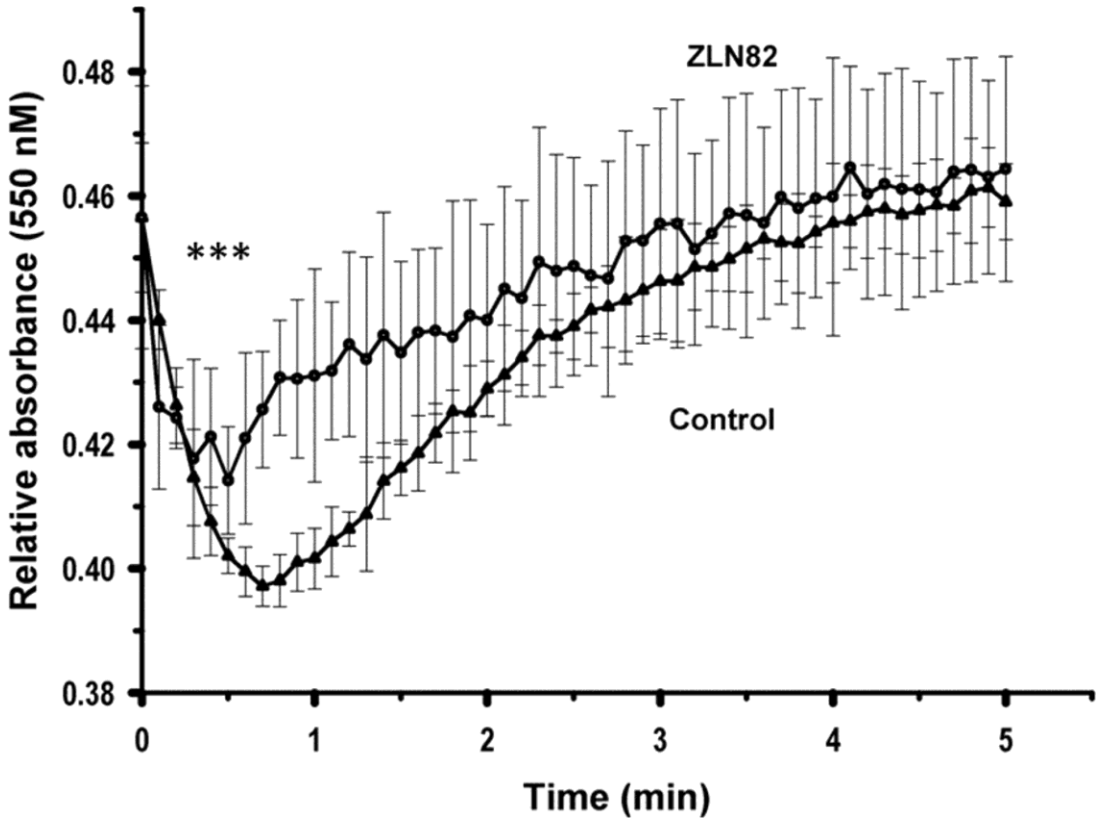

Figure 5.5

Effect of ZLN82 on regulatory volume decrease. Epimastigotes suspended in Iso-Cl buffer were diluted with water to a final osmolarity of 150 mOsm at time 0, and relative changes in cell volume were followed by monitoring the absorbance at 550 nm as described in the Material and methods section. Note that cells preincubated for 10 min with ZLN82 (8.7 µM, upper curve) did not swell as the controls (bottom curve) and recover their volume earlier than controls. Values are means ± S.E.M, n = 3, all in triplicate. Asterisks indicate significant differences (measured using a Student's *t* test).

Supplemental Figures

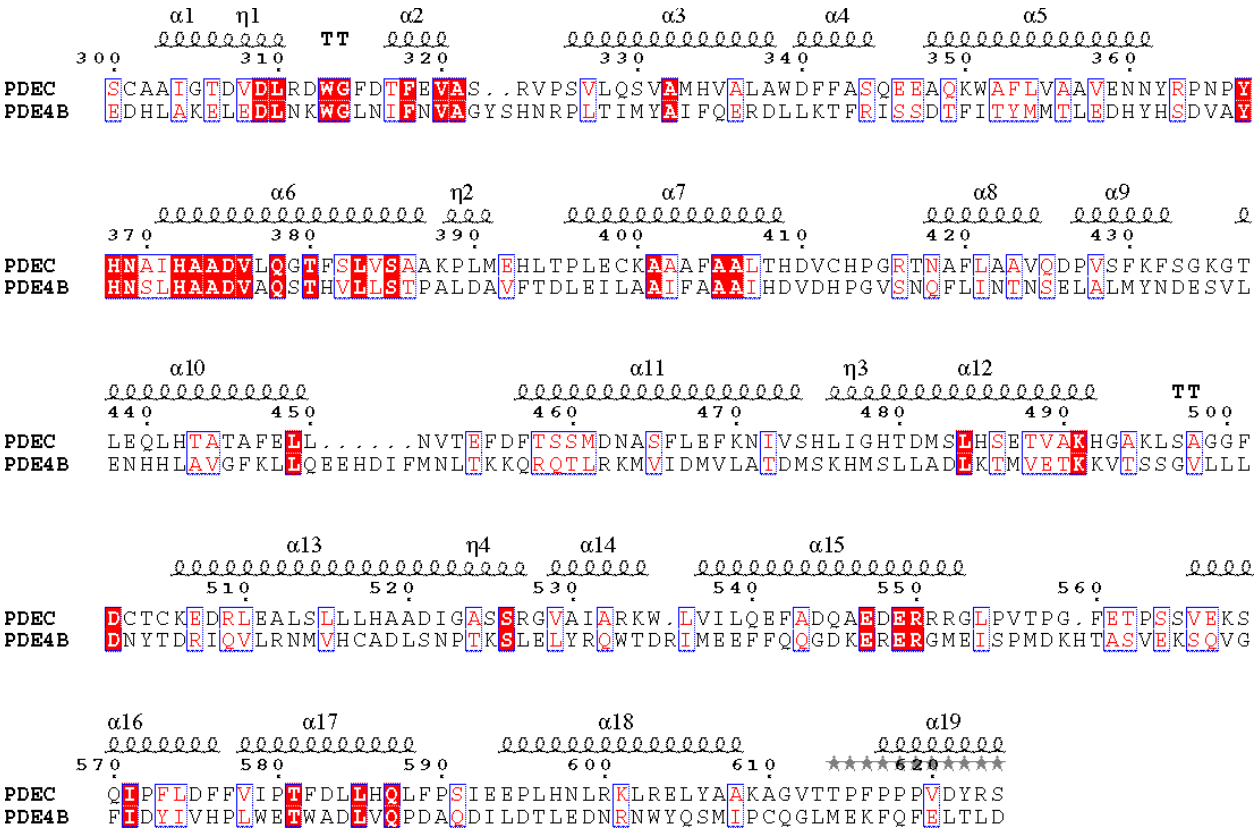

Figure 5.6: Sequence alignment of *Trypanosoma cruzi* PDEC and human PDE4B

Sequence alignment between *Trypanosoma cruzi* PDEC (UniProtKB/TrEMBL accession number Q53I60_TRYCR) and human PDE4B, PDB entry 1XMY). Identical residues are in red boxes and white characters, similar residues are in red characters. Alpha helices are displayed as squiggles.

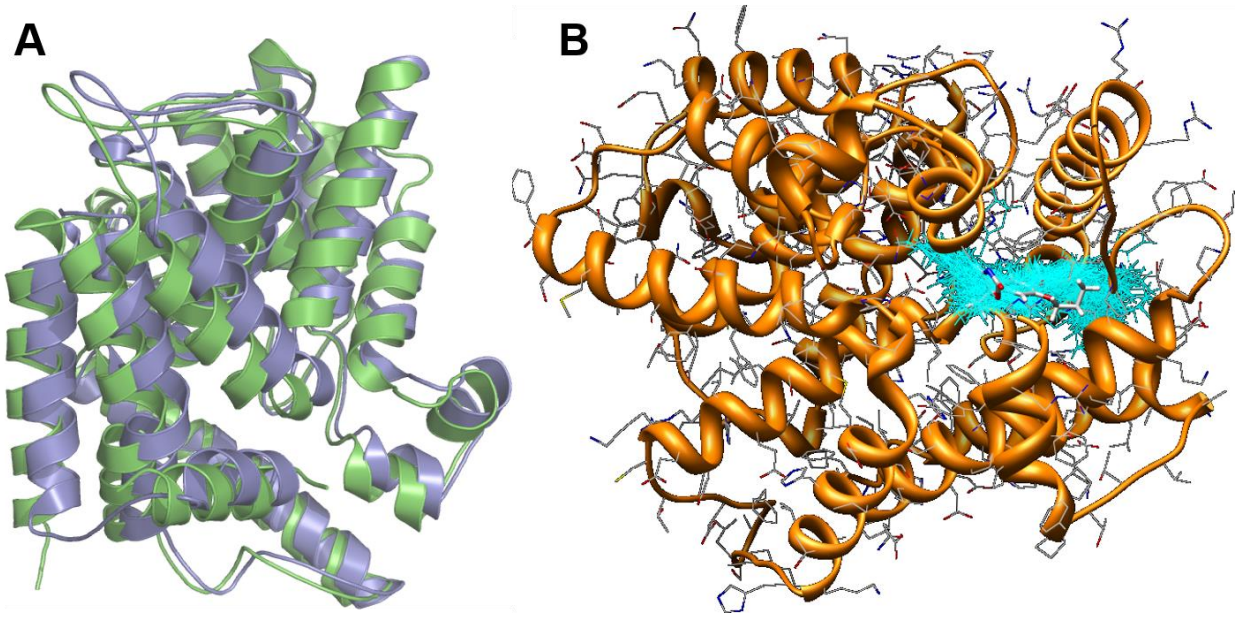

Figure 5.7: Homology modeling

(A) The overlay of human PDE4B crystal structure (green ribbons) and *Trypanosoma cruzi* PDEC homology model (purple ribbons). (B) The docking conformations of identified compounds around the active site of PDEC.

CHAPTER 6

CONCLUSIONS

6.1 Summary of Key Findings (PI-PLC)

At the beginning of this thesis work, very little information was known concerning the existence of an IP_3/DAG pathway in Trypanosomes. IP_3 had been detected in parasites (Moreno *et al*, 1992) and DAG had been implicated in endocytosis (Subramanya and Mensa-Wilmot, 2010). The phospholipase C that can generate these second messengers had only been investigated in *Trypanosoma cruzi* (Furuya *et al*, 2000; Okura *et al*, 2005; Martins *et al*, 2010; Martins *et al*, 2010). However, limitations, such as lack of RNAi machinery and arduous strategy for gene knock outs in *Trypanosoma cruzi* prevented further investigations into the functional role of the PI-PLC. The presence of these genetic tools made *Trypanosoma brucei* an attractive model for functional analysis.

Our work demonstrated that PI-PLC gene codes for a phospholipase C by demonstrating activity in the recombinant protein that was sensitive to low amounts (nM) of calcium. The enzymatic characterization also showed that the enzymes prefers PIP_2 as a substrate compared to PI. *Tb*PI-PLC enzyme lacks a traditional PH domain found in most mammalian PLCs. Like the *Tc*PI-PLC, the *T. brucei* enzyme has a myristoylation sequence. This sequence demonstrated a role in localization to the plasma membrane in *T. cruzi* (Martins *et al*, 2010). The *Tb*PI-PL enzyme shows a complex intracellular localization as demonstrated by our overexpression of the myristoylation sequence and a truncated version (without the myristoylation sequence). The overexpression of the myristoylation sequence localized to the plasma membrane whereas the

truncated version localized to the cytosol. We also demonstrated that our overexpression constructs can be modified by fatty acid attachment which, when absent, disrupted plasma membrane localization. Moreover, our tagging of the endogenous enzyme localized to intracellular vesicles. Further analysis highlighted a similar distribution of the substrate, PIP_2, to intracellular vesicles. *Tc*PI-PLC associated with lipid rafts when dually acylated (Martins *et al*, 2010) which could assist in bringing enzyme in contact with the substrate suggesting mechanisms for targeting to areas of substrate enrichment. Collectively, our data suggest that the *T. brucei* enzyme may be localized differently in the absence of the necessary modifications and the enzyme may be targeted to these intracellular vesicles where there is an enrichment of substrate.

Enzymatic activity was sensitive to low amounts of calcium. Site-directed mutagenesis within the calcium-binding region of the EF hand illustrated calcium could be regulating activity through the EF hand domain rather than through the C2 domain, but calcium sensitivity remained unchanged. However, the sensitivity to low amounts of calcium suggests that this enzyme may be constitutively active and could be contributing to the basal level of calcium. This could support the substrate level phosphorylation needed for the growth of procyclic form cells (Bochud-Alleman and Schneider, 2002). Understanding how the *Tb*PI-PLC enzyme could be contributing to cellular bioenergetics would be important for understanding the role of the IP_3/DAG signaling pathway in the parasite.

Using RNAi, we were able to knock down the PI-PLC transcript, but we did not observe any effects on growth or the ability to establish an acute infection. With that, we were keenly interested in demonstrating that the enzyme is active in the parasites. Using a PIP_2 hydrolysis assay, we demonstrated that the enzyme is active in both procyclics and bloodstream forms,

more so in procyclics. However, we noticed an increase of dead cells in the cells overexpressing *Tb*PI-PLC compared to the parental line. To further analyze this observation, we labeled cells with propidium iodide that were induced to overexpress the PI-PLC and we noticed an increase from less than 0.5 percent to over 3%. Treatment with H_2O_2 has been shown to induce programmed cell death in parasites (Das *et al,* 2001). When treated with 100 µM of H_2O_2 for 3 hours, cells induced to overexpress PI-PLC had 3.3% of dead cells compared to the 0.59% in the uninduced cells. This suggests that overexpression of the PI-PLC makes the cells more susceptible to programmed cell death and highlights further roles of the IP_3/DAG pathway.

6.2 Future Direction (PI-PLC)

This work suggests new and additional avenues to explore the role of this enzyme. Previous data identifying only detectable amount of IP_3 bloodstream form and more substantial amounts in procyclics (Moreno *et al,* 1992) as well as our unsuccessful attempts to overexpress the PI-PLC in bloodstream forms suggests that the enzyme may upregulated or expressed only in the procyclic form. Expression profiles from the TriTrypDB demonstrate at least a two-fold increase of transcript and protein in procyclics compared to the bloodstream form. Bloodstream form RNAi cells could be subjected to in vitro differentiation and analyzed for ability to differentiate.

Another interesting avenue to explore is the role of PI-PLC expression in causing the overload of calcium in the mitochondrion and therefore contributing to programmed cell death. This could be accomplished by measuring mitochondrial Ca^{2+} and mitochondrial superoxide radicals in cells overexpressing PI-PLC using MitoSOX. In addition, measurements of cytosolic Ca^{2+} levels in cells that are not overexpressing and those overexpressing PI-PLC with or without ionomycin to increase cytosolic Ca^{2+} would demonstrate that a rise in cytosolic calcium alone does not cause programmed cell death. The ionomycin would cause Ca^{2+} mobilization out of the

mitochondrion as well. This could demonstrate that mitochondrial Ca^{2+} overload causes superoxide formation and that cytosolic Ca^{2+} would induce necrosis instead. The IP_3 receptor in *T. brucei* has recently been shown to be functional and can release intracellular calcium when stimulated with IP_3 (Huang *et al*, 2013). The experiments investigating the formation of superoxides could highlight how PI-PLC expression and the IP_3/DAG pathway could mediate constitutive IP_3 receptor-mediated calcium release regulating cellular metabolism. It is speculated that low-level IP_3 receptor calcium release promotes oxidative phosphorylation through activation of the ATP synthase (Balaban, 2009; Cárdenas, 2010). The overexpression of PI-PLC could cause the formation of superoxides damaging to cells mediated by an increase of IP_3 receptor calcium release beyond the normal basal level contributing to cell death.

6.3 Summary of Key Findings (PDEC)

In this work, we demonstrated that homology modeling could be used to build a 3D model to guide drug discovery for TcrPDEC. Due to the structural similarity between the PDEC and the mammalian PDE4B crystal structure, we tested compounds originally synthesized for the PDE4B. Six compounds selectively inhibited the parasite PDEC rather than the mammalian or both. The homology model was also used to screen compounds from a database looking for compound that could bind to active sites and inhibit the PDEC. We tested these compounds for amastigote growth inhibition and for inhibition of recombinant enzyme activity. Some of the drugs also were able to significantly increase cAMP levels in cells with prior incubation thus demonstrating the enzyme as a drug target. To illustrate that the drug that most significantly increased the level of cAMP was targeting the TcrPDEC involved in osmotic stress response, we incubated epimastigotes in the presence of the drug and then subjected them to hyposmotic

stress. The cells preincubated with the inhibitor did not swell as much as the untreated and were able to recover faster.

6.4 Future Direction (PDEC)

Currently, the crystal structure of TcrPDEC is providing insight into the interaction between the N-terminal and the catalytic suggesting that the N-terminal may regulate activity via the active site residues (Wang *et al,* 2012). A PDE5 inhibitor with an IC_{50} of 230 nM for PDEC binds differently compared to the human inhibitor and could be used as a starting model for drug design (Wang *et al,* 2012). Human PDEs as targets have been extensively explored leading to the development of specific inhibitors for certain families. It has been proposed that drug development to target the parasite PDEs need to build upon the knowledge gained from human studies. This would take advantage of the similarity of the homologues in host and parasite by applying previously developed technology to target the PDE (Seebeck *et al,* 2011). Any issues regarding host versus parasite specificities would be worked out by medicinal chemistry as it has been demonstrated in humans. Even though there is great similarity between the PDE families in humans, selective inhibitors are possible. This work provides a strong foundation in the use of homology modeling coupled with inhibitor testing for the screening of compounds and how this information can be used to optimize lead compounds.